AD-A093 052 MARK RESOURCES INC MARINA DEL REY CA F/G 17/9
RFSS. VOLUME 1. DISTRIBUTED CLUTTER MODEL: REAL-TIME FFT PROGRA--ETC(U)
NOV 78 R L MITCHELL DAAK40-78-C-0031
UNCLASSIFIED MRI-149-38 NL

1 OF 2
AD A
093052

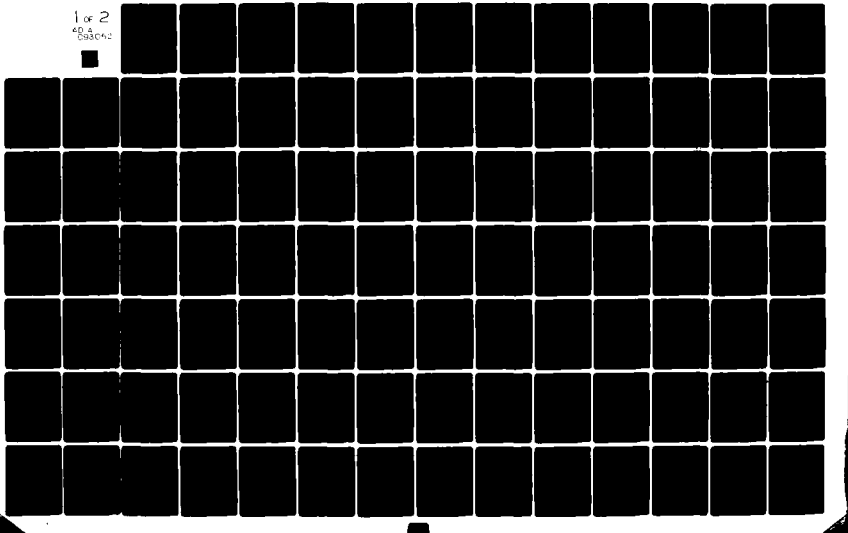

RFSS - Volume I.

DISTRIBUTED CLUTTER MODEL: REAL-TIME FFT PROGRAM
(VOL 1 OF FINAL TECHNICAL REPORT)

TECH NOTE 105-051

27 NOV 78

Final Technical Report
M-149-38, L
MIRADCOM TN-105-051

PREPARED FOR: RF SYSTEMS BRANCH (DRDMI-TDR)
SYSTEMS SIMULATION DIRECTORATE
TECHNOLOGY LABORATORY
US ARMY MIRADCOM
REDSTONE ARSENAL, AL 35809

DAAK40-78-C-0431

PREPARED BY: DR. R. L. MITCHELL
MARK RESOURCES, INC.
4676 ADMIRALTY WAY
SUITE 303
MARINA DEL REY, CA 90291

341760

80 9 22 16

MARK RESOURCES INCORPORATED

DISTRIBUTED CLUTTER MODEL: REAL-TIME FFT PROGRAM

MRI REPORT 149-38

R. L. MITCHELL

27 NOVEMBER 1978

Volume 1 of a Final Technical Report under
Contract DAAK40-78-C-0031

Under the Sponsorship of:

U.S. Army Missile R&D Command (DRDMI-TDR)
Redstone Arsenal, AL 35809

pages 65 + 67
(not missing - just numbered wrong.)

4676 ADMIRALTY WAY / SUITE 303 / MARINA DEL REY, CALIFORNIA 90291 / (213) 822-4955

TABLE OF CONTENTS

LIST OF FIGURES

LIST OF FIGURES (Cont'd)

LIST OF TABLES

LIST OF FIGURES (Cont'd)

FOREWORD

The work performed under Contract DAAK40-78-C-0031 that resulted in specific deliverables (principally computer programs) is described in two volumes of a final report. This is Volume 1, which describes the work that led to the distributed clutter model. Volume 2, entitled "Extended Target Model: Real-Time Simulation Program," describes the work relevant to that subject.

The AP120B array processor programs described in this report (but documented elsewhere) were designed and developed by Dr. I. P. Bottlik, as well as the interfaces to the host computer and Digital Signal Generator. Dr. Bottlik was assisted by Mr. D. L. Brandon.

1. INTRODUCTION AND SUMMARY

This report describes a real-time simulation procedure for generating replicas of the gound clutter signal as received on the three monopulse channels of an airborne radar. The procedure is based on first computing the power spectra of the clutter (on the three monopulse channels) according to the engagement geometry, then randomizing these power spectra, and finally executing an FFT in real time to create the quadrature video components of the clutter sequences.

The procedure permits any spectral shape to be simulated, so that it is inherently very accurate. However, the computation is time-consuming so that its application in real time is limited. With one AP120B array processor interfaced to a Datacraft/6 computer, only a single range gate of clutter can be simulated in real time.

Listings of a Fortran program are included. The program has been tailored to a specific missile system under test at the RFSS.

2. GENERATING CLUTTER SEQUENCES IN REAL TIME

The use of an FFT to generate finite-length sequences of correlated random samples is described in Reference 1. First, a sequence of independent, complex random samples is generated throughout one frequency repetition interval. Next, given an amplitude spectrum of interest (the square-root of the ensemble-averaged power spectrum) we multiply the random samples by the corresponding samples of the amplitude spectrum. Finally, the complex spectral sequence is Fourier transformed (via an FFT) to obtain the quadrature components of the correlated time sequence.

The above time sequences have the property that they are circularly periodic; i.e., the sequence repeats with a period $1/\Delta f$ where Δf is the sample spacing in the frequency domain. If the random process is stationary we can make Δf small enough (at least in theory) so that the repetition period will be longer than the process time of interest. However, if the process is nonstationary, as with clutter received on a missile radar, the power or amplitude spectrum of the process will be continually changing and any procedure based on a single FFT will not lead to the proper time sequence.

One procedure that does work, however, is to take a sequence of FFT's where the spectrum for any one FFT will be relatively stationary. The procedure is discussed in Reference 2 (Section 6). In order to avoid the abrupt transition that would result if one resulting time sequence directly followed another, it is imperative that the sequences overlap as shown in Figure 1. Different weighting functions are discussed in Reference 2, and the conclusion is that linear weighting, as shown in Figure 1, is satisfactory with an overlap that is about 1/8 of the FFT length. More overlap would provide slightly lower residual sidelobes but at the expense of a more time-consuming computation.

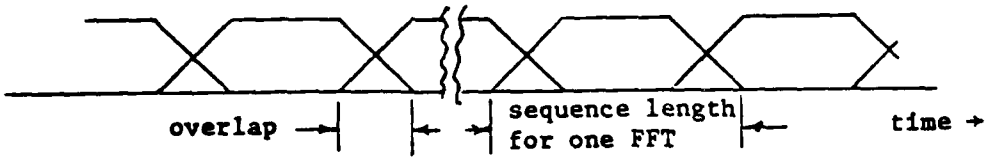

Figure 1. Sequence of Weighting Functions

3. GROUND CLUTTER SPECTRA

The ground clutter spectra on the three monopulse channels are determined by the engagement geometry and the antenna pattern shapes. In this section we will derive the basic relationships for a pulse-Doppler radar with the antenna pointing within about 30° of the velocity vector.

3.1 Engagement Geometry

In Reference 2 (Section 4) it was shown that the clutter spectral shapes on the three monopulse channels are functions of only five angles, where the geometry is given in Figure 2:

1) azimuth angle of antenna boresight, α
2) depression angle of antenna boresight, β
3) depression angle of range ring of interest, γ
4) missile dive angle, δ
5) missile roll angle, ω

Two additional parameters are required to complete the specification of the clutter spectra:

6) missile altitude, h
7) missile velocity, V

The engagement geometry may not be expressed directly in terms of the five angles above. Instead of (α,β) it is most likely that the azimuth and elevation of the antenna boresight (θ_o, ϕ_o) relative to the missile velocity vector will be given. The transformation of (θ_o, ϕ_o) to (α,β) is derived in Appendix A.

The missile altitude and slant range are related by

$$r = h/\sin \beta \tag{1}$$

3.2 Assumed Antenna Patterns

In the analysis that follows we will assume the following set of receive voltage gain patterns:

sum channel: $$g_\Sigma(\theta,\phi) = g_\Sigma(\theta)\, g_\Sigma(\phi) \tag{2}$$

ΔAz channel: $$g_{\Delta A}(\theta,\phi) = g_\Delta(\theta)\, g_\Sigma(\phi) \tag{3}$$

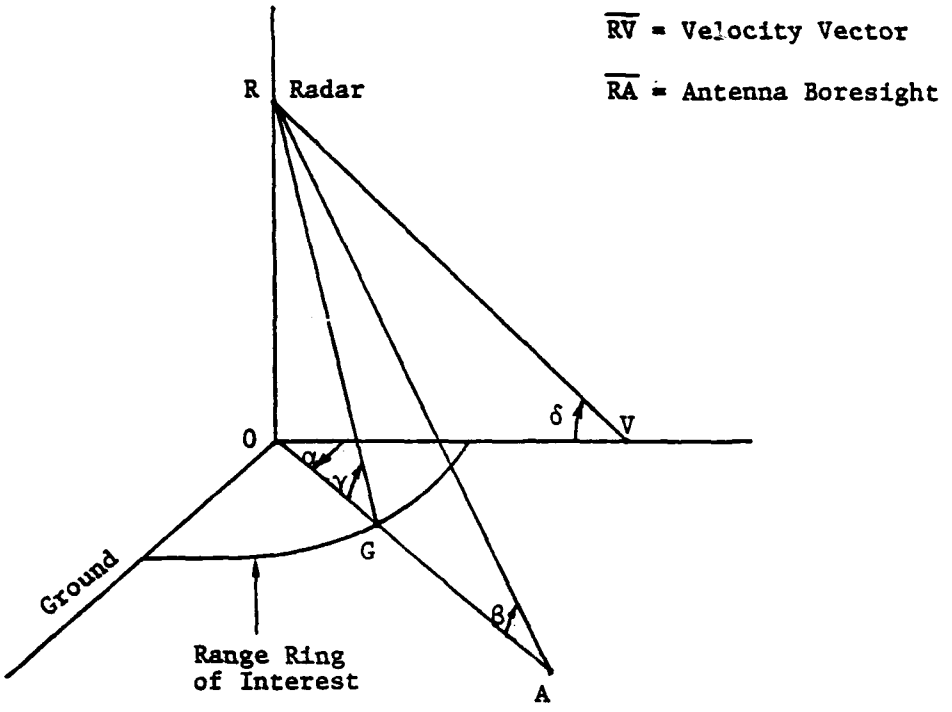

Figure 2. Engagement Geometry for Ground Clutter

$$\Delta El \text{ channel: } g_{\Delta E}(\theta,\phi) = g_{\Sigma}(\theta)\, g_{\Delta}(\phi) \tag{4}$$

where θ and ϕ are the azimuth and elevation angles, respectively, and

$$g_{\Sigma}(\zeta) = \exp\,(-a|\zeta|^{b}) \tag{5}$$

$$g_{\Delta}(\zeta) = k\zeta \quad \exp\,(-c|\zeta|^{d}) \tag{6}$$

where ζ designates either angle. We also assume the specific parameters

$$k = .084$$
$$a = .00389$$
$$b = 2.30$$
$$c = .00309$$
$$d = 2.10$$

where ζ is in degrees in (5) and (6). The half-power width of the sum pattern is about 14°. It is assumed that the radar transmits on the sum channel. The patterns for the sum and one difference channel are plotted in Figure 3.

3.3 Spectral Shape

In Reference 2 (Section 4) it was shown that the spectral shapes of clutter are primarily a function of two parameters, α and ω. The remaining parameters in the list in Section 3.1 act as scaling parameters, either in frequency or power.

> **Note:**
> Throughout the remainder of this report clutter spectra will be shown for the three monopulse channels. Unless otherwise indicated, all plots will be in the format of Figure 4.

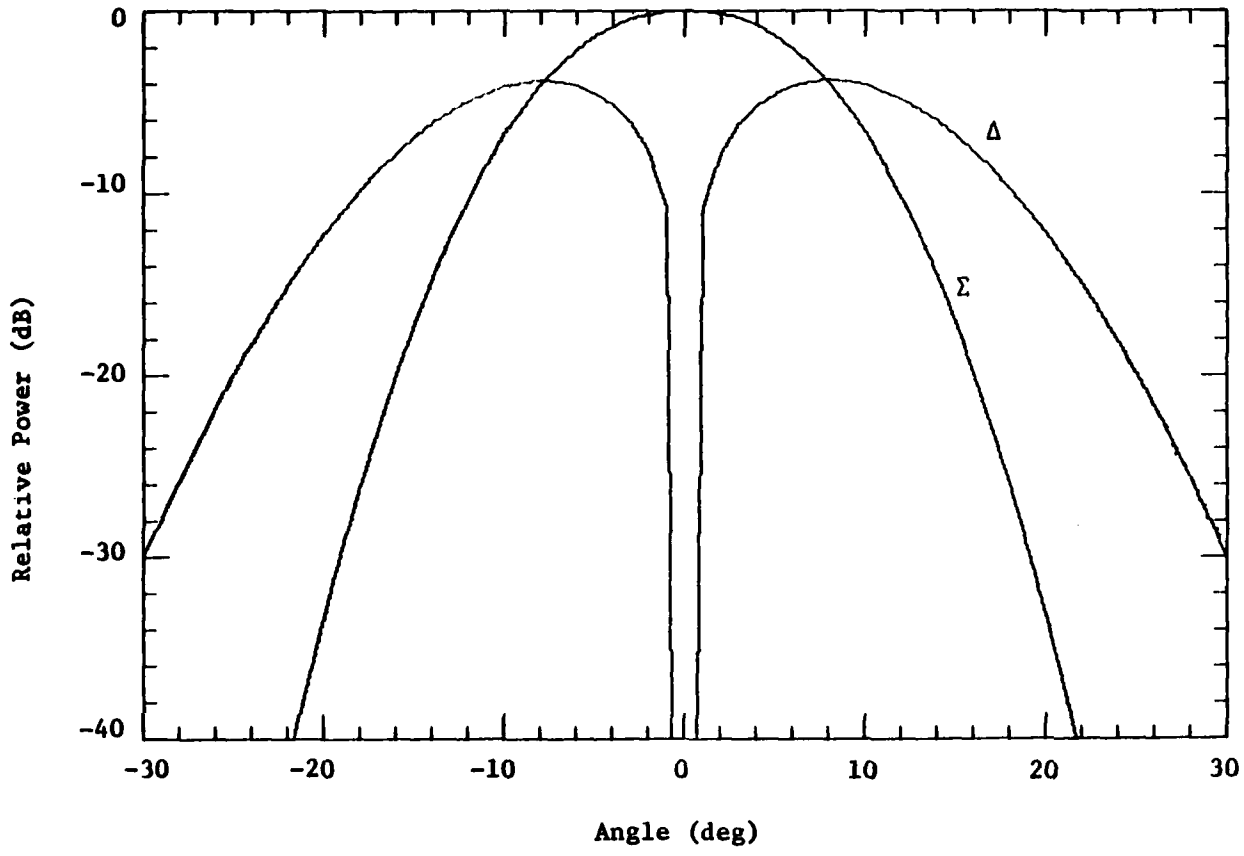

Figure 3. Assumed Sum and Difference Channel Antenna Patterns

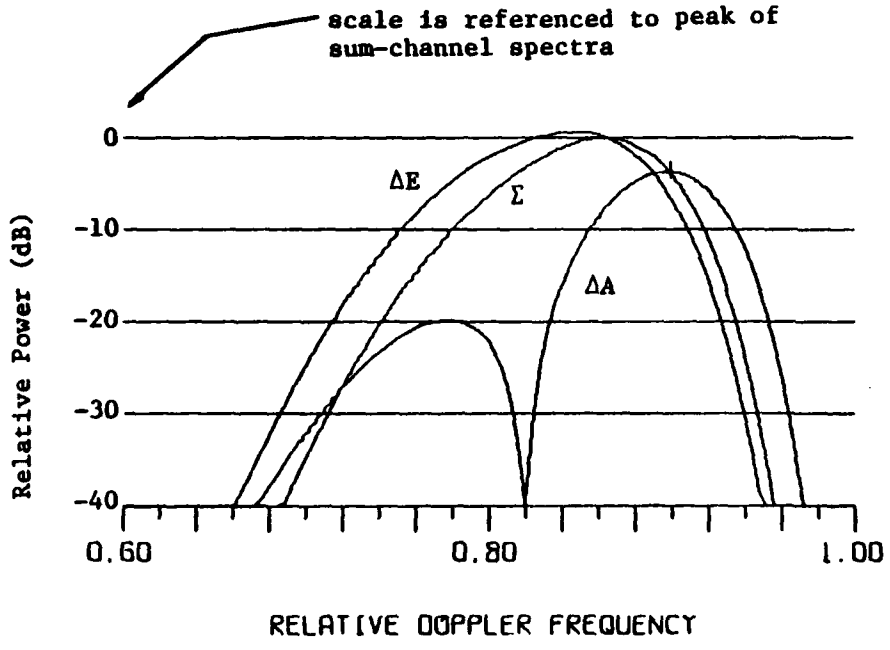

Actual Doppler Frequency =

$(2V/\lambda)$ × Relative Doppler Frequency

Σ = sum-channel spectrum

ΔA = del-az channel spectrum

ΔE = del-el channel spectrum

Figure 4. Format for Plots of Clutter Spectra

The azimuth angle, α, strongly affects the spectra on all three monopulse channels as is shown in Figure 5 through 8 for $\alpha = 0$, 10°, 20°, and 30°, respectively (in all cases $\beta = \delta = \omega = 0$ and $\gamma = 10°$, and frequency is relative to $2V/\lambda$). Note the different scales in frequency. When the azimuth angle is small (less than about 50% of the antenna half-power beamwidth), all spectra are truncated sharply at the relative Doppler frequency given by $\cos(\delta-\gamma)$, which in the case of the figures is 0.985. It is this strong variation with respect to the azimuth angle that greatly limits the use of a single spectral shape to describe the clutter spectra.

The missile roll angle, ω, affects primarily the monopulse difference channels as is shown in Figures 9 through 17 for $-45° \leq \omega \leq 45°$ in steps of 11.25° (in all cases $\beta = \delta$ and $\alpha = \gamma = 10°$). Due to the symmetry in the antenna patterns of Section 3.2, the spectra for ω and $\omega \pm 180°$ are identical. The spectra for ω and $\omega \pm 90°$ are also identical except the monopulse difference channels are interchanged (e.g., see Figures 9 and 17). Note that the sum channel spectrum is not a strong function of the missile roll angle.

3.4 Frequency Scaling

The maximum Doppler frequency within the range gate of interest is given by

$$f_{max} = \frac{2V}{\lambda} \cos(\delta-\gamma) \qquad (7)$$

In Reference 2 (Section 4.6) it was suggested that (7) represents a valid frequency scaling of the spectra for most cases of interest. In other words, spectra computed at one combination of δ and γ could be simply scaled in frequency for other values by the use of (7). The approximation is good as long as δ and γ are not large.

In order to demonstrate how well the spectra can be scaled we show in Figures 18 through 23 cases for which $|\delta-\gamma| = 10°$ ($\alpha = 10°$, $\beta = \delta$, and $\omega = 0$). The first three cases where $\delta \leq 20°$ and $\gamma \leq 30°$ are practically identical. In Figure 21 there is some deviation in the tail of the ΔA spectrum, but otherwise the spectra are still within a few dB of the other cases. It is only when we go to the steeper geometries in Figures 22 and 23 that

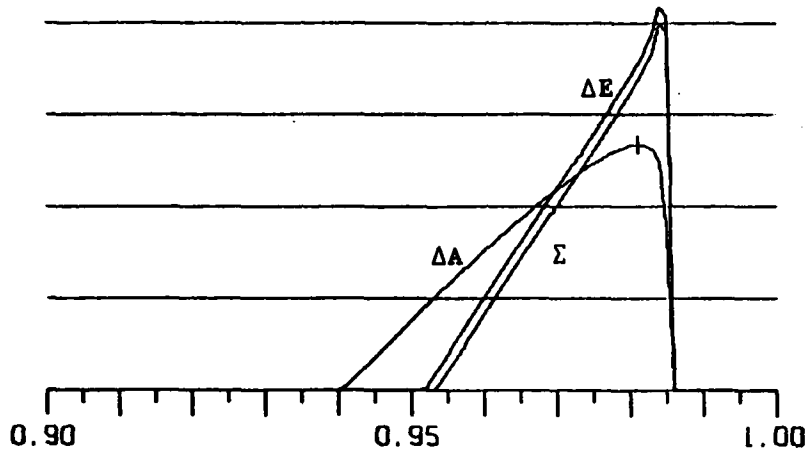

Figure 5. Clutter Spectra for $\alpha = 0$

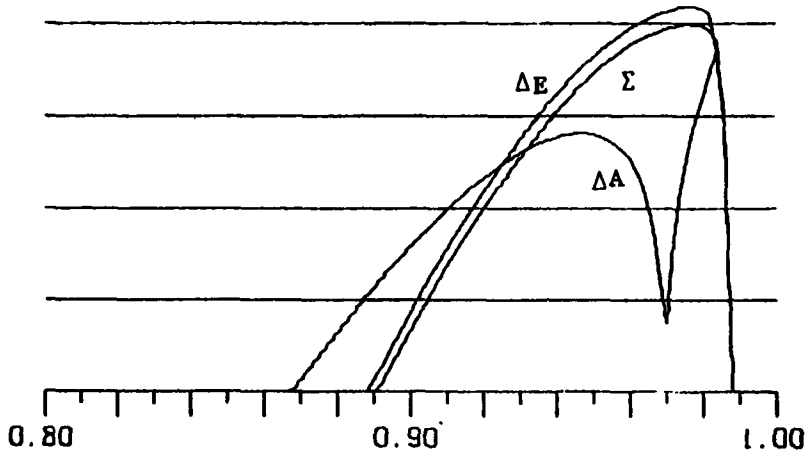

Figure 6. Clutter Spectra for $\alpha = 10°$

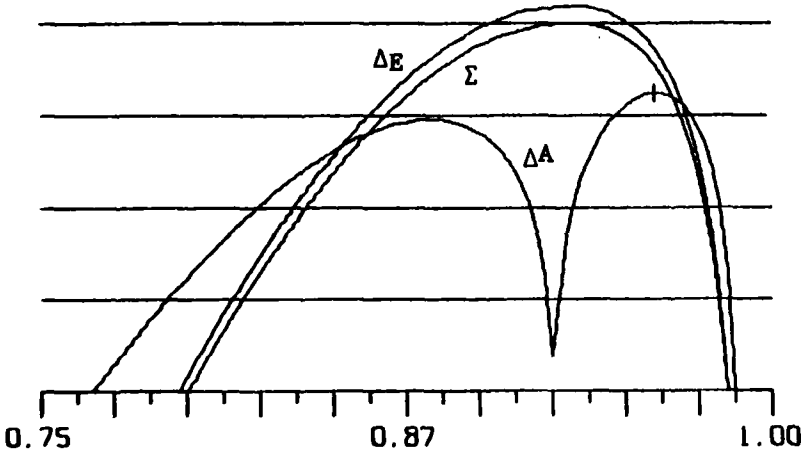

Figure 7. Clutter Spectra for $\alpha = 20°$

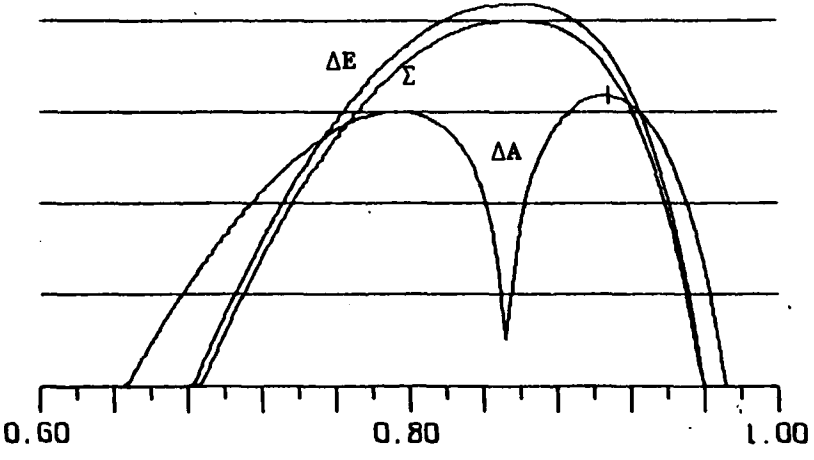

Figure 8. Clutter Spectra for $\alpha = 30°$

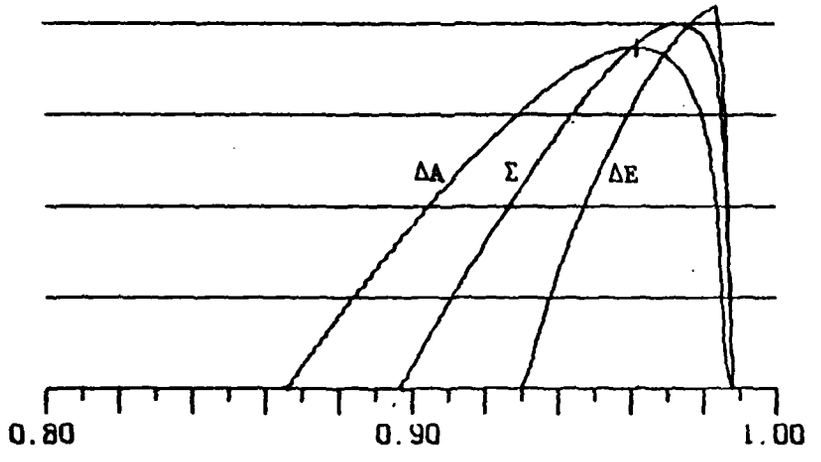

Figure 9. Clutter Spectra for $\omega = -45°$

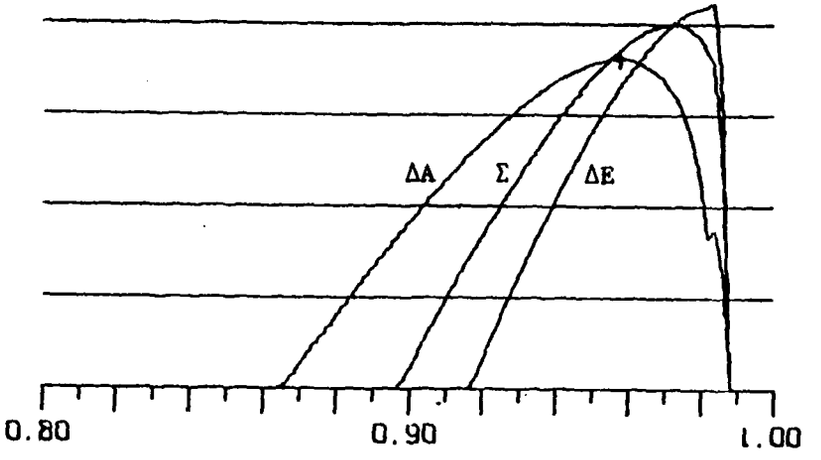

Figure 10. Clutter Spectra for $\omega = -33.75°$

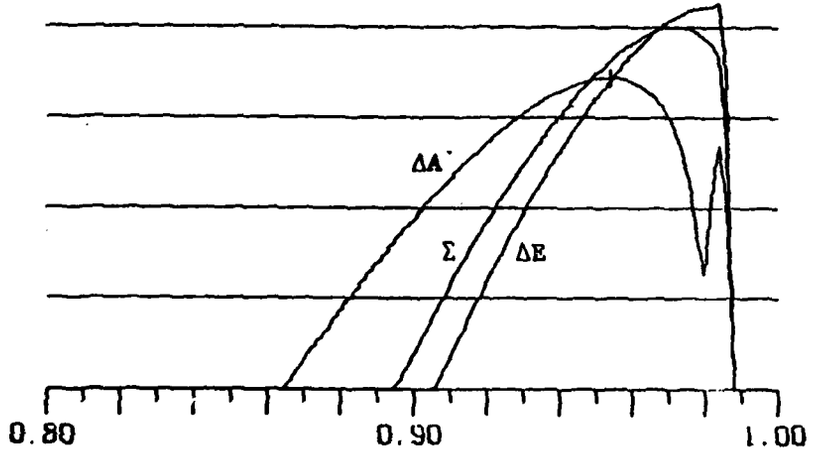

Figure 11. Clutter Spectra for $\omega = 22.5°$

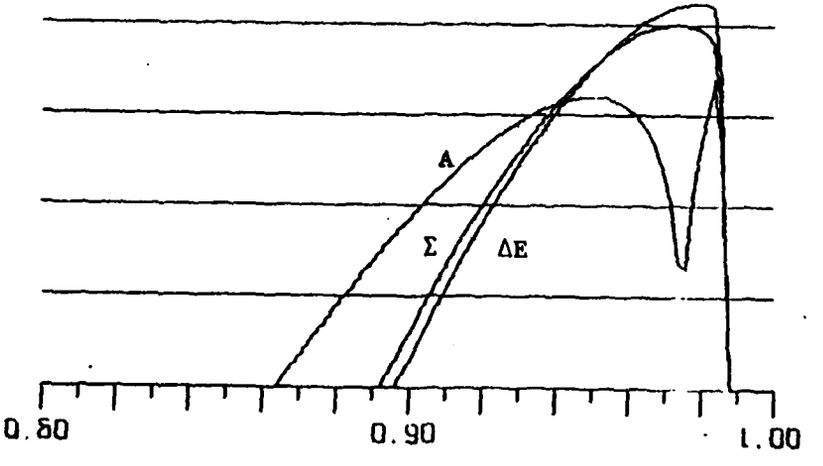

Figure 12. Clutter Spectra for $\omega = -11.25°$

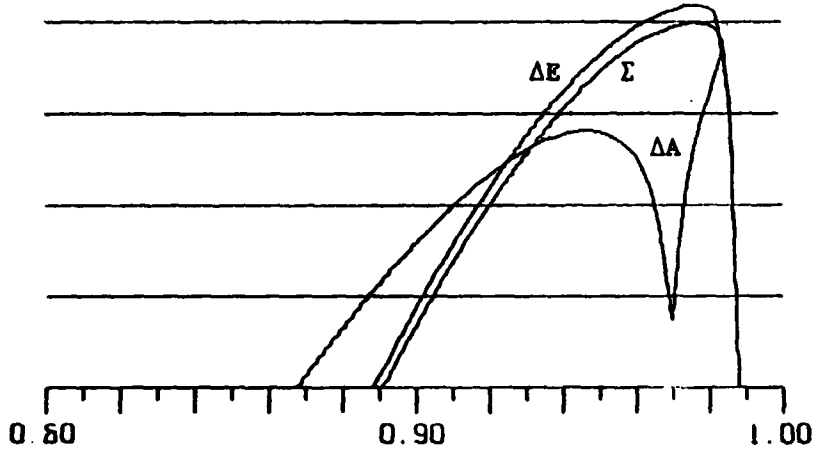

Figure 13. Clutter Spectra for ω = 0

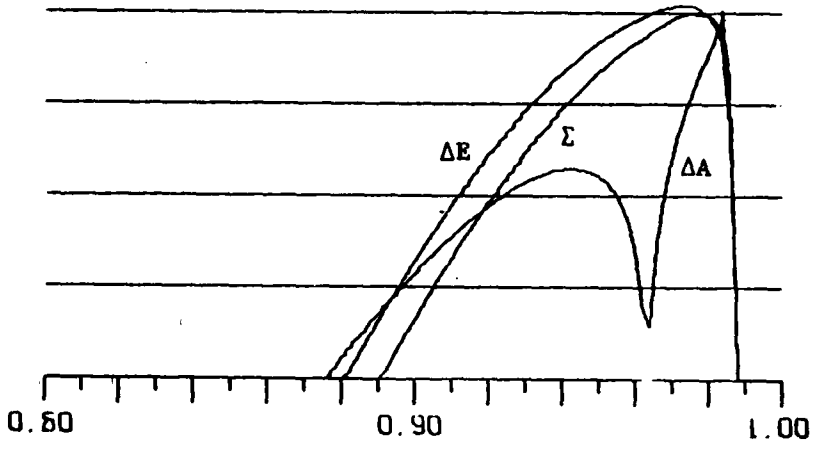

Figure 14. Clutter Spectra for ω = 11.25°

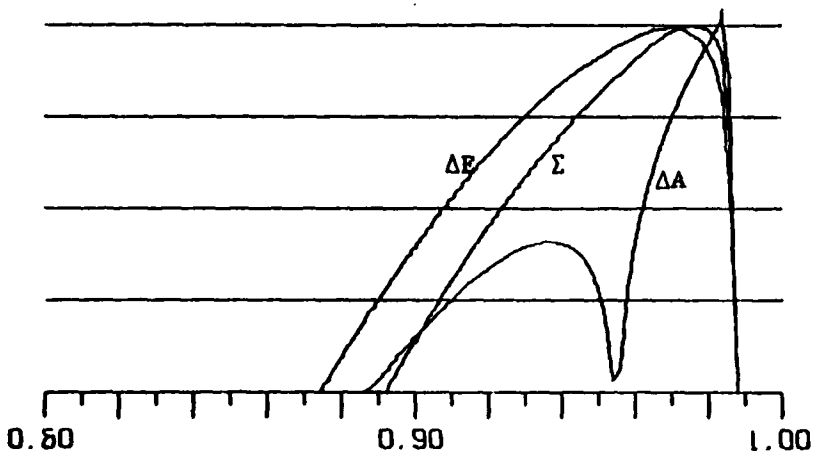

Figure 15. Clutter Spectra for ω = 22.5°

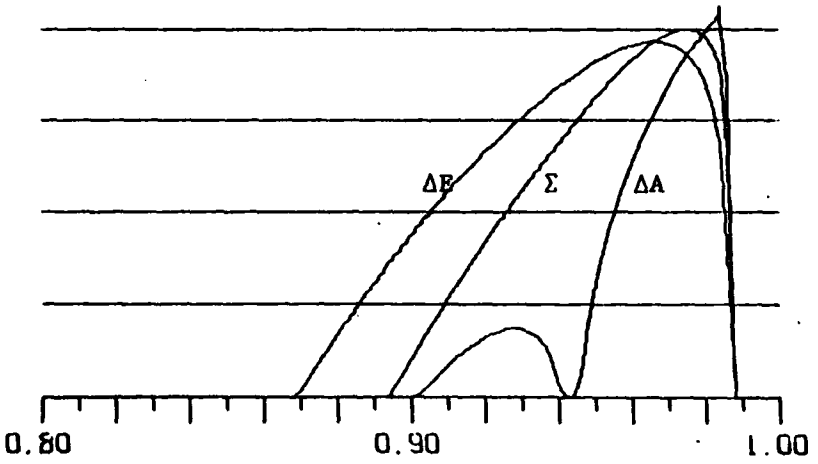

Figure 16. Clutter Spectra for ω = 33.75°

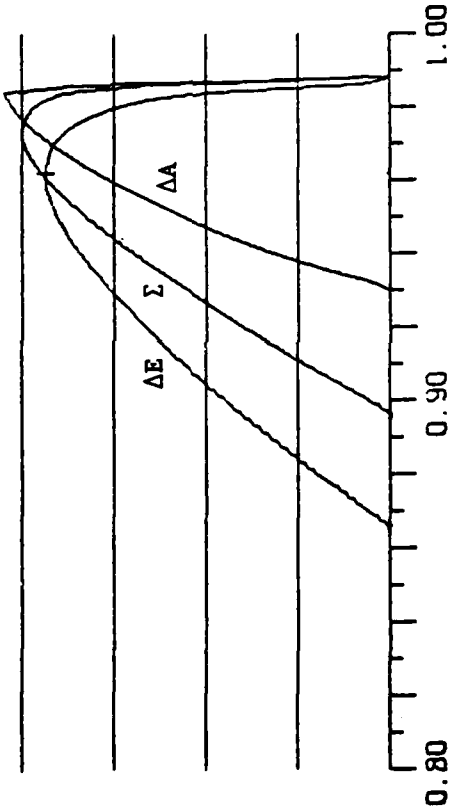

Figure 17. Clutter Spectra for ω = 45°

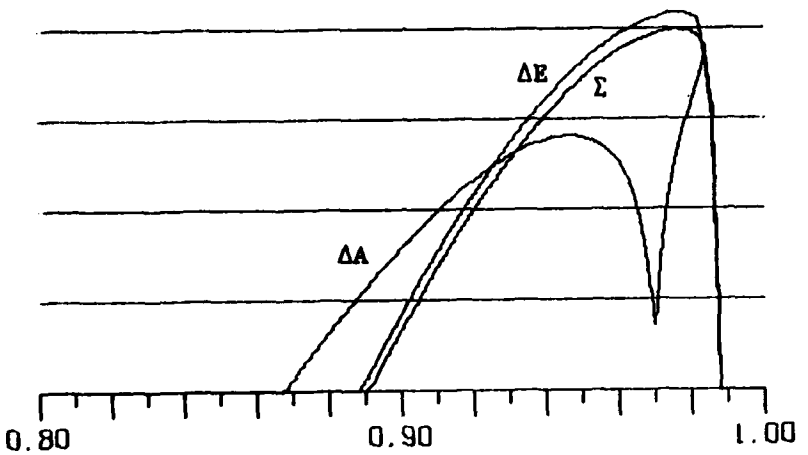

Figure 18. Clutter Spectra for $\beta = \delta = 0$, $\gamma = 10°$

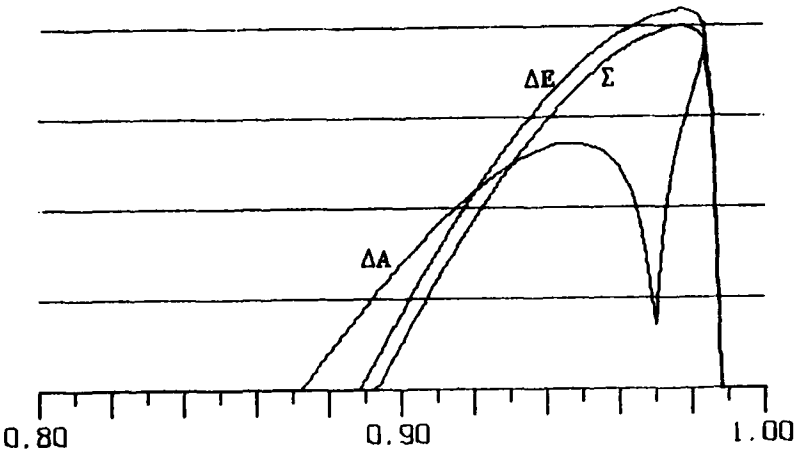

Figure 19. Clutter Spectra for $\beta = \delta = 10°$, $\gamma = 20°$

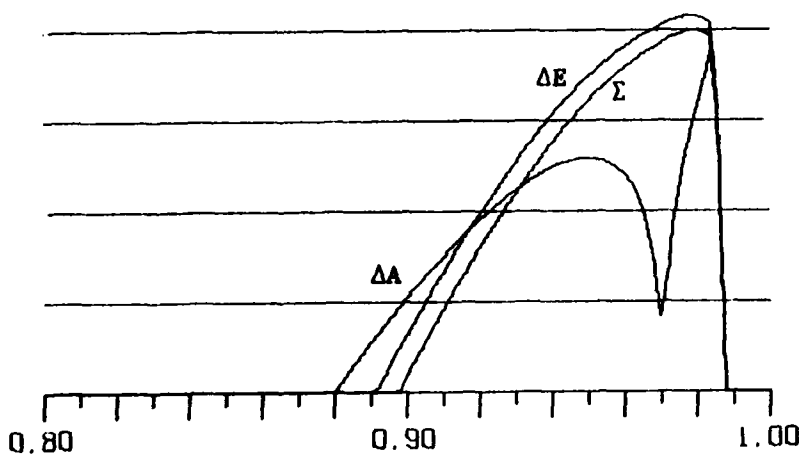

Figure 20. Clutter Spectra for $\beta = \delta = 20°$, $\gamma = 30°$

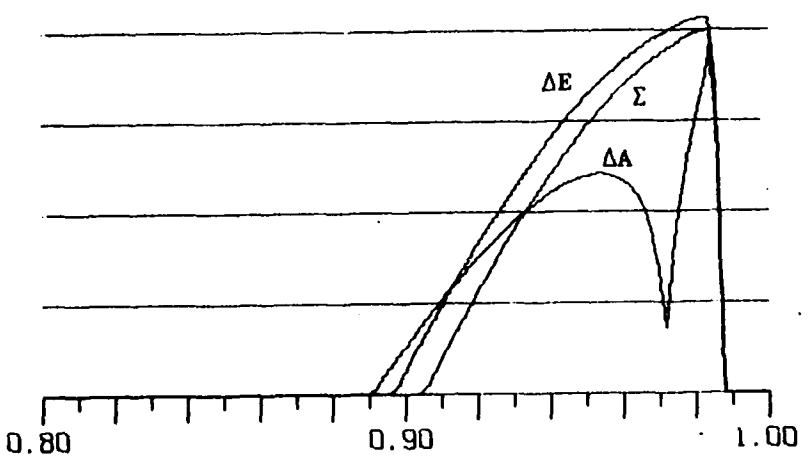

Figure 21. Clutter Spectra for $\beta = \delta = 30°$, $\gamma = 40°$

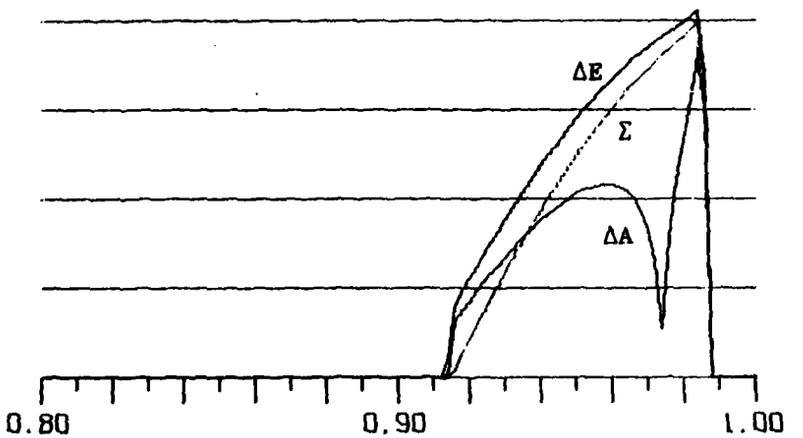

Figure 22. Clutter Spectra for $\beta = \delta = 40°$, $\gamma = 50°$

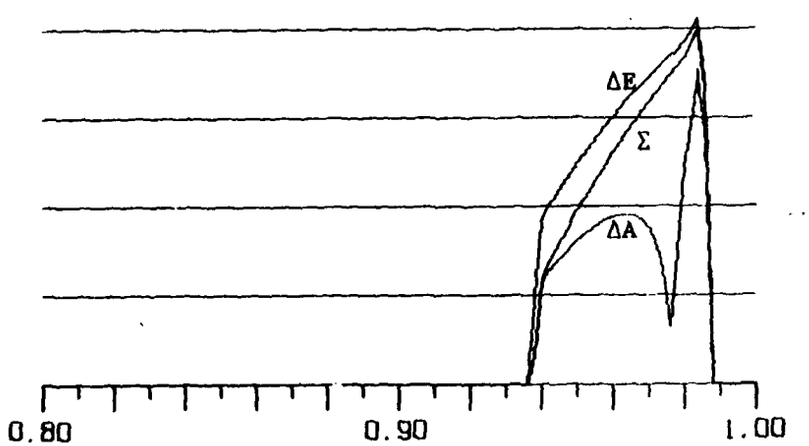

Figure 23. Clutter Spectra for $\beta = \delta = 50°$, $\gamma = 60°$

the differences become significant. These results indicate that the simple frequency scaling law of cos $(\delta-\gamma)$ applies with reasonable accuracy as long as δ and γ do not exceed about 35 or 40°.

3.5 Clutter Power for Sum Channel

With the use of Figure 24, the power received from the clutter cell of area $r_g \Delta r_g \Delta\alpha$ is given by

$$\Delta P_R = \frac{P_T G^2 \lambda^2 \sigma_o (r_g \Delta r_g \Delta\alpha)}{(4\pi)^3 r^4} \tag{8}$$

where P_T is the peak transmit power, G is the one-way power gain in the direction of the clutter cell, λ is the wavelength, r is the range, and σ_o is the clutter backscatter coefficient (radar cross section per unit area on the ground). The ground range, r_g, is related to the slant range, r, by

$$r_g = r \cos \gamma \tag{9}$$

The intersection of the range resolution cell on the ground is Δr_g. It is straightforward to show that

$$r_g \Delta r_g = r \Delta r \tag{10}$$

where we define Δr to be the range resolution (range gate width). Thus (8) becomes

$$\Delta P_R = \frac{P_T G^2 \lambda^2 \sigma_o \Delta r \Delta\alpha}{(4\pi)^3 r^3} \tag{11}$$

The total received power is obtained by integrating (11) over all azimuth angles within the range gate intersection on the ground. If σ_o is constant (as it will be for homogeneous clutter), the total power is

$$P_R = \frac{P_T \lambda^2 \sigma_o \Delta r}{(4\pi)^3 r^3} \int G^2(\alpha)\, d\alpha \tag{12}$$

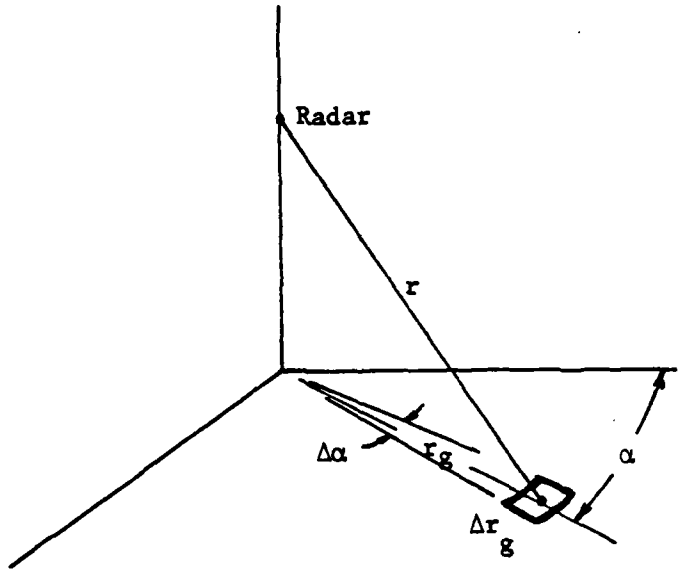

Figure 24. Clutter Geometry

where $G(\alpha)$ is defined as the one-way power gain in the direction of a point at an azimuth α within the range gate intersection on the ground.

3.6 Effective Radiated Power

In the RFSS the clutter signal will be radiated from the RFSS array at a distance D from the radar receiver. Let us designate the effective radiated power as P_e. Thus the power density at the receive antenna will be

$$P_d = P_e/4\pi D^2 \tag{13}$$

The received power will be

$$P_R = P_d A = P_e A/4\pi D^2 \tag{14}$$

where A is the antenna aperture area. Since the peak gain is given by $G_o = 4\pi A/\lambda^2$, we can write

$$P_e = P_R \frac{(4\pi)^2 D^2}{G_o \lambda^2} \tag{15}$$

so that with (12) we obtain

$$P_e = \frac{P_T \sigma_o \Delta r D^2}{4\pi G_o r^3} \int G^2(\alpha)\, d\alpha \tag{16}$$

It is more convenient to work with normalized antenna patterns, so we define

$$G_n(\alpha) = G(\alpha)/G_o \tag{17}$$

where G_o is the peak gain on the sum channel. Thus (16) becomes

$$P_e = \frac{(P_T G_o D^2)\ \sigma_o\ \Delta r}{4\pi r^3} \int G_n^2(\alpha)\ \ d\alpha \tag{18}$$

which is our final result.* In some cases σ_o is defined as a function of the grazing angle, γ, such as a sin γ dependence.

For several types of antenna patterns, it has been empirically determined that for the sum channel

$$\int G_n^2(\alpha)\, d\alpha = \text{const} \times G_n^2(\gamma-\beta) \tag{19}$$

which is accurate to within about 0.2 dB for all engagement geometries. For the antenna pattern defined in Section 3.2 the constant has a value of .20 so that

$$P_e = 0.16 \frac{(P_T G_o D^2)\ \sigma_o \Delta r}{r^3}\ G_n^2(\gamma-\beta) \tag{20}$$

---

*The integral in (18) is the quantity "POWER" computed by a subroutine (SPCTRA) written by the author.

Note that the antenna patterns in (2) through (6) are defined in the normalized form.

3.7 Clutter Spectral Parameters

Let us refer to Figure 2. As viewed from the radar, the range ring intersection with the ground plane will be approximately a straight line, at least for γ not too large and for points on the range ring that are not too far away from the vertical plane ROA. Thus we have the approximate geometry given by Figure 25, where points A and G represent vectors $\overline{RA}$ and $\overline{RG}$ in Figure 2, respectively. The apparent angle between the two points is $\Delta = \gamma - \beta$. The skewed coordinates in Figure 25 represent the principal planes of the antenna, θ being the azimuth axis and ϕ the elevation axis. The angle ξ is the angle between the ϕ-axis and the vertical plane, which is derived in Appendix B as a function of the engagement geometry. Point Q is some arbitrary point along the ground "line" at an angular distance η from Point G. In the following discussion we will assume that Δ, the angular distance between Points A and G, is smaller than about 20° so that the actual spherical geometry reduces to the plane geometry in Figure 25.

The two-way antenna gain pattern for any of the three monopulse channels is assumed to be the product of two functions (see Section 3.2) as

$$G(\theta,\phi) = G_1(\theta)\, G_2(\phi) \tag{21}$$

where $G_1(\phi)$ and $G_2(\phi)$ are given in the following table:

Channel	$G_1(\theta)$	$G_2(\phi)$
sum	$g_\Sigma^4(\theta)$	$g_\Sigma^4(\phi)$
Δ-Az	$g_\Delta^2(\theta)g_\Sigma^2(\theta)$	$g_\Sigma^4(\phi)$
Δ-El	$g_\Sigma^4(\theta)$	$g_\Delta^2(\phi)g_\Sigma^2(\phi)$

with $g_\Sigma(\ )$ and $g_\Delta(\ )$ being defined in (5) and (6), respectively. From Figure 25 we can write for an arbitrary point Q on the ground within the range ring of interest

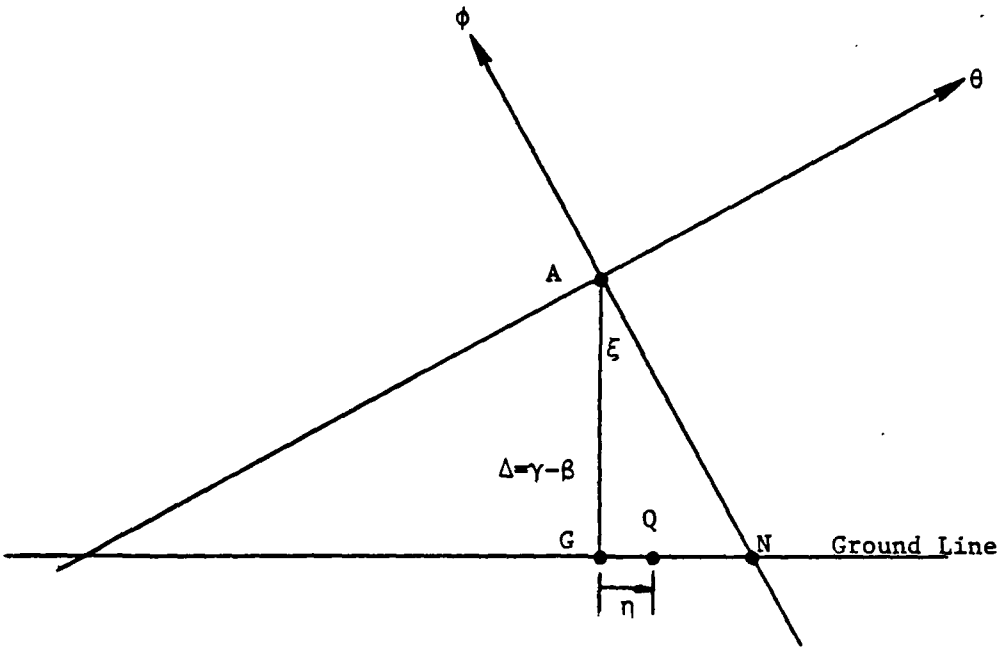

Figure 25. Engagement Geometry as Viewed from Radar

$$\theta = -\Delta \sin \xi + \eta \cos \xi \tag{22}$$

$$\phi = -\Delta \cos \xi - \eta \sin \xi \tag{23}$$

where η is the angular distance of Point Q from Point G. Thus we can write the two-way antenna gain along the ground line as

$$\begin{aligned} G(\eta) &= G_1(-\Delta \sin \xi + \eta \cos \xi)\, G_2(-\Delta \cos \xi - \eta \sin \xi) \\ &= G_1(\Delta \sin \xi - \eta \cos \xi)\, G_2(\Delta \cos \xi + \eta \sin \xi) \end{aligned} \tag{24}$$

where symmetry was assumed to obtain the second result in (24).

For the monopulse sum channel the two-way pattern will be nearly circularly symmetric about Point A in Figure 25, assuming the pattern in (2). Therefore, the peak gain along the ground line occurs at Point G, and the angle from the boresight axis is $\Delta = \gamma - \beta$. This is the reason why the effective radiated power for the sum channel scales as $G_n^2(\gamma-\beta)$ in (20).

For the monopulse difference channels the reasoning is similar, except that there is no longer any dominant circular symmetry about the boresight axis. Instead, the symmetry is about the principal antenna axes. For

example, the azimuth difference pattern has a null along the ϕ-axis, so that Point N on the ground line corresponds to a null. The angular separation of the null from Point G is

$$\eta_N = \Delta \tan \xi \tag{25}$$

By referring to Figure 2 we see that the azimuth angle of the null is $\alpha + \eta_N$. The normalized Doppler frequency of the null (ψ_N is the corresponding Doppler angle) is

$$\cos \psi_N = \cos \gamma \cos \delta \cos(\alpha + \eta_N) + \sin \gamma \sin \delta \tag{26}$$

If we use the approximation derived in Reference 2 (Section 4.6), we can write for most cases of interest

$$\cos \psi_N = \cos(\delta - \gamma) \cos (\alpha + \eta_N) \tag{27}$$

With the use of (7) we can write the Doppler frequency of the null as

$$f_N = f_{max} \cos (\alpha + \eta_N)$$

For the azimuth difference channel there will be two points along the ground line in Figure 25 for which the two-way gain will be a local maximum. One of these points will lie to the left of Point N and one will lie to the right. (When $\xi \approx \pm 90°$ there will be only one local maximum of significance which occurs near $\eta = 0$, and the null will occur so far away from Point G that the small-angle approximation will no longer be valid. In effect, the clutter spectrum will be unimodal for the azimuth difference channel when ξ is in the neighborhood of $\pm 90°$, and for the elevation difference channel when $\xi \approx 0$ and $180°$ as can be seen in Figure 13.) There is no convenient way to find these peaks other than to perform a computer search for them. Since the geometry is specified by only two parameters, Δ and ξ, we have tabulated the peak gain of the azimuth difference channel that occurs to the left of Point N in Figure 25 as a function of these two angles. The peak gain is shown in Table 1 (referenced to the peak gain of the sum channel) and the location of the peak, η_L, is shown in Table 2. Because of the symmetry we

Table 1. Two-way Gain of Left-Side Peak (dB)

	ANGLE BETWEEN PLANES, ξ (DEG)									
λ(DEG)	0	10	20	30	40	50	60	70	80	90
-18	-61.2									
-17	-54.8	-62.6								
-16	-48.9	-56.1	-65.6							
-15	-43.4	-50.0	-58.7							
-14	-38.4	-44.4	-52.3	-63.4						
-13	-33.8	-39.3	-46.4	-56.4						
-12	-29.6	-34.6	-41.0	-49.9	-63.3					
-11	-25.9	-30.4	-36.1	-43.9	-55.6					
-10	-22.6	-26.6	-31.7	-38.5	-48.6	-65.6				
-9	-19.7	-23.2	-27.7	-33.7	-42.3	-56.6				
-8	-17.2	-20.2	-24.1	-29.3	-36.7	-48.5				
-7	-15.1	-17.6	-21.0	-25.4	-31.6	-41.4	-59.8			
-6	-13.3	-15.4	-18.2	-22.0	-27.2	-35.2	-49.5			
-5	-11.9	-13.6	-15.9	-19.0	-23.4	-29.7	-40.8	-67.2		
-4	-10.8	-12.1	-13.9	-16.5	-20.0	-25.1	-33.5	-52.1		
-3	-10.0	-10.9	-12.4	-14.4	-17.2	-21.2	-27.5	-40.1		
-2	-9.5	-10.1	-11.1	-12.7	-14.9	-18.0	-22.6	-31.0	-57.5	
-1	-9.2	-9.5	-10.2	-11.3	-13.0	-15.3	-18.7	-24.2	-37.0	
0	-9.1	-9.2	-9.6	-10.3	-11.5	-13.2	-15.7	-19.2	-25.2	
1	-9.2	-9.1	-9.2	-9.6	-10.4	-11.6	-13.3	-15.6	-18.6	-21.6
2	-9.5	-9.2	-9.1	-9.3	-9.7	-10.4	-11.6	-13.0	-14.7	-15.8
3	-10.0	-9.4	-9.2	-9.1	-9.3	-9.7	-10.3	-11.2	-12.1	-12.7
4	-10.8	-9.9	-9.4	-9.2	-9.1	-9.2	-9.6	-10.0	-10.5	-10.8
5	-11.9	-10.7	-9.9	-9.4	-9.2	-9.1	-9.2	-9.4	-9.6	-9.7
6	-13.3	-11.7	-10.7	-9.9	-9.5	-9.2	-9.1	-9.1	-9.2	-9.2
7	-15.1	-13.1	-11.7	-10.8	-10.1	-9.6	-9.4	-9.3	-9.2	-9.2
8	-17.2	-14.9	-13.2	-11.9	-11.0	-10.4	-10.0	-9.7	-9.6	-9.6
9	-19.7	-17.0	-14.9	-13.4	-12.2	-11.4	-10.9	-10.6	-10.5	-10.4
10	-22.6	-19.5	-17.0	-15.2	-13.8	-12.9	-12.2	-11.8	-11.7	-11.6
11	-25.9	-22.3	-19.5	-17.3	-15.7	-14.6	-13.8	-13.4	-13.2	-13.2
12	-29.6	-25.6	-22.4	-19.9	-18.0	-16.7	-15.8	-15.3	-15.1	-15.1
13	-33.8	-29.3	-25.7	-22.8	-20.7	-19.2	-18.1	-17.6	-17.4	-17.4
14	-38.4	-33.4	-29.3	-26.1	-23.7	-22.0	-20.8	-20.2	-20.0	-20.0
15	-43.4	-37.9	-33.4	-29.8	-27.1	-25.1	-23.8	-23.1	-23.0	-23.0
16	-48.9	-42.9	-37.9	-33.9	-30.8	-28.6	-27.2	-26.4	-26.2	-26.4
17	-54.8	-48.3	-42.9	-38.4	-35.0	-32.5	-30.9	-30.1	-29.9	-30.0
18	-61.2	-54.2	-48.2	-43.3	-39.5	-36.7	-35.0	-34.1	-33.9	-34.1
19		-60.6	-54.1	-48.6	-44.4	-41.3	-39.4	-38.4	-38.2	-38.4
20		-67.4	-60.3	-54.3	-49.7	-46.3	-44.1	-43.1	-42.9	-43.2
21			-67.0	-60.5	-55.3	-51.6	-49.3	-48.1	-47.9	-48.3
22				-67.0	-61.4	-57.4	-54.8	-53.5	-53.3	-53.7
23					-67.9	-63.4	-60.6	-59.2	-59.1	-59.5
24								-65.3	-65.2	-65.7

Table 2. Location of Left-Side Peak, η_L (deg)

	ANGLE BETWEEN PLANES, ξ (DEG)									
Δ(DEG)	0	10	20	30	40	50	60	70	80	90
-18	-6.5									
-17	-6.5	-7.4								
-16	-6.5	-7.4	-8.9							
-15	-6.5	-7.3	-8.7							
-14	-6.5	-7.3	-8.5	-10.5						
-13	-6.5	-7.2	-8.4	-10.1						
-12	-6.5	-7.1	-8.2	-9.8	-12.1					
-11	-6.5	-7.1	-8.0	-9.4	-11.5					
-10	-6.5	-7.1	-7.9	-9.0	-10.8	-13.7				
-9	-6.5	-7.0	-7.7	-8.7	-10.3	-12.7				
-8	-6.5	-7.0	-7.6	-8.4	-9.7	-11.7				
-7	-6.5	-6.9	-7.4	-8.1	-9.1	-10.8	-13.9			
-6	-6.5	-6.9	-7.3	-7.8	-8.6	-10.0	-12.5			
-5	-6.5	-6.8	-7.2	-7.6	-8.2	-9.2	-11.1	-15.3		
-4	-6.5	-6.8	-7.1	-7.3	-7.8	-8.4	-9.8	-13.0		
-3	-6.5	-6.7	-7.0	-7.1	-7.4	-7.8	-8.7	-10.8		
-2	-6.5	-6.7	-6.8	-6.9	-7.0	-7.2	-7.6	-8.8	-13.2	
-1	-6.5	-6.6	-6.7	-6.7	-6.7	-6.7	-6.8	-7.2	-8.9	
0	-6.5	-6.5	-6.5	-6.5	-6.4	-6.2	-6.0	-5.9	-5.8	
1	-6.5	-6.4	-6.4	-6.3	-6.1	-5.9	-5.5	-5.0	-4.0	0.0
2	-6.5	-6.3	-6.2	-6.0	-5.8	-5.5	-5.0	-4.3	-3.1	0.0
3	-6.5	-6.2	-5.9	-5.7	-5.5	-5.2	-4.6	-3.7	-2.5	0.0
4	-6.5	-6.1	-5.7	-5.4	-5.1	-4.8	-4.1	-3.3	-2.0	0.0
5	-6.5	-6.1	-5.6	-5.1	-4.6	-4.2	-3.7	-2.9	-1.7	0.0
6	-6.5	-6.0	-5.5	-4.9	-4.3	-3.7	-3.0	-2.4	-1.4	0.0
7	-6.5	-6.0	-5.4	-4.8	-4.1	-3.4	-2.6	-1.8	-0.9	0.0
8	-6.5	-6.0	-5.3	-4.6	-3.9	-3.2	-2.4	-1.5	-0.7	0.0
9	-6.5	-5.9	-5.3	-4.6	-3.8	-3.0	-2.2	-1.3	-0.5	0.0
10	-6.5	-5.9	-5.3	-4.5	-3.7	-2.9	-2.0	-1.1	-0.4	0.0
11	-6.5	-5.9	-5.3	-4.5	-3.7	-2.8	-1.9	-1.0	-0.3	0.0
12	-6.5	-5.9	-5.3	-4.5	-3.6	-2.8	-1.9	-1.0	-0.2	0.0
13	-6.5	-5.9	-5.3	-4.5	-3.7	-2.8	-1.8	-0.9	-0.1	0.0
14	-6.5	-5.9	-5.3	-4.6	-3.7	-2.8	-1.8	-0.8	-0.1	0.0
15	-6.5	-6.0	-5.4	-4.6	-3.7	-2.8	-1.8	-0.8	0.0	0.0
16	-6.5	-6.0	-5.4	-4.7	-3.8	-2.8	-1.8	-0.8	0.0	0.0
17	-6.5	-6.0	-5.5	-4.8	-3.9	-2.9	-1.8	-0.8	0.1	0.0
18	-6.5	-6.1	-5.6	-4.9	-4.0	-2.9	-1.8	-0.8	0.1	0.0
19		-6.1	-5.7	-5.0	-4.1	-3.0	-1.8	-0.7	0.1	0.0
20		-6.1	-5.8	-5.1	-4.2	-3.1	-1.8	-0.7	0.2	0.0
21			-5.9	-5.2	-4.3	-3.1	-1.8	-0.7	0.3	0.0
22				-5.4	-4.4	-3.2	-1.9	-0.7	0.3	0.0
23					-4.5	-3.3	-1.9	-0.7	0.3	0.0
24								-0.7	0.3	0.0

can write the location of the peak on the right side of the ground line as

$$\eta_R(\Delta,\xi) = -\eta_L(-\Delta,\xi) \tag{29}$$

For the peaks we also have the symmetry

$$\eta_R(\Delta,\xi) = -\eta_L(\Delta, -\xi) \tag{30}$$

Note that nothing changes if $\xi \pm 180°$ is substituted for ξ. For the elevation difference channel we can use the above results by substituting either $\xi + 90°$ or $\xi - 90°$ for ξ.

In converting the azimuth location of either peak to Doppler frequency we can write for any η

$$f = f_{max} \cos(\alpha + \eta) \tag{31}$$

Note, however, that the left peak will generally be at a *higher* frequency than the right peak (as defined above) so that $f_R < f_L$ (at least for $\alpha > 0$). When $\alpha < \eta_L$ we get a foldover or wraparound effect that results in the spectrum being sharply truncated at f_{max}. In this case only the lower-frequency peak, namely the one at $f = f_{max} \cos(\alpha + \eta_R)$, will be relatively undistorted.

In the process of converting a power distribution in angle to a power distribution in frequency, we must also include the effect of the Jacobian. Thus the peak gains in Table 1 (in linear units) must be divided by $\sin(\alpha + \eta)$ where η is the corresponding entry in Table 2 (provided $\alpha + \xi > 0$.

3.8 Two Examples

Let us refer to the parameters of Figure 15, for which $\alpha = 10°$, $\beta = 0$, $\gamma = 10°$, $\delta = 0$, and $\omega = 22.5°$. Immediately we note that $\Delta = 10°$ and from (B-3) we have $\xi = 22.2°$. The parameters that were discussed in Section 3.7 are summarized in Table 3. The peak gain for the sum channel is defined as $G_n^2(\gamma-\beta)$, where $G_n(\ )$ is the one-way power of the antenna pattern, and the Jacobian is defined as $1/\sin(\alpha+\eta)$. The normalized Doppler is designated by f in Table 3. In the last column the "corrected gains" are referenced

Table 3. Summary of Example I

α=10°, β=0, γ=10°, δ=0, ω=22.5°

ξ=22.2°, ξ-90°=-67.8°, Δ=10°

Refer to Figure 15 for spectral plots

Channel	Feature	η	$\alpha+\eta$	f	Gain	Jacobian	Corrected Gain	Gain Rel. to Σ
sum	peak	0°	10.0°	.970	-13.0 dB	+7.6 dB	-5.4 dB	-
Az	null	4.1	14.1	.955				
	R-peak	8.1	18.1	.936	-33.2	+5.1	-28.1	-22.7 dB
	L-peak	-5.1	4.9	.981	-16.6	+10.8	-5.8	-0.4
El	null	-24.5	-14.5*					
	R-peak	1.3	11.3	.966	-11.9	+7.1	-4.8	+0.6
	L-peak				**			

*spectrum folds over for $\alpha + \eta < 0$

**peak is below -60 dB in Table 2

Note that "R-peak" appears at a lower frequency than "L-peak"

to the corrected gain in the sum channel. If we compare the results of Table 3 with Figure 15 we note that the location of the peaks and nulls is in excellent agreement, and the peak values of the various lobes agrees to within 1 dB.

As a second example we have arbitrarily selected $\alpha = 30°$, $\beta = 5°$, $\gamma = 10°$, $\delta = 15°$, and $\omega = 20°$. The results are summarized in Table 4 along with a plot of the "exact" sprectum. The agreement is again excellent as noted on the figure.

Table 4. Summary of Example II

α=30°, β=5°, γ=10°, δ=15° ω=20°

ξ=25.2°, ξ-90°= -64.8°, Δ=5°

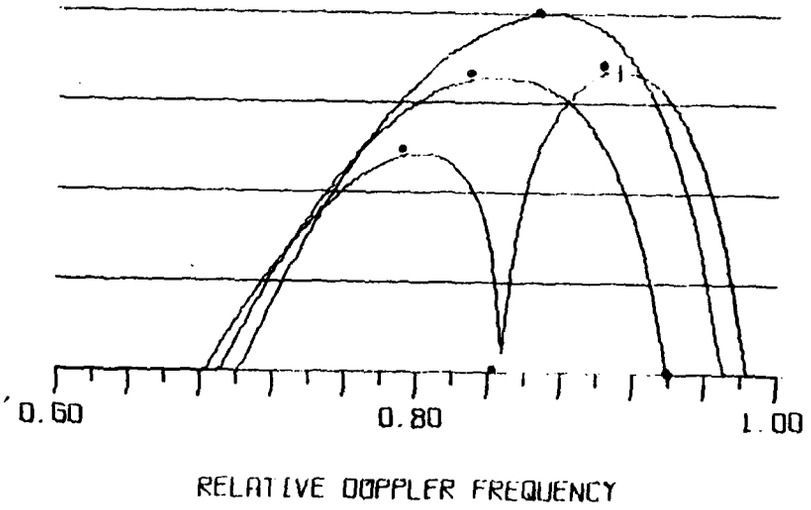

Channel	Feature	η	$\alpha+\eta$	f	Gain	Jacobian	Corrected Gain	Gain Rel. to Σ
sum	peak	0°	30.0°	.866	-3.0 dB	+3.0 dB	0.0 dB	--
Az	null	2.4	32.4	.842				
	R-peak	7.4	37.4	.791	-17.5	+2.2	-15.3	-15.3 dB
	L-peak	-5.3	24.7	.905	-9.6	+3.8	-5.8	-5.8
El	null	-10.6	19.4	.940				
	R-peak	3.3	33.3	.829	-9.3	+2.6	-6.7	-6.7
	L-peak	-13.2	16.8	.954	-54.0	+5.4	-48.6	-48.6

4. APPROXIMATING SPECTRA IN REAL TIME

As was concluded in Reference 2 (Section 4.6) one cannot implement the "exact" computation of the clutter spectra in real time, at least in a practical sense. One is forced to use some approximation technique. In this section we discuss one possibility that is based on describing the clutter spectra by a few parameters that are functions of the engagement geometry.

4.1 Description of Method

In the format of the plots in Figure 4 through 23, all spectra are composed of either a single lobe or two adjacent lobes where the lobes are either distorted parabolas or triangular-shaped functions. For any of the lobes we have decided to implement the parametric description that is diagramed in Figure 26. First of all, a reference level (base) is established that is, say, 40 dB below the sum channel peak. On the log-scale of the figure a second level is established that is midway between the lobe peak and the reference base. Five normalized frequencies can then be determined, f_1 through f_5 for Points 1 through 5, respectively, in Figure 26. The sixth parameter in Figure 26 is the peak height. A seventh parameter, as shown in Figure 27, describes the shape of the lobe. To reconstruct the spectral lobe in the format of Figure 26, a straight line is drawn between Points 1 and 2. Between Points 2 and 3 either a straight line (TYPE = 0) or a parabola with zero slope at Point 3 (TYPE > 0) is drawn. Between Points 3 and 4 either a straight line (TYPE $\leq$ 1) or a parabola with zero slope at Point 3 (TYPE = 2) is drawn. A straight line is drawn between Points 4 and 5.

4.2 Application to Specific System

For the system based on the antenna patterns in Section 3.2 we have determined the spectral parameters for all combinations of α = 0, 10°, 20°, 30° and ω = -45° to 45° in steps of 11.25° (in all cases $\beta = \delta = 0$ and γ = 10°). The results are shown in Figures 28 through 59, where the a. figure designates the "exact" case and the b. figure designates the approximate one. The agreement is generally within 1 dB throughout the 40 dB range for all cases. The parameters are summarized in Tables 5 through 8. All power values

(text continues on Page 49)

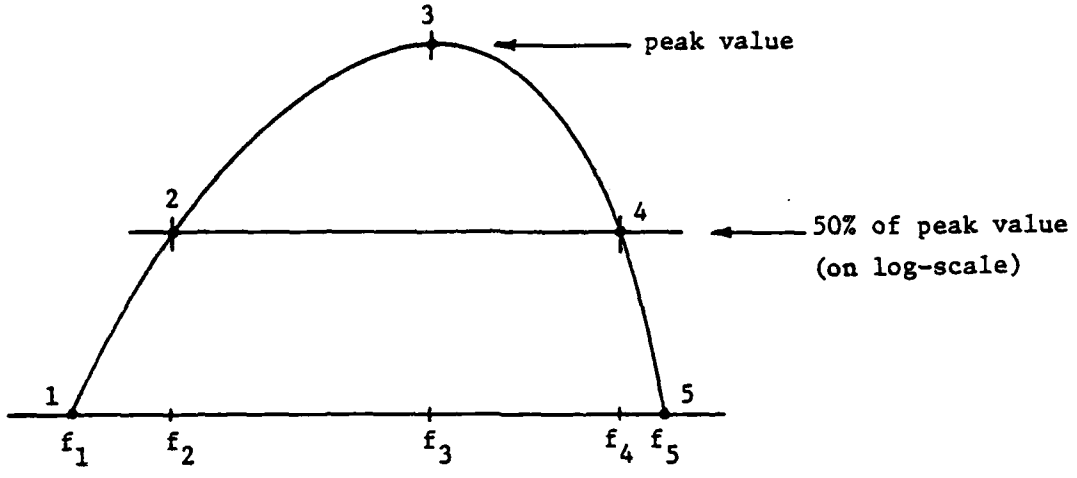

Figure 26. Determination of Six of the Parameters that Describe Spectral Lobe

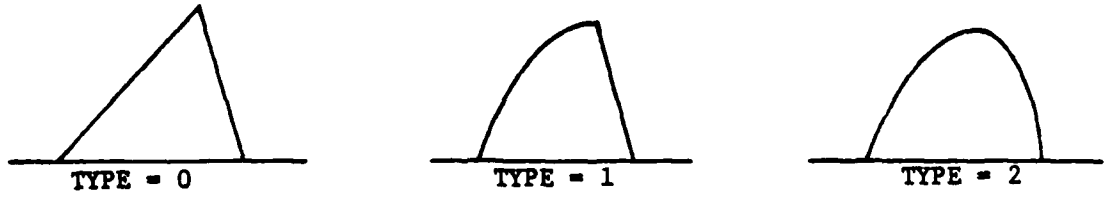

Figure 27. Three Types of Lobe Shapes

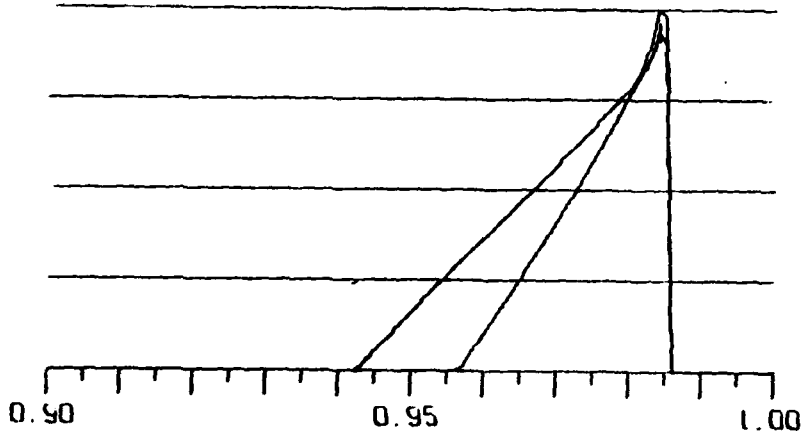

Figure 28a. Clutter Spectra for $\alpha = 0$, $\omega = -45°$

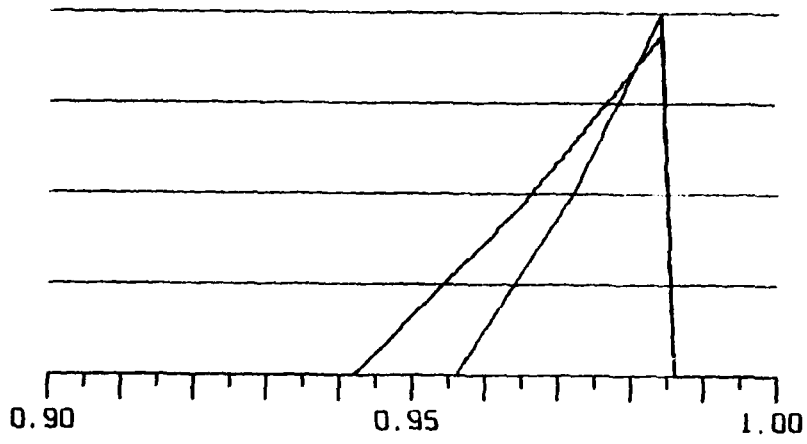

Figure 28b. Approximation to Figure 28a

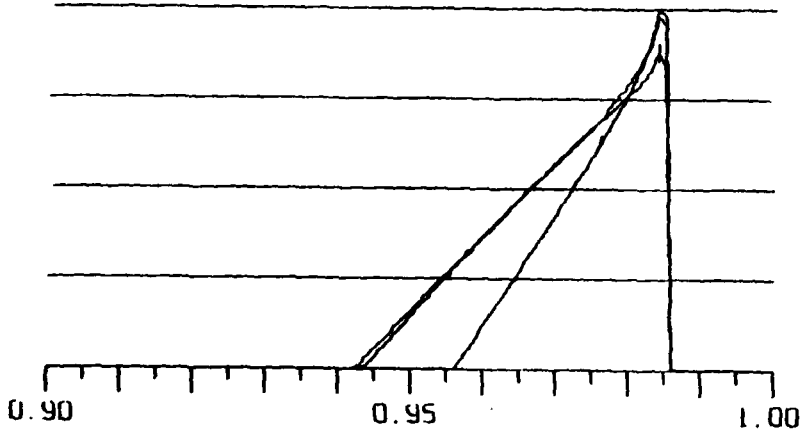

Figure 29a. Clutter Spectra for $\alpha = 0$, $\omega = 33.75°$

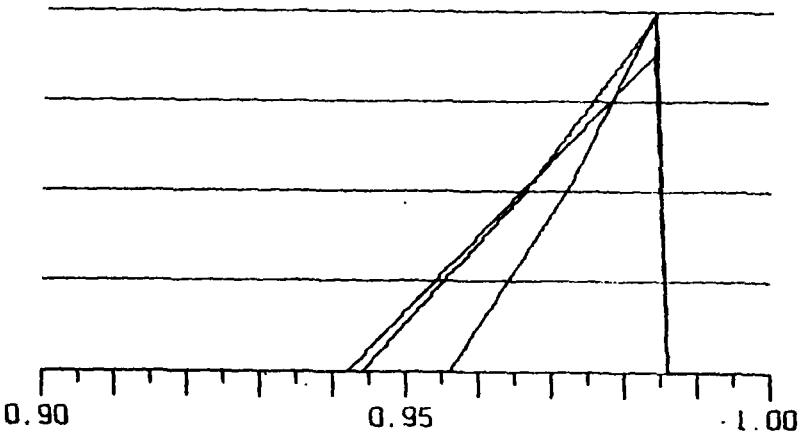

Figure 29b. Approximation to Figure 29a

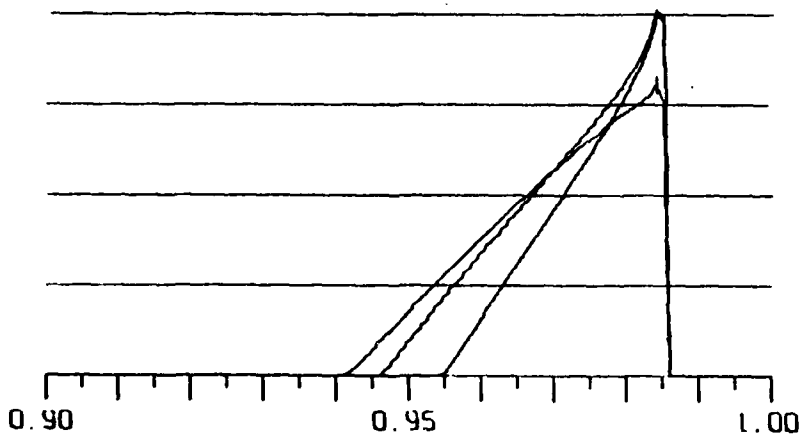

Figure 30a. Clutter Spectra for $\alpha = 0$, $\omega = -22.5°$

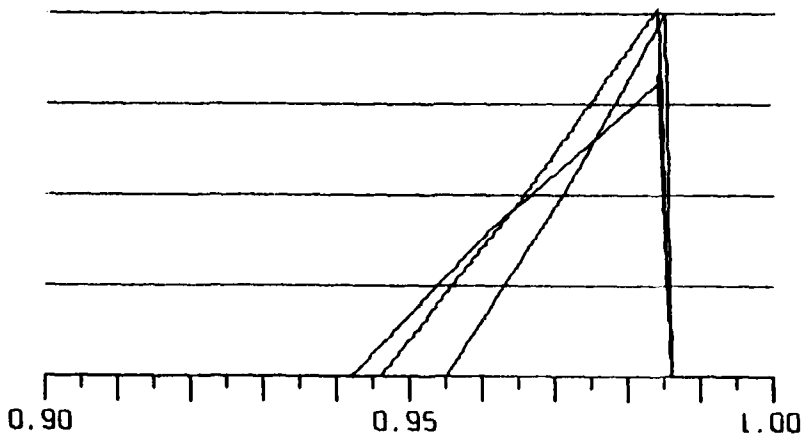

Figure 30b. Approximation to Figure 30a

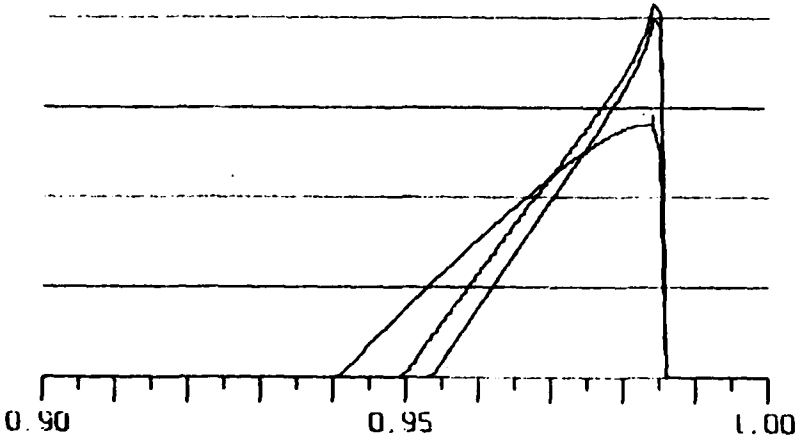

Figure 31a. Clutter Spectra for $\alpha = 0$, $\omega = -11.25°$

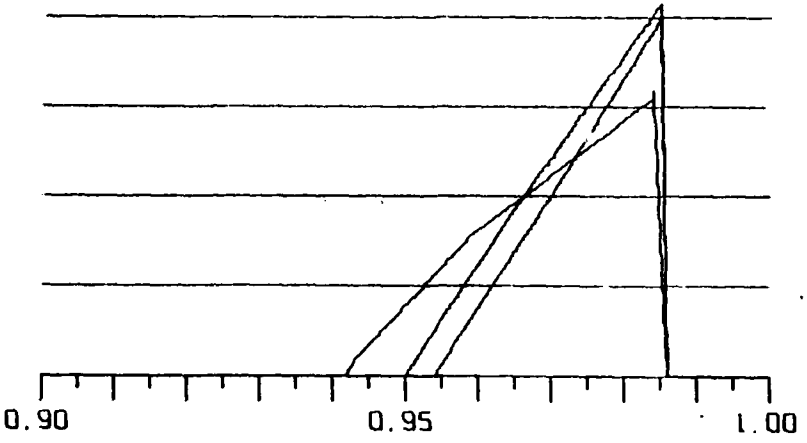

Figure 31b. Approximation to Figure 31a

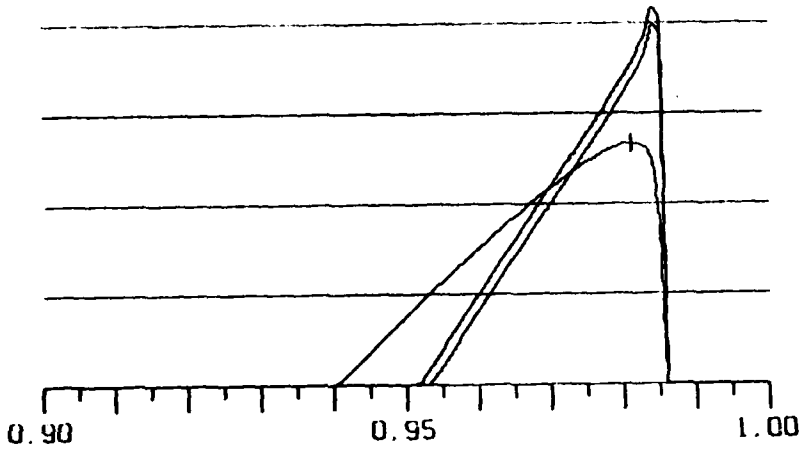

Figure 32a. Clutter Spectra for $\alpha = 0$, $\omega = 0$

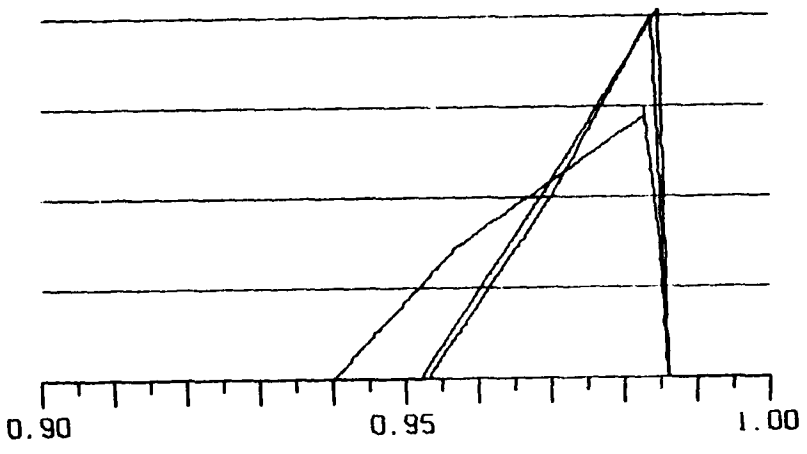

Figure 32b. Approximation to Figure 32a

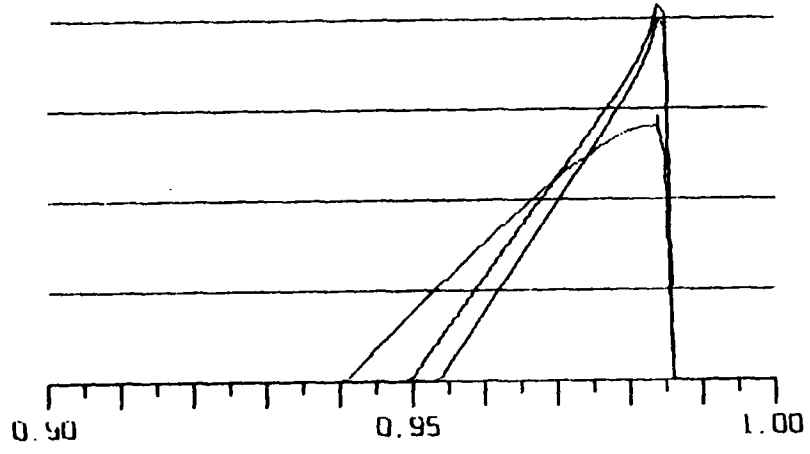

Figure 33a. Clutter Spectra for $\alpha = 0$, $\omega = 11.25°$

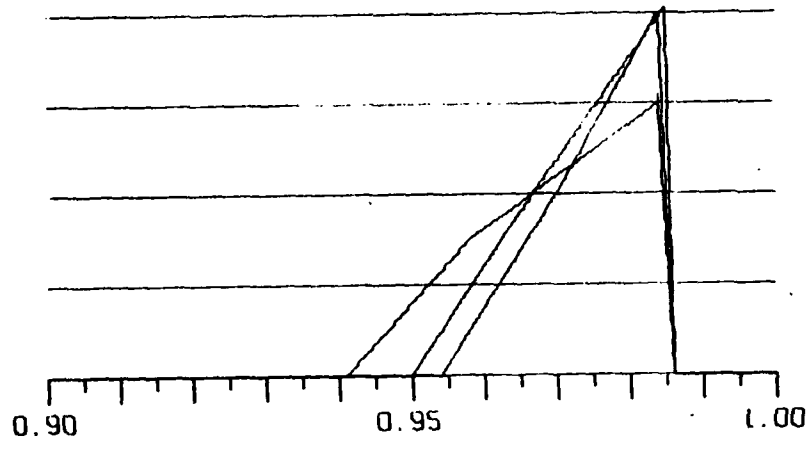

Figure 32b. Approximation to Figure 33a

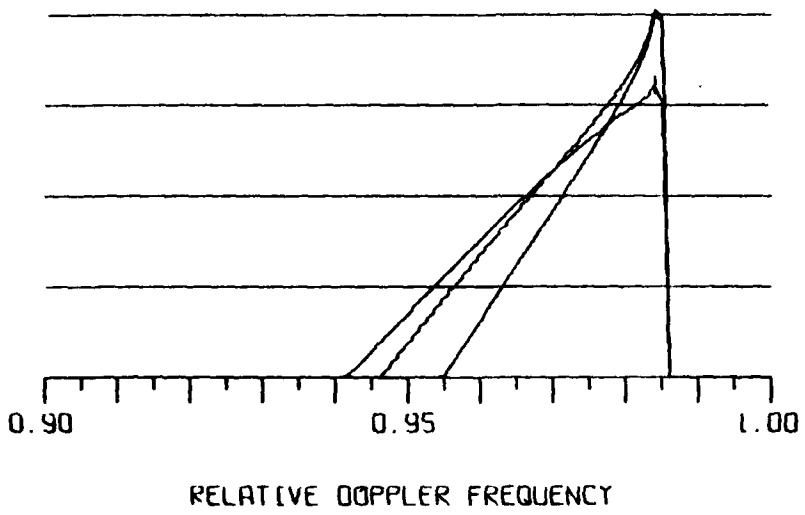

Figure 34a. Clutter Spectra for $\alpha = 0$, $\omega = 22.5°$

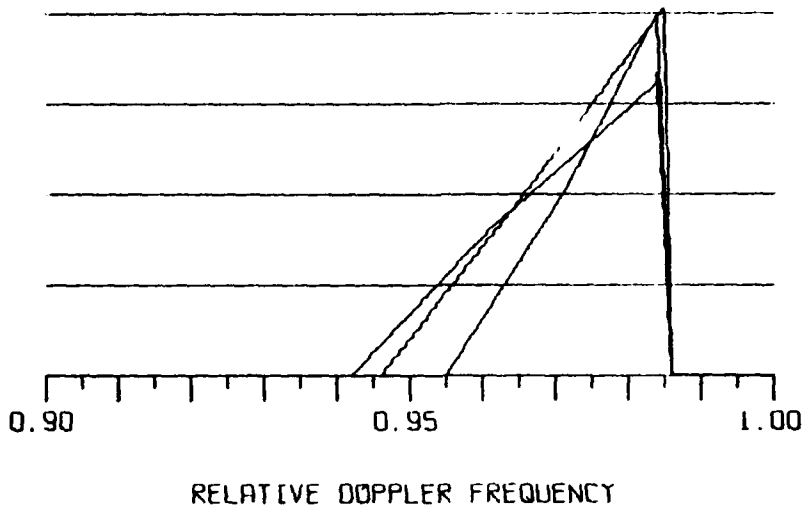

Figure 34b. Approximation to Figure 34a

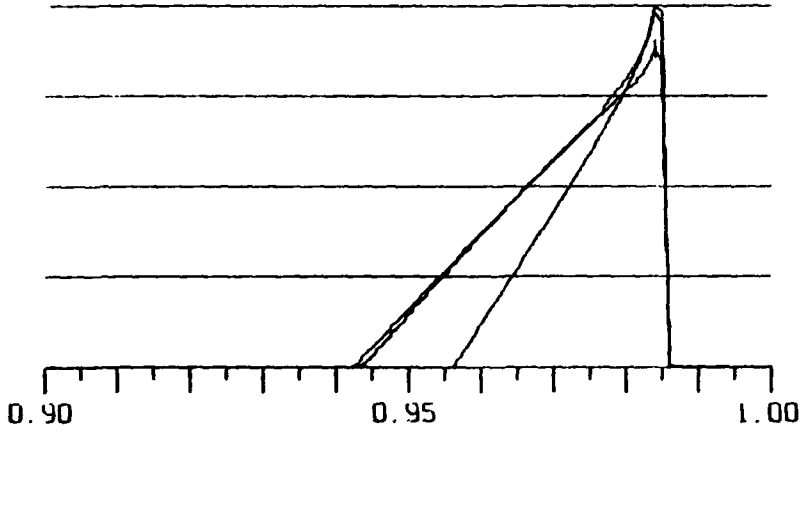

Figure 35a. Clutter Spectra for $\alpha = 0$, $\omega = 33.75°$

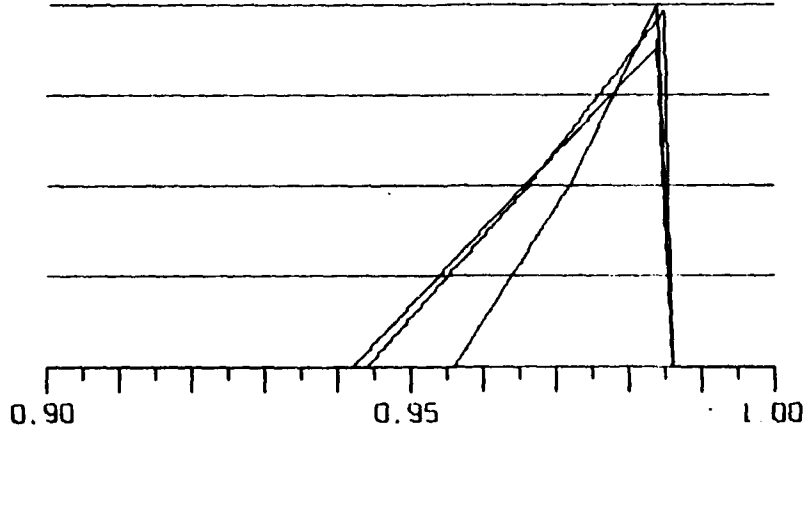

Figure 35b. Approximation to Figure 35a

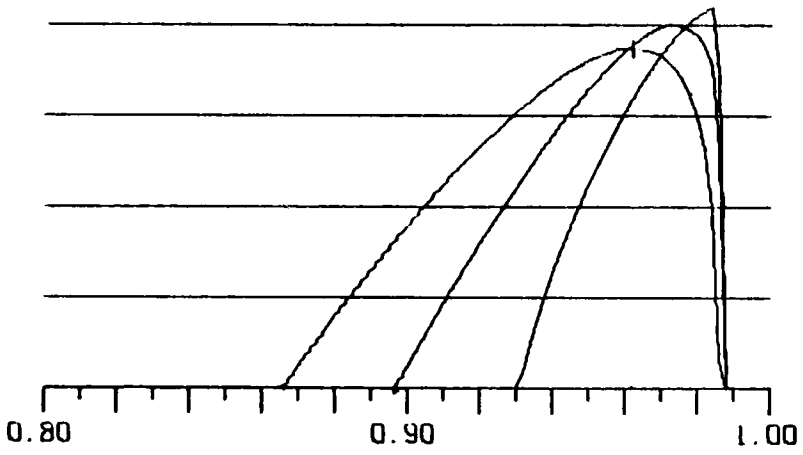

Figure 36a. Clutter Spectra for $\alpha = 10°$, $\omega = -45°$

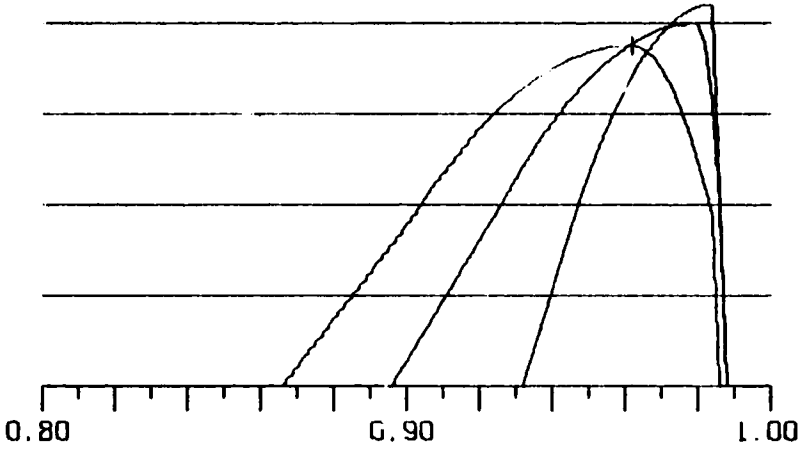

Figure 36b. Approximation to Figure 36a

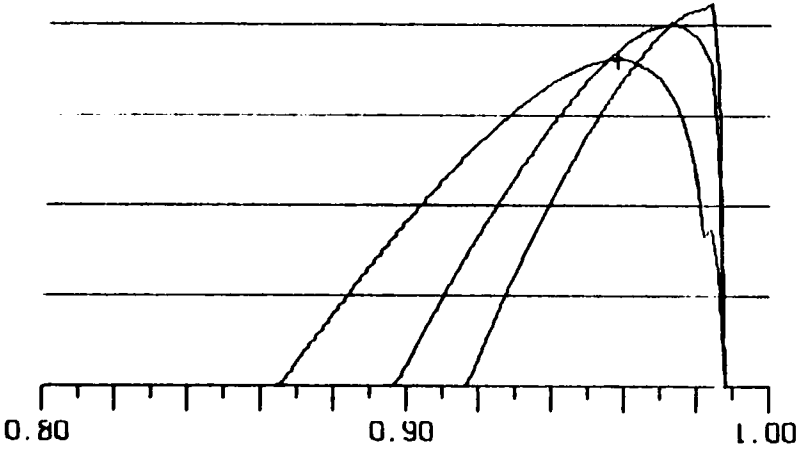

Figure 37a. Clutter Spectra for $\alpha = 10°$, $\omega = -33.75°$

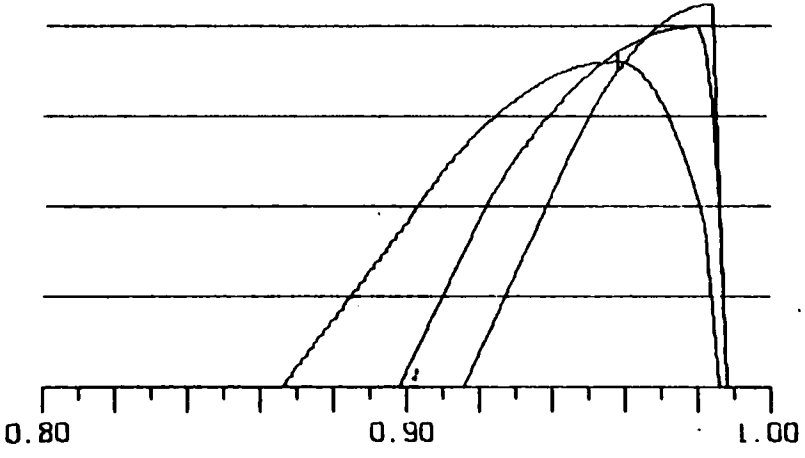

Figure 37b. Approximation to Figure 37a

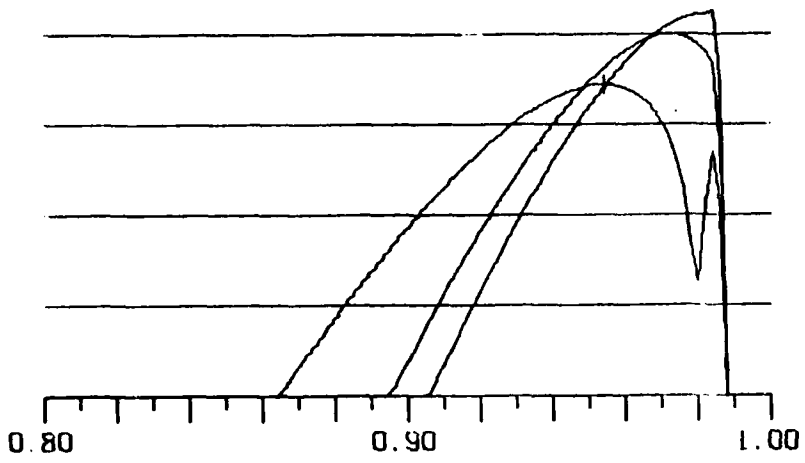

Figure 38a. Clutter Spectra for $\alpha = 10°$, $\omega = -22.5°$

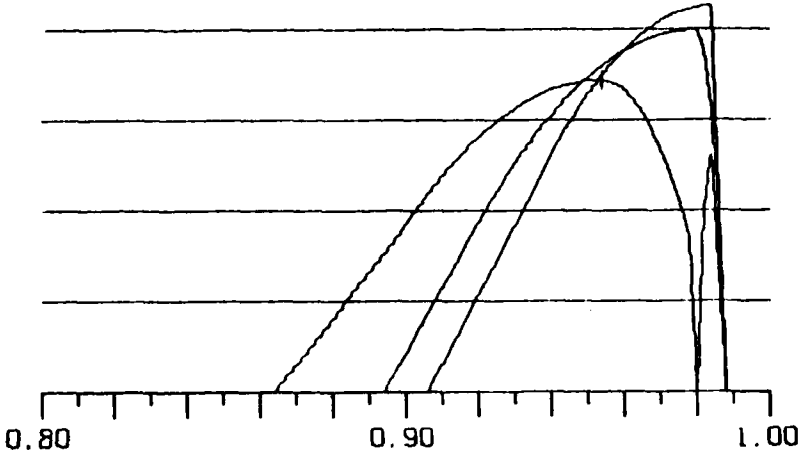

Figure 38b. Approximation to Figure 38a

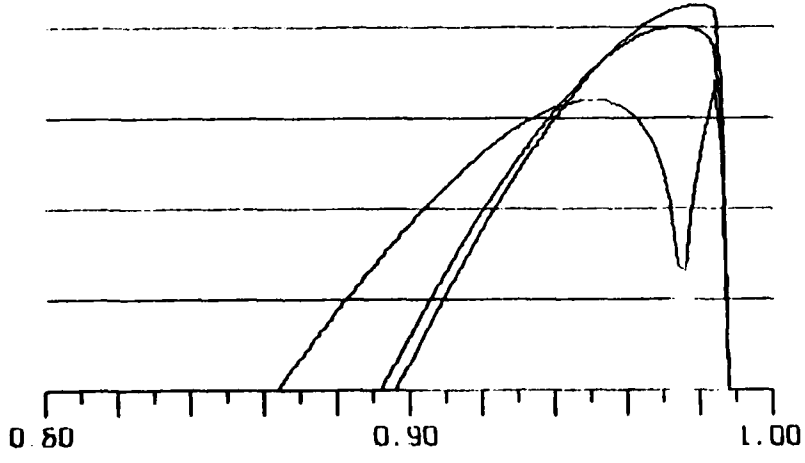

Figure 39a. Clutter Spectra for $\alpha = 10°$, $\omega = -11.25°$

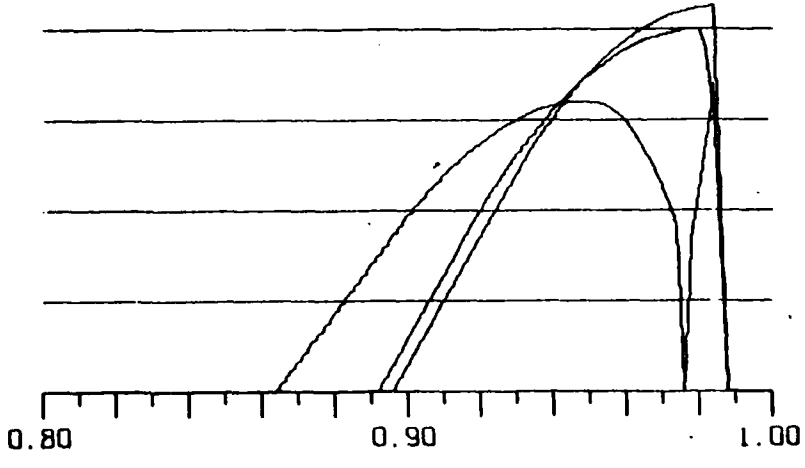

Figure 39b. Approximation to Figure 39a

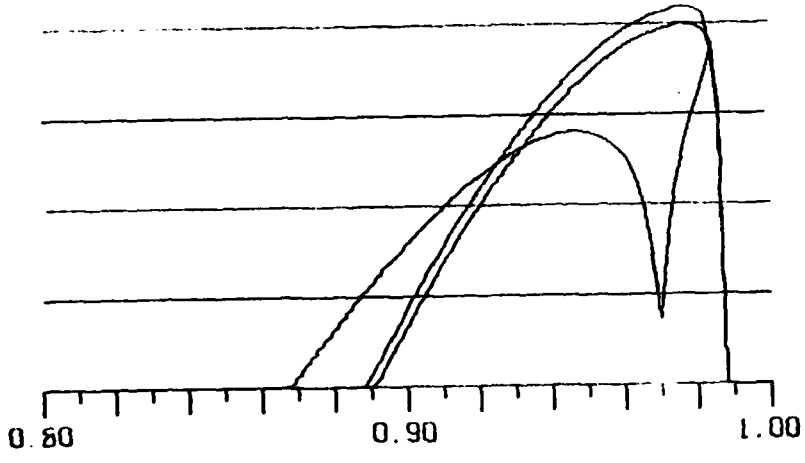

Figure 40a. Clutter Spectra for $\alpha = 10°$, $\omega = 0$

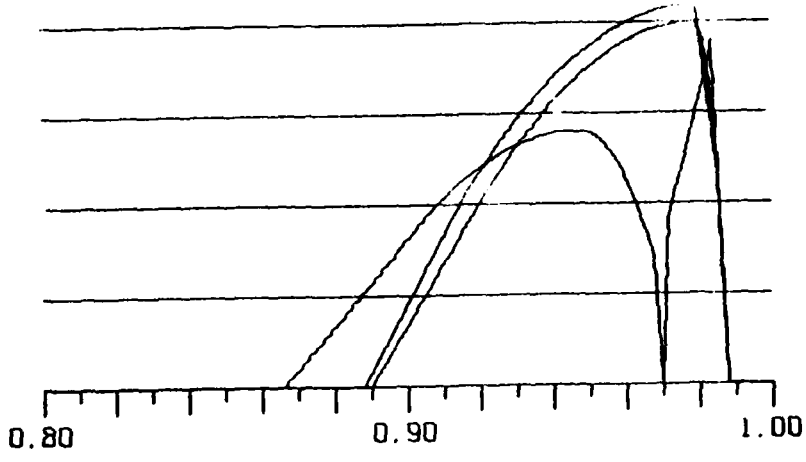

Figure 40b. Approximation to Figure 40a

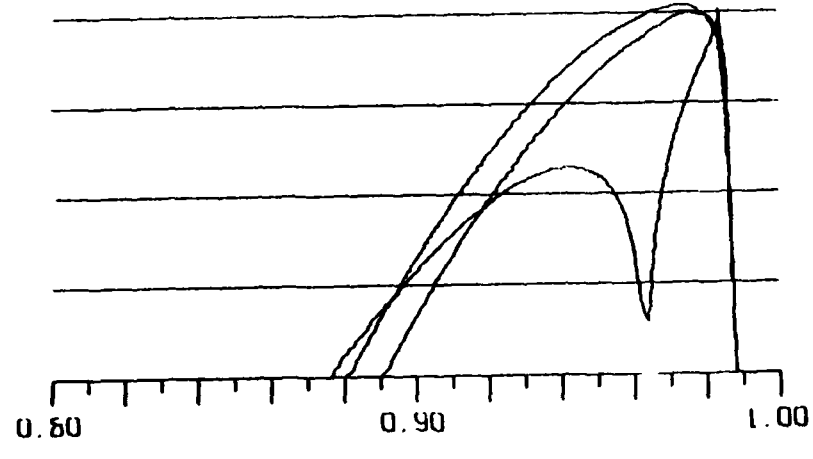

Figure 41a. Clutter Spectra for $\alpha = 10°$, $\omega = 11.25°$

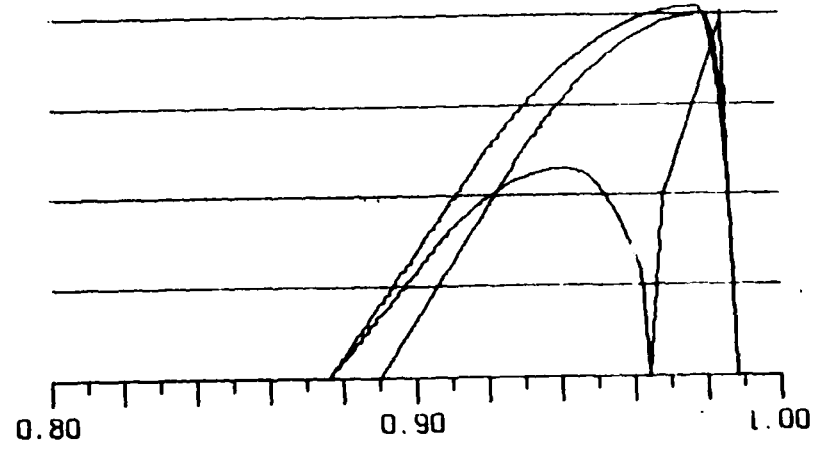

Figure 41b. Approximation to Figure 41a

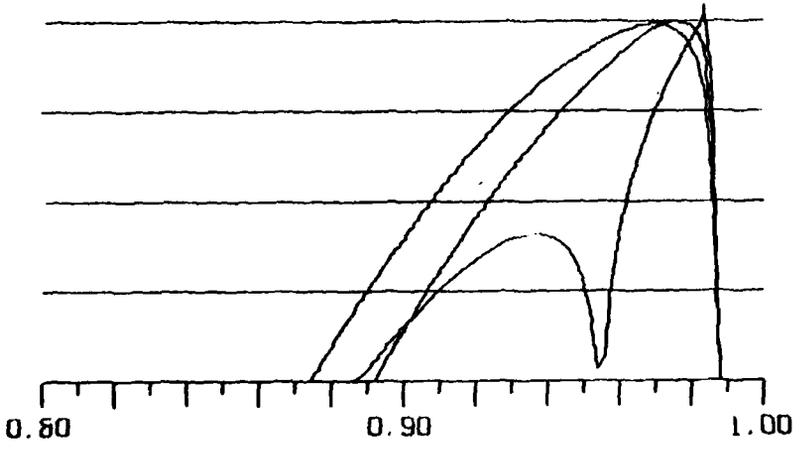

Figure 42a. Clutter Spectra for $\alpha = 10°$, $\omega = 22.5°$

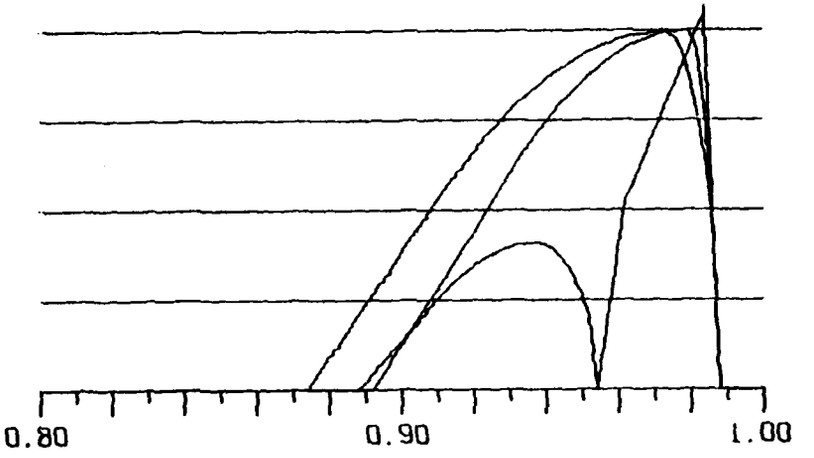

Figure 42b. Approximation to Figure 42a

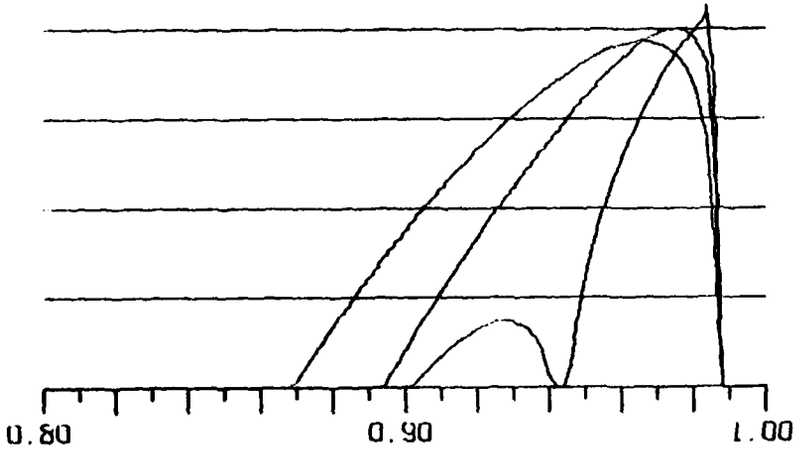

Figure 43a. Clutter Spectra for $\alpha = 10°$, $\omega = 33.75°$

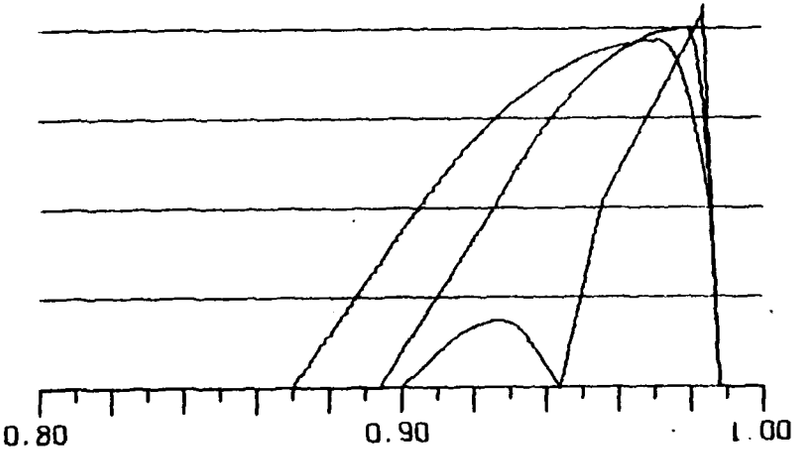

Figure 43b. Approximation to Figure 43a

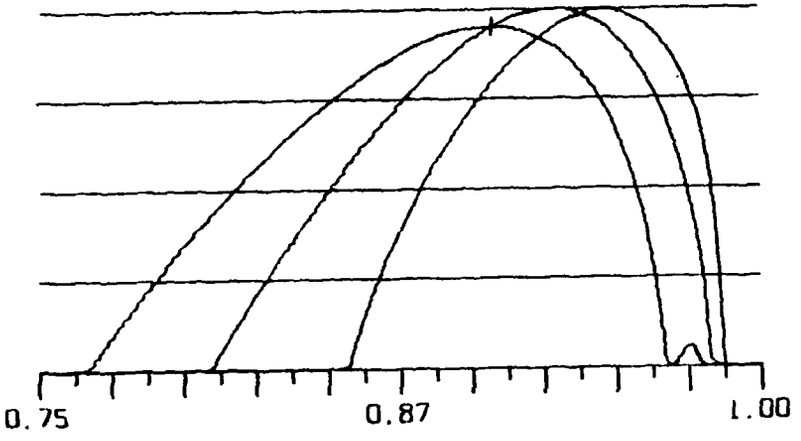

Figure 44a. Clutter Spectra for $\alpha = 20°$, $\omega = -45°$

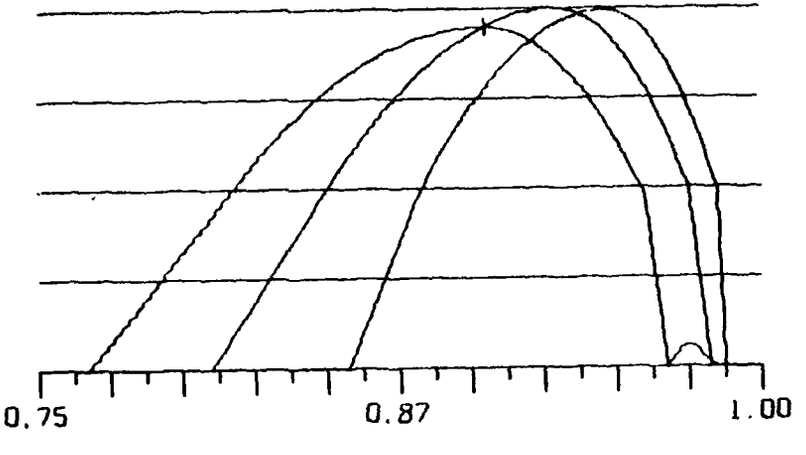

Figure 44b. Approximation to Figure 44a

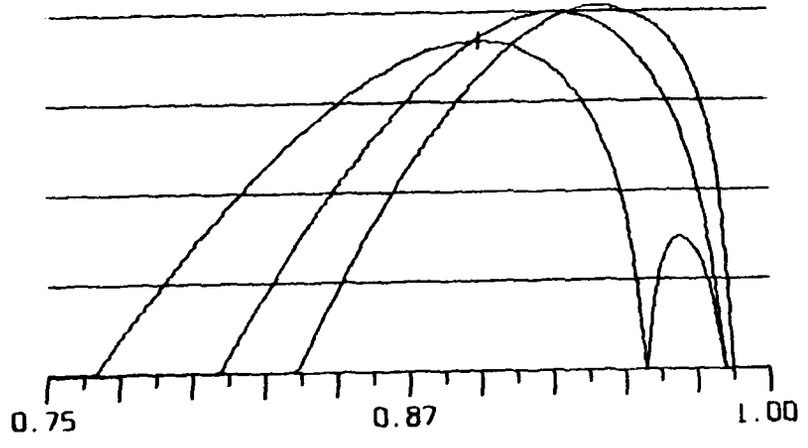

Figure 45a. Clutter Spectra for $\alpha = 20°$, $\omega = 33.75°$

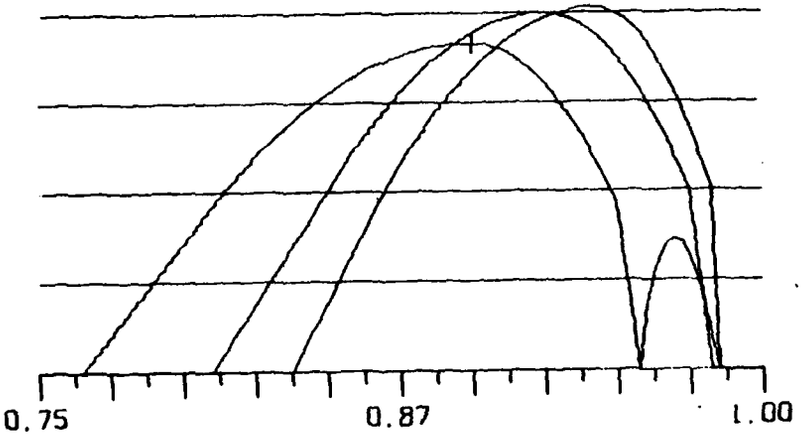

Figure 45b. Approximation to Figure 45a

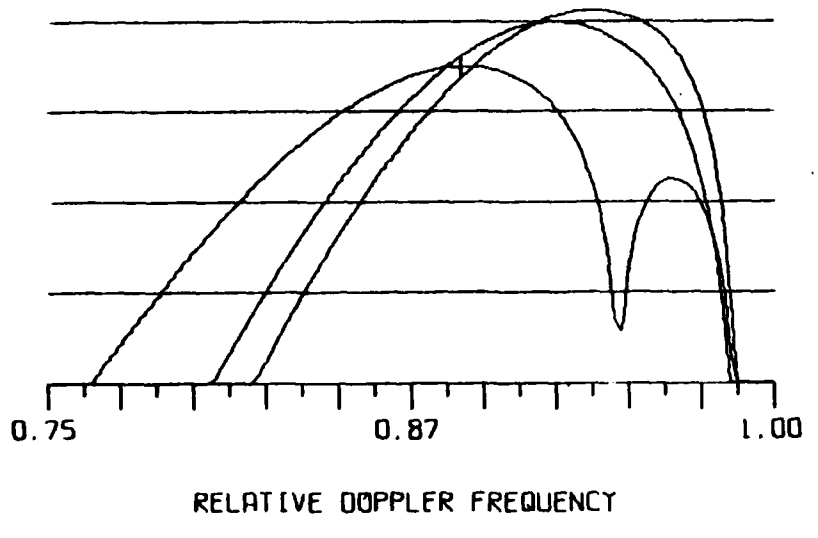

Figure 46a. Clutter Spectra for $\alpha = 20°$, $\omega = -22.5°$

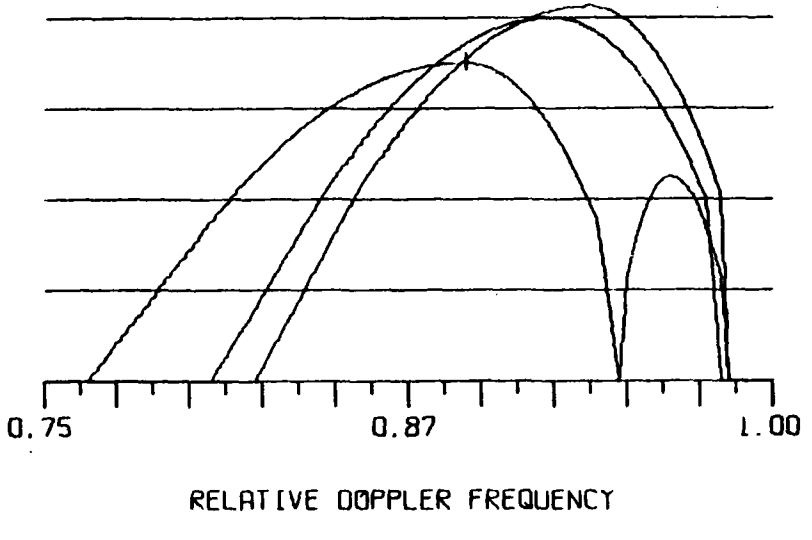

Figure 46b. Approximation to Figure 46a

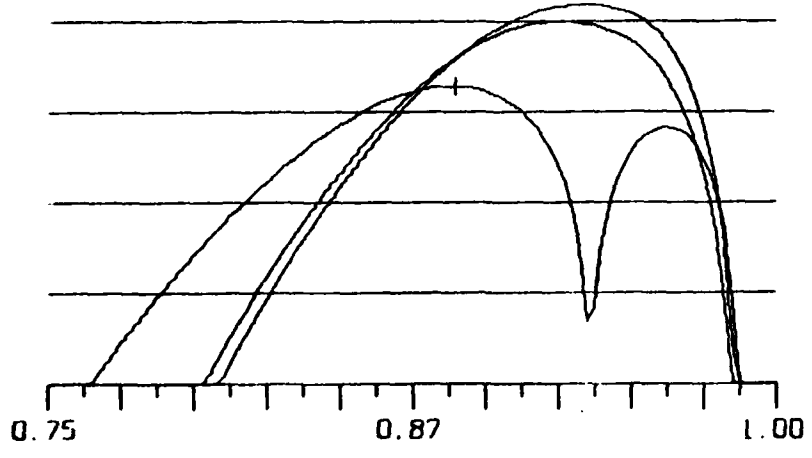

Figure 47a. Clutter Spectra for $\alpha = 20°$, $\omega = -11.25°$

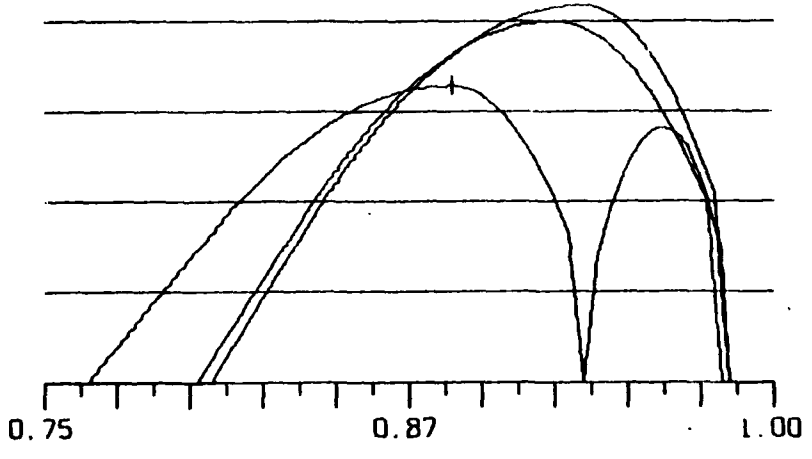

Figure 47b. Approximation to Figure 47a

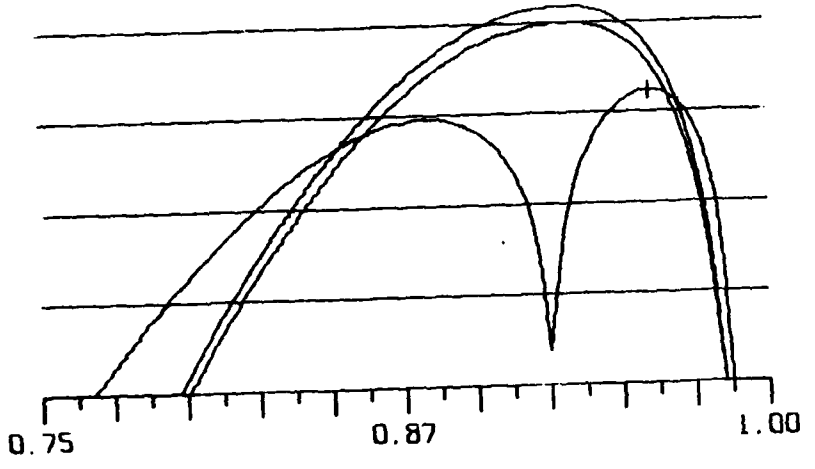

Figure 48a. Clutter Spectra for $\alpha = 20°$, $\omega = 0$

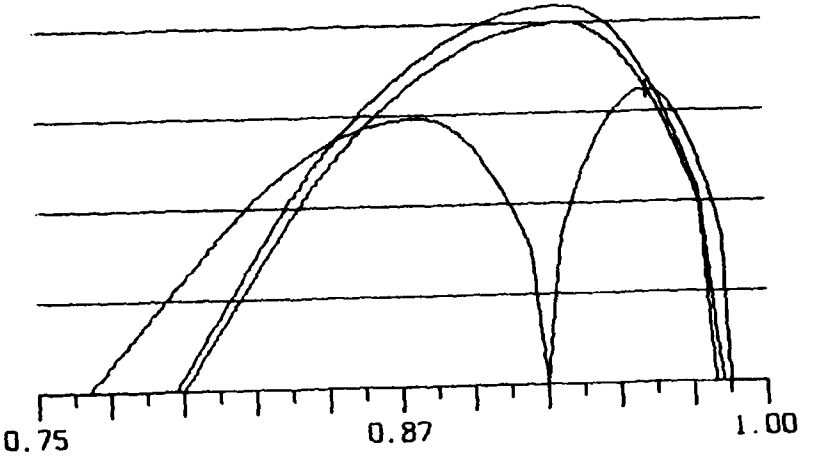

Figure 48b. Approximation to Figure 48a

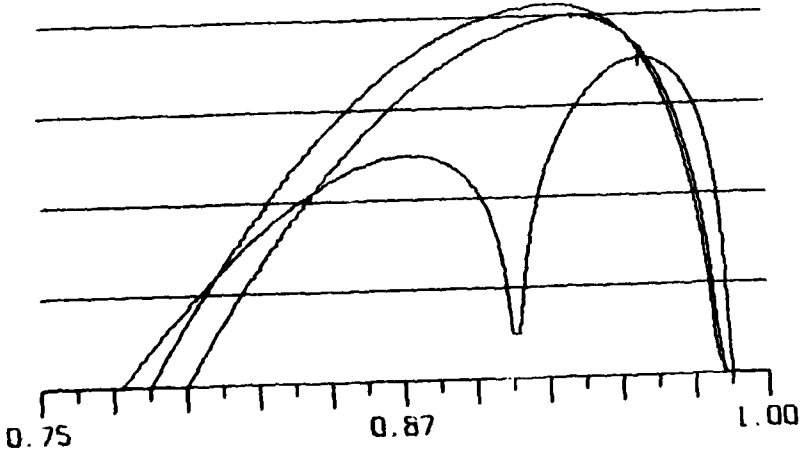

Figure 49a. Clutter Spectra for $\alpha = 20°$, $\omega = 11.25°$

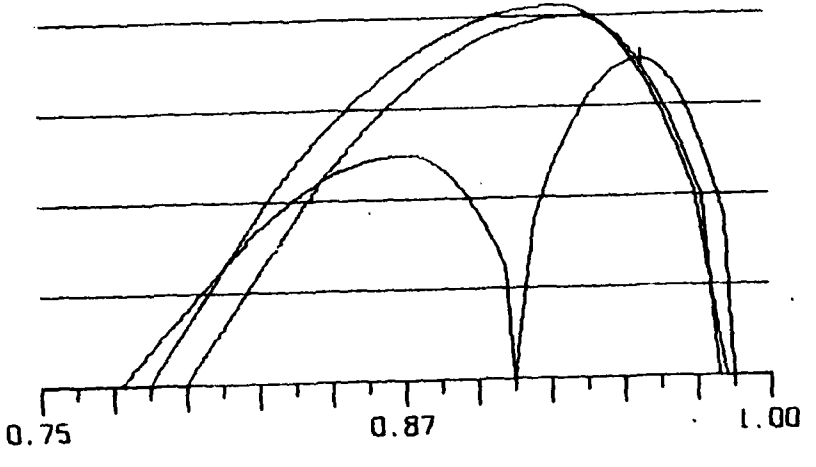

Figure 49b. Approximation to Figure 49a

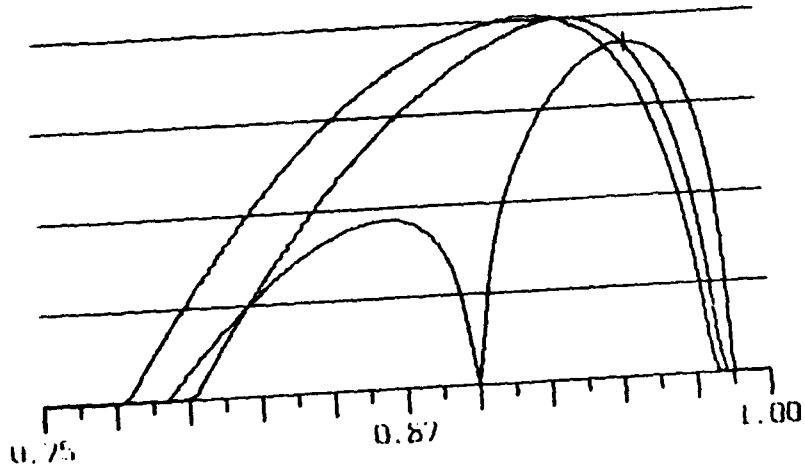

Figure 50a. Clutter Spectra for $\alpha = 20°$, $\omega = 22.5°$

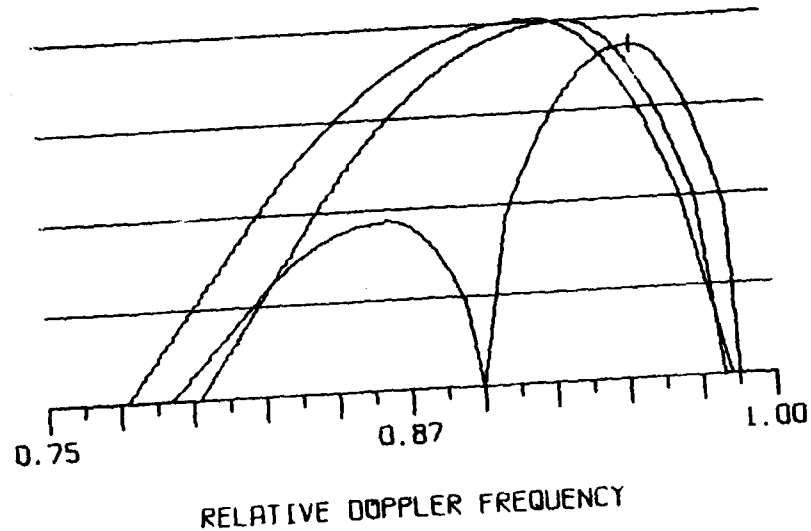

Figure 50b. Approximation to Figure 50a

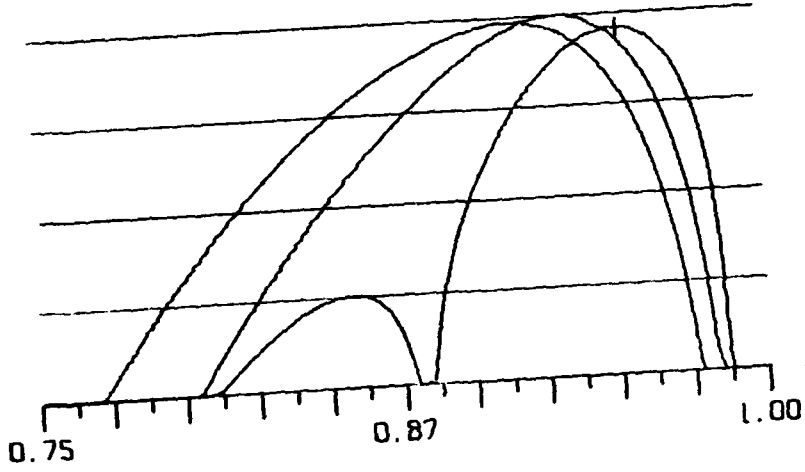

Figure 51a. Clutter Spectra for $\alpha = 20°$, $\omega = 33.75°$

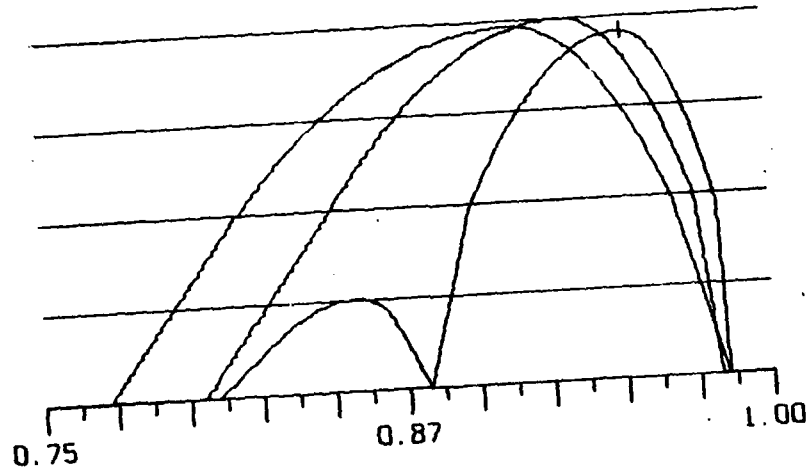

Figure 51b. Approximation to Figure 51a

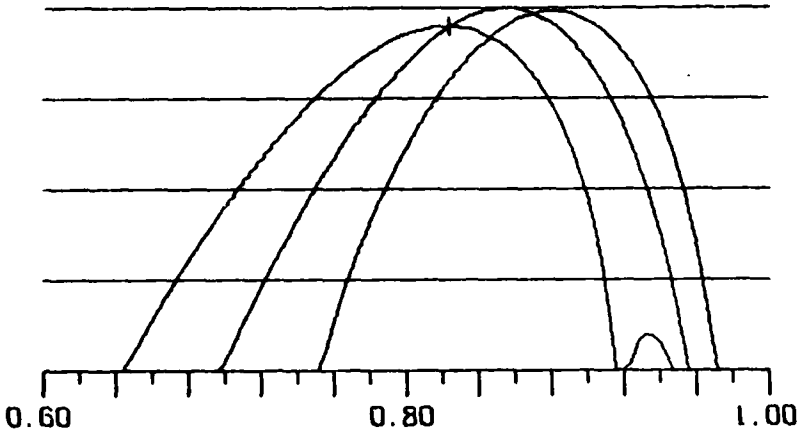

Figure 52a. Clutter Spectra for $\alpha = 30°$, $\omega = -45°$

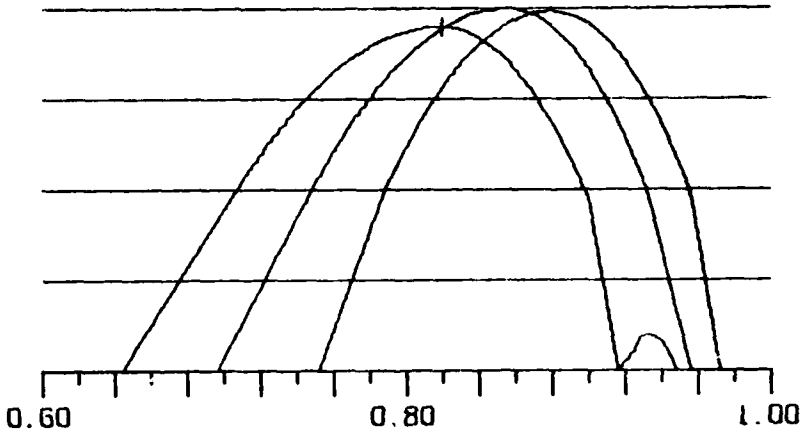

Figure 52b. Approximation to Figure 52a

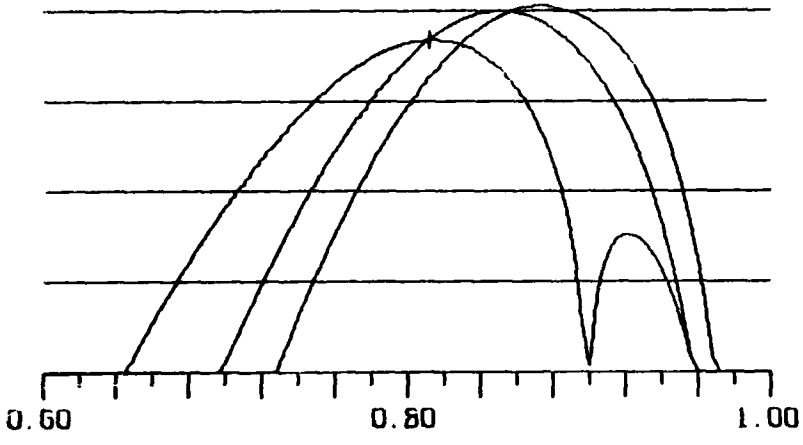

Figure 53a. Clutter Spectra for $\alpha = 30°$, $\omega = -33.75°$

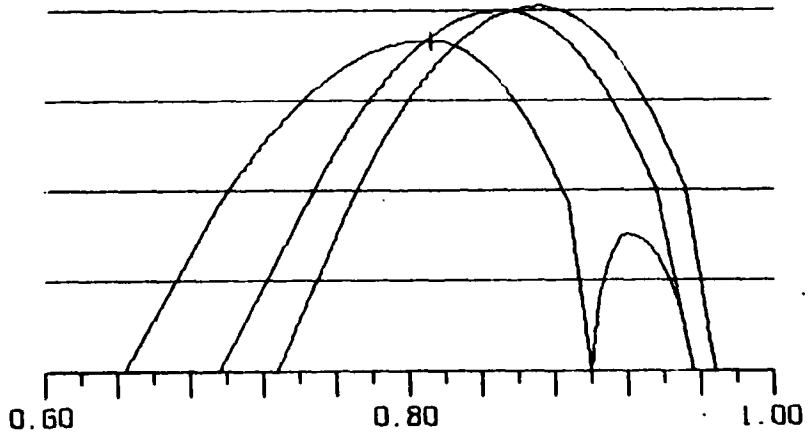

Figure 53b. Approximation to Figure 53a

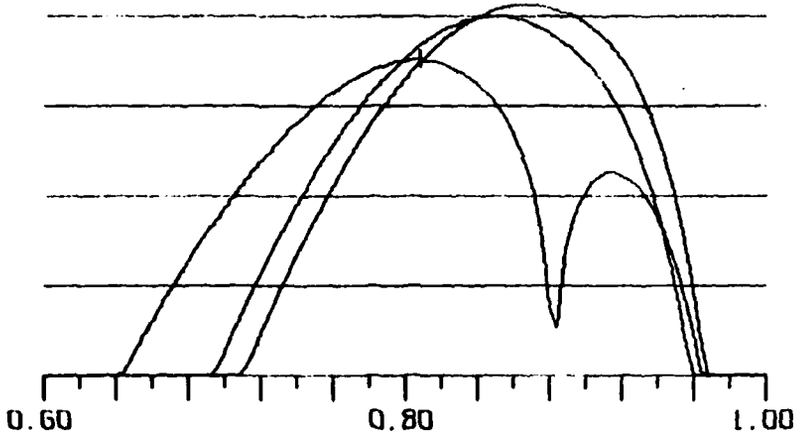

Figure 54a. Clutter Spectra for $\alpha = 30°$, $\omega = -22.5°$

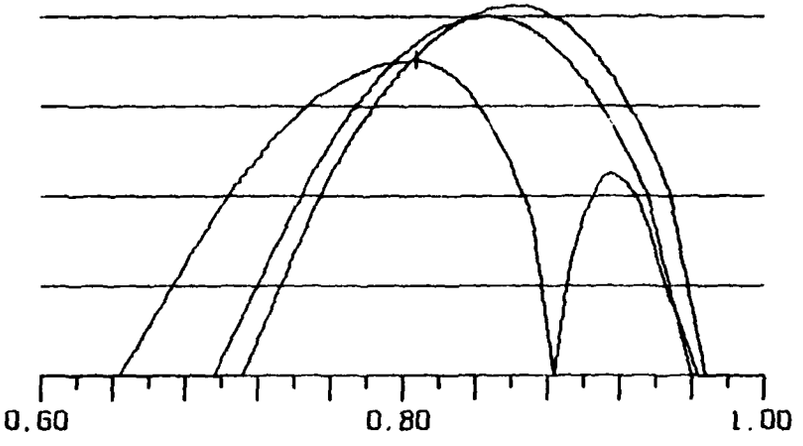

Figure 54b. Approximation to Figure 54a

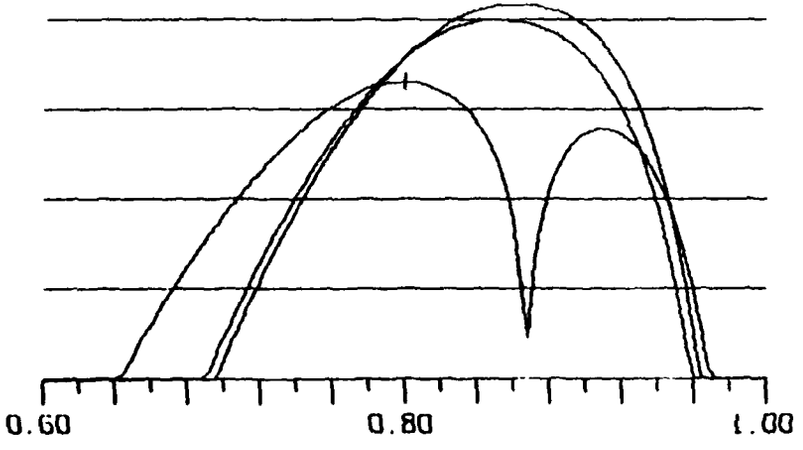

Figure 55a. Clutter Spectra for $\alpha = 30°$, $\omega = -11.25°$

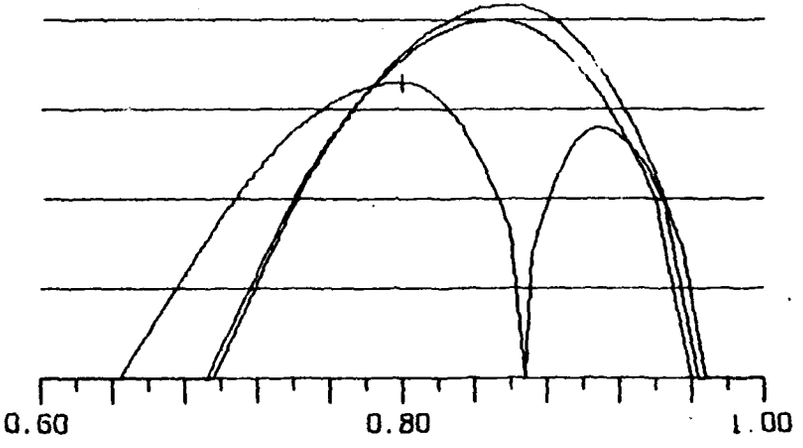

Figure 55b. Approximation to Figure 55a

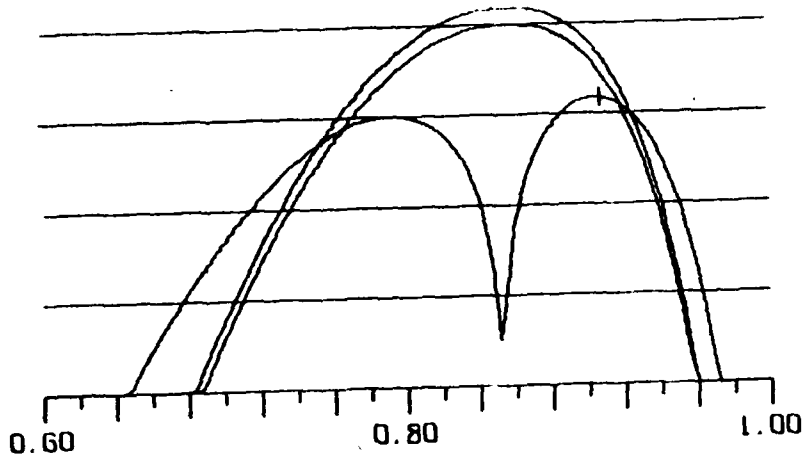

Figure 56a. Clutter Spectra for $\alpha = 30°$, $\omega = 0$

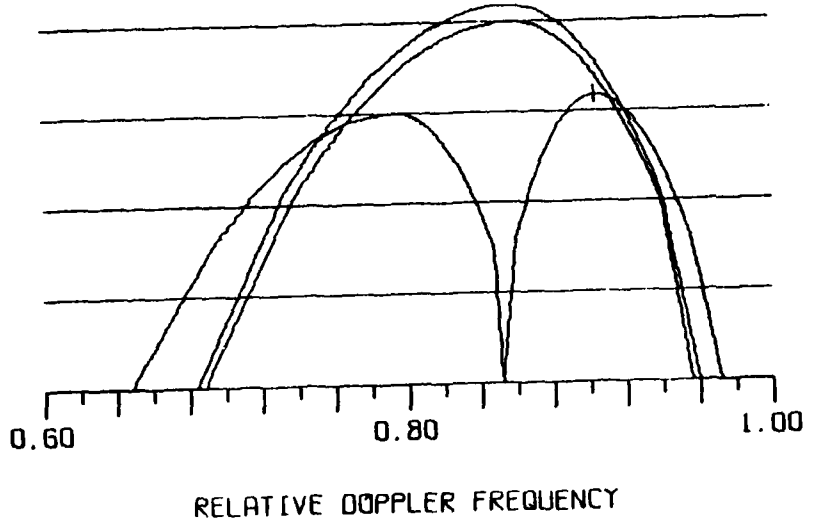

Figure 56b. Approximation to Figure 56a

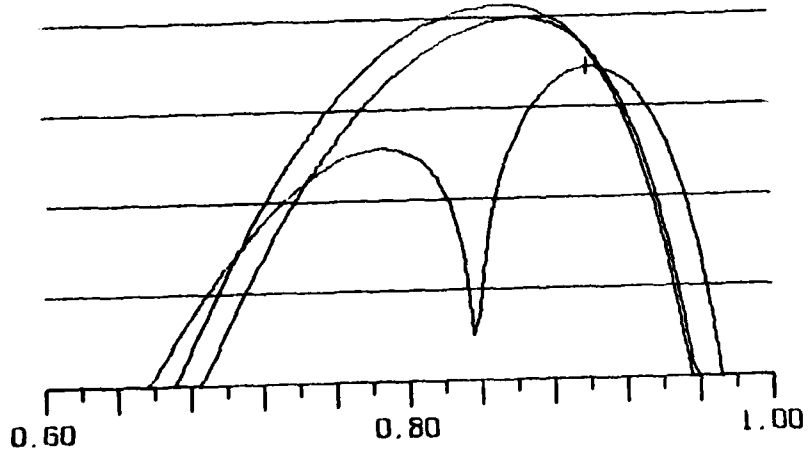

Figure 57a. Clutter Spectra for $\alpha = 30°$, $\omega = 11.25°$

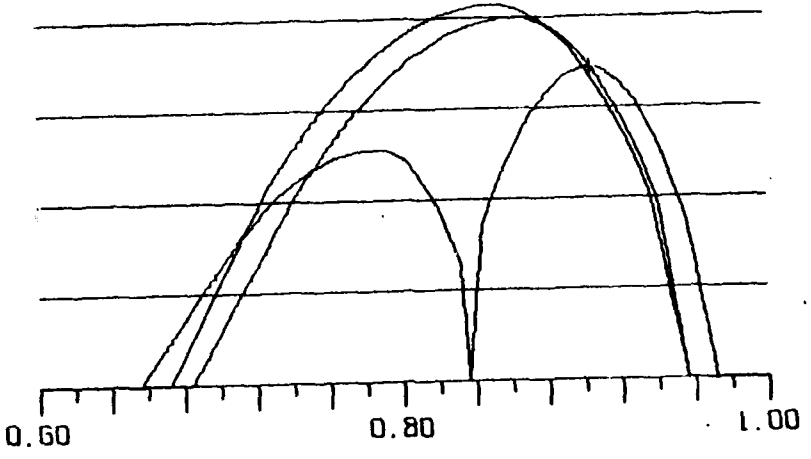

Figure 57b. Approximation to Figure 57a

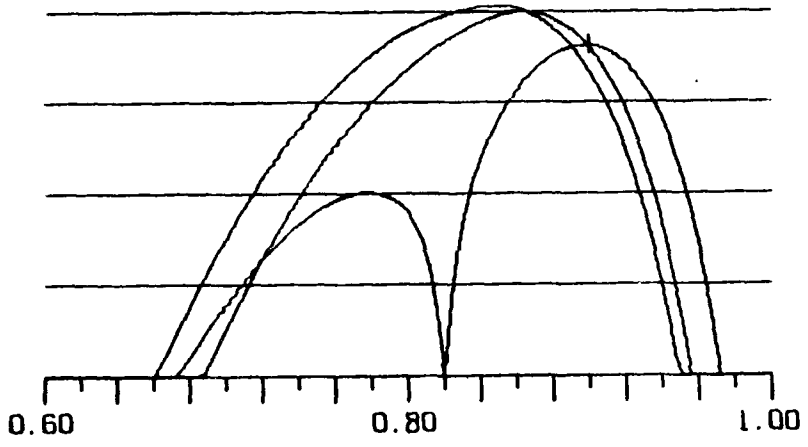

Figure 58a. Clutter Spectra for $\alpha = 30°$, $\omega = 22.5°$

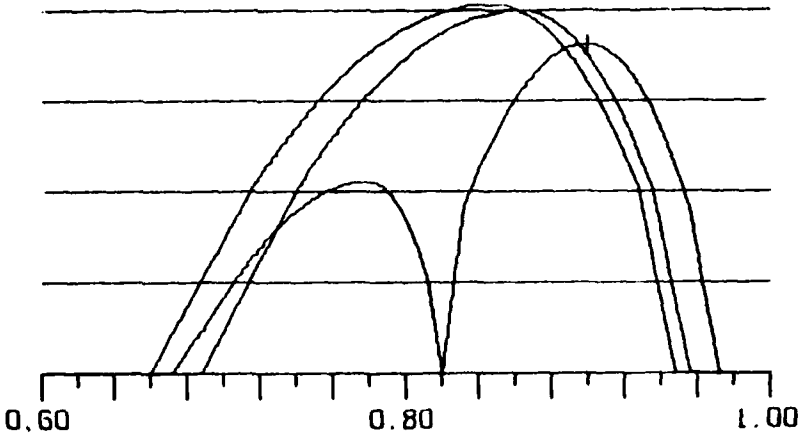

Figure 58b. Approximation to Figure 58a

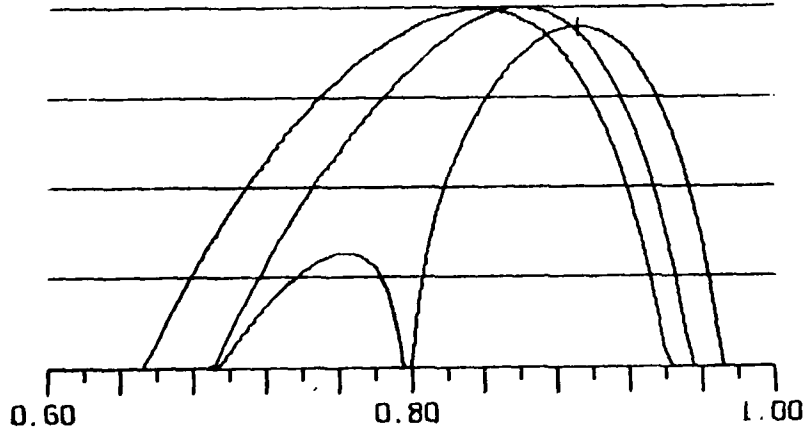

Figure 59a. Clutter Spectra for $\alpha = 30°$, $\omega = 33.75°$

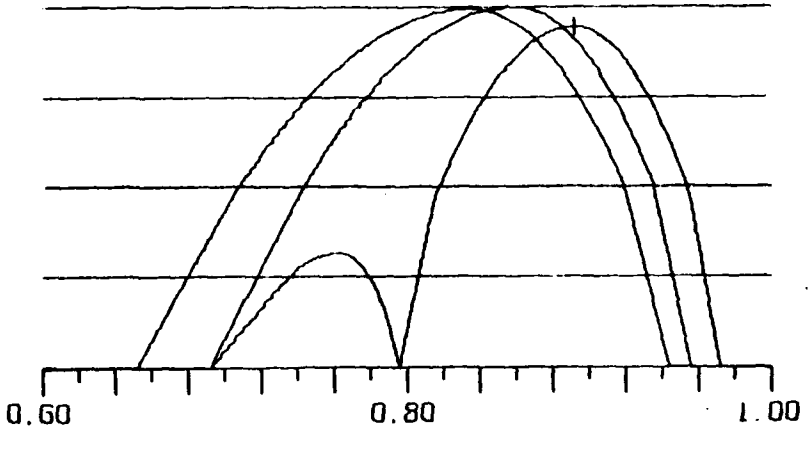

Figure 59b. Approximation to Figure 59a

Table 5. Clutter Spectrum Parameters for Sum Channel

(frequencies are normalized to $2V/\lambda$, PEAK is in dB)

						OMEGA				
	ALPHA	-45.00	-33.75	-22.50	-11.25	0.00	11.25	22.50	33.75	45.00
F1	0	.956	.956	.955	.954	.953	.954	.955	.956	.956
	10	.896	.897	.894	.892	.890	.890	.892	.894	.896
	20	.810	.810	.808	.803	.800	.800	.802	.805	.810
	30	.697	.698	.697	.690	.688	.686	.688	.692	.697
F2	0	.972	.972	.971	.970	.970	.970	.971	.972	.972
	10	.926	.922	.920	.920	.920	.922	.924	.926	.926
	20	.850	.849	.845	.843	.841	.843	.845	.849	.850
	30	.749	.747	.743	.740	.736	.739	.741	.745	.749
F3	0	.984	.984	.985	.985	.984	.984	.984	.984	.984
	10	.980	.980	.980	.980	.980	.980	.980	.980	.980
	20	.930	.925	.925	.925	.933	.935	.933	.930	.930
	30	.856	.852	.848	.852	.860	.864	.864	.860	.856
F4	0	.985	.985	.985	.985	.985	.985	.985	.985	.985
	10	.985	.985	.985	.985	.985	.985	.985	.985	.985
	20	.975	.976	.977	.978	.978	.977	.976	.975	.975
	30	.933	.935	.938	.939	.940	.939	.936	.934	.933
F5	0	.985	.985	.985	.985	.985	.985	.985	.985	.985
	10	.985	.985	.985	.985	.985	.985	.985	.985	.985
	20	.983	.983	.983	.983	.983	.983	.983	.983	.983
	30	.956	.958	.959	.959	.958	.958	.956	.956	.956
PEAK	0	40.0	40.0	40.0	40.0	40.0	40.0	40.0	40.0	40.0
	10	40.0	40.0	40.0	40.0	40.0	40.0	40.0	40.0	40.0
	20	40.0	40.0	40.0	40.0	40.0	40.0	40.0	40.0	40.0
	30	40.0	40.0	40.0	40.0	40.0	40.0	40.0	40.0	40.0
TYPE	0	0	0	0	0	0	0	0	0	0
	10	2	2	2	2	2	2	2	2	2
	20	2	2	2	2	2	2	2	2	2
	30	2	2	2	2	2	2	2	2	2

Table 6. Clutter Spectrum Parameters for Left-lobe of ΔAz Channel

(frequencies are normalized to 2V/λ, PEAK is in dB)

	ALPHA	-45.00	-33.75	-22.50	-11.25	OMEGA 0.00	11.25	22.50	33.75	45.00
F1	0	.942	.942	.942	.941	.940	.941	.942	.942	.942
	10	.866	.866	.864	.864	.866	.876	.888	.900	.913
	20	.768	.766	.765	.765	.767	.778	.790	.810	.830
	30	.645	.645	.644	.644	.648	.657	.673	.694	.716
F2	0	.965	.963	.961	.959	.957	.959	.961	.963	.965
	10	.902	.900	.898	.894	.896	.900	.906	.910	.916
	20	.815	.810	.808	.808	.808	.813	.820	.828	.840
	30	.704	.698	.696	.695	.693	.700	.708	.720	.730
F3	0	.984	.984	.984	.984	.983	.984	.984	.984	.984
	10	.962	.958	.954	.950	.947	.942	.938	.928	.915
	20	.906	.899	.895	.889	.883	.878	.870	.859	.848
	30	.822	.812	.808	.800	.794	.786	.780	.764	.750
F4	0	.985	.985	.985	.985	.985	.985	.985	.985	.985
	10	.984	.982	.978	.976	.968	.961	.952	.938	.920
	20	.959	.950	.941	.931	.920	.910	.895	.876	.860
	30	.900	.887	.874	.860	.847	.832	.814	.789	.765
F5	0	.985	.985	.985	.985	.985	.985	.985	.985	.985
	10	.985	.985	.980	.975	.970	.964	.958	.944	.932
	20	.968	.958	.948	.938	.925	.912	.900	.883	.858
	30	.914	.900	.884	.869	.852	.836	.820	.796	.753
PEAK	0	37.5	35.3	32.3	31.0	29.0	30.0	32.3	35.3	37.5
	10	37.5	36.1	34.4	32.1	28.1	23.0	16.4	7.4	.0
	20	38.0	36.7	35.1	32.9	29.6	24.8	18.7	10.2	.0
	30	38.0	36.7	35.1	33.0	30.0	25.7	21.1	12.6	.0
TYPE	0	0	0	0	0	0	0	0	0	0
	10	2	2	2	2	2	2	2	2	2
	20	2	2	2	2	2	2	2	2	2
	30	2	2	2	2	2	2	2	2	2

Table 7. Clutter Spectrum Parameters for Right-lobe of ΔAz Channel

(frequencies are normalized to 2V/λ, PEAK is in dB)

		OMEGA							
	ALPHA	-45.00	-33.75	-22.50	-11.25	0.00	11.25	22.50	33.75	45.00
F1	0	.000	.000	.000	.000	000	.000	.000	.000	.000
	10	.000	.000	.980	.975	.970	.964	935	944	.932
	20	.962	.956	.948	.935	925	.912	.900	883	.868
	30	.914	.900	.884	.869	.852	836	.820	.796	.753
F2	0	.000	.000	.000	.000	.000	.000	000	000	.000
	10	.000	.000	980	977	972	.968	962	956	948
	20	.971	.960	949	939	930	920	910	899	883
	30	.926	.904	.891	.872	860	.844	832	.816	.788
F3	0	.000	.000	.000	000	000	.000	000	.000	.000
	10	.000	.000	.994	984	984	.994	984	.984	.984
	20	.975	.970	.965	.963	.960	.958	956	.953	.948
	30	.932	.920	.914	.908	.906	.902	.900	.892	.580
F4	0	.000	.000	.000	.000	000	.000	.000	.000	.000
	10	.000	.000	.985	.985	.985	.985	.985	.985	.985
	20	.979	.981	.983	.982	.984	.985	985	.983	.984
	30	.942	.948	.944	.955	.957	.958	.957	.955	.954
F5	0	.000	.000	.000	.000	.000	.000	.000	.000	.000
	10	.000	.000	.985	.985	.985	.985	.985	985	985
	20	.984	.984	.985	.985	.985	.985	985	.985	985
	30	.948	.958	.964	.968	.971	.971	.971	.971	.971
PEAK	0	.0	.0	.0	.0	.0	.0	.0	.0	.0
	10	.0	.0	27.0	33.1	37.0	39.4	41.9	41.7	42.0
	20	2.5	14.7	22.6	28.3	32.5	35.2	37.1	38.4	39.8
	30	4.0	15.2	22.5	27.9	31.8	34.4	36.3	37.8	39.7
TYPE	0	0	0	0	0	0	0	0	0	0
	10	0	0	0	0	0	0	0	0	0
	20	2	2	2	2	2	2	2	2	2
	30	2	2	2	2	2	2	2	2	2

Table 8. Clutter Spectrum Parameters for ΔE1 Channel

(frequencies are normalized to $2V/\lambda$, PEAK is in dB)

		OMEGA							
	ALPHA	-45.00	-33.75	-22.50	-11.25	0.00	11.25	22.50	33.75	45.00
F1	0	.942	.944	.946	.950	.952	.950	.946	.944	.942
	10	.932	.916	.906	.896	.888	.876	.874	.870	.866
	20	.858	.808	.822	.808	.798	.788	.778	.772	.768
	30	.753	.728	.711	.696	.684	.672	.661	.652	.646
F2	0	.965	.966	.966	.967	.969	.967	.966	.966	.965
	10	.948	.940	.934	.926	.916	.912	.908	.904	.902
	20	.883	.870	.858	.848	.838	.830	.824	.818	.815
	30	.788	.772	.758	.744	.732	.724	.716	.709	.704
F3	0	.984	.984	.984	.985	.985	.985	.985	.985	.985
	10	.984	.984	.984	.983	.980	.977	.974	.972	.970
	20	.948	.943	.938	.935	.933	.929	.923	.916	.906
	30	.880	.874	.866	.862	.860	.854	.848	.836	.822
F4	0	.985	.985	.985	.985	.985	.985	.985	.985	.985
	10	.985	.985	.985	.985	.985	.985	.985	.985	.984
	20	.984	.982	.982	.980	.978	.975	.971	.967	.959
	30	.954	.952	.950	.945	.941	.935	.928	.919	.900
F5	0	.985	.985	.985	.985	.985	.985	.985	.985	.985
	10	.985	.985	.985	.985	.985	.985	.985	.985	.985
	20	.985	.985	.985	.985	.985	.985	.985	.985	.985
	30	.971	.969	.967	.964	.960	.955	.949	.942	.935
PEAK	0	37.5	39.3	40.6	41.6	40.8	40.6	40.6	39.3	37.5
	10	42.0	42.4	42.6	42.5	41.9	40.9	39.8	38.7	37.5
	20	39.8	40.6	41.3	41.8	41.9	41.2	40.4	39.4	38.0
	30	39.7	40.5	41.2	41.7	41.9	41.4	40.7	39.3	38.0
TYPE	0	0	0	0	0	0	0	0	0	0
	10	1	1	1	1	1	2	2	2	2
	20	2	2	2	2	2	2	2	2	2
	30	2	2	2	2	2	2	2	2	2

are referenced to the -40 dB level below the sum-channel peak (i.e., the sum channel peak has a value of 40 dB). The azimuth-difference channel is characterized by two lobes, designated by "right" and "left" in the tables, where the orientation is with respect to the spectrum. In some cases the right lobe is below the reference level; the parameters are set to zero to designate this situation.

In Tables 5 through 8 a constant value of $\Delta = \gamma - \beta = 10°$ was assumed. In Section 3.7 it was shown that the spectral parameters are also a function of Δ. The dependence is slight for all parameters except the peak power values for the various azimuth-and elevation-difference channel lobes. Here the effect is strong as we see in Table 1. To include the dependence of Δ on the peak power values, the parameters in Tables 6 through 8 should be adjusted by the values in Table 1 in a procedure that is consistent with the examples in Section 3.8.

5. SIMULATION ARCHITECTURE

The computer resources that are available at the RFSS to generate clutter signals consist of a Datacraft/1 minicomputer that acts as a host to the AP120B array processor built by Floating Point Systems. The input to the host computer consists of the state of the engagement geometry (θ_o, ϕ_o, r, δ, ω, h, V) and the output of the AP120B is the set of three clutter time-sequences. In deciding which operations are to be assigned to the two processors, the following factors were applied:

1) the array processor works best on arrays where the number of operations on each sample is few;
2) the program construction is costly for the array processor so that program should be fairly stable;
3) modifications are best made in the host computer; and
4) there should be relatively little traffic over the real-time interface between the host computer and the array processor.

With these factors in mind, the assignment of the various processing steps to generate clutter signals reduces naturally to:

The host computer

1. derive and/or transform engagement geometry
2. compute spectral parameters

The array processor

1. compute power spectral arrays
2. randomize spectra
3. take Fourier transform to time domain
4. weight, overlap, and sum time sequences
5. normalize time sequences to reference power

In order to minimize the computation load on the host computer, one should take advantage of table-lookup procedures to compute the spectral parameters. The real-time interface between the host computer and the array processor consists of, at most, 28 parameters if the format of Section 4 is used.

In Appendix C we describe and give listings for a clutter simulation program that conforms to the above architecture.

References

1. Mitchell, R. L., *Radar Signal Simulation*, Artech House, 1976, p. 113.

2. Mitchell, R. L., and I. P. Bottlik, "Design Requirements for Simulating Realistic RF Environment Signals on the RFSS," MRI Report 132-44, 23 Sept. 1977.

APPENDIX A

COORDINATE TRANSFORMATIONS FOR GROUND CLUTTER

There are several coordinate systems involved for the ground clutter as observed by a missile-borne radar. The transformations from one system to another are derived here. We begin with a transformation derived in Reference 2 (Appendix A), where one typographical error is corrected.

Arbitrary Point on Ground to Antenna Coordinates

Let us begin with the geometry of Figure 60 where R designates the location of the radar at the origin of a rectangular coordinate system referenced to the ground, $\overline{RV}$ designates the velocity vector which is contained in the y-z plane by definition, and P is the point of interest. We can define the dive angle of the missile as δ, the azimuth and depression angles of point P as ζ and γ, respectively, and ψ as the Doppler angle. Designating the direction cosines a_x, a_y, a_z on the x, y, z axes, we can write

$$\begin{aligned} a_x &= \cos\gamma \sin\zeta \\ a_y &= \cos\gamma \cos\zeta \\ a_z &= -\sin\gamma \end{aligned} \tag{A-1}$$

To define missile coordinates we can rotate the x-axis clockwise (looking in) by δ so that the new y-axis corresponds to the velocity vector. Now the direction cosines in the new coordinate system are

$$\begin{aligned} b_x &= a_x \\ b_y &= a_y\cos\delta - a_z\sin\delta \\ b_z &= a_y\sin\delta + a_z\cos\delta \end{aligned} \tag{A-2}$$

Note that $\cos\delta = b_y$ or

$$\cos\psi = \cos\gamma \cos\zeta \cos\delta + \sin\gamma \sin\delta \tag{A-3}$$

If the missile rotates (rolls) by an amount ω counterclockwise looking out the velocity vector, then we can rotate the previous y-axis by the corresponding angle. Defining the new z-axis to be the missile "vertical" axis, we obtain new direction cosines as

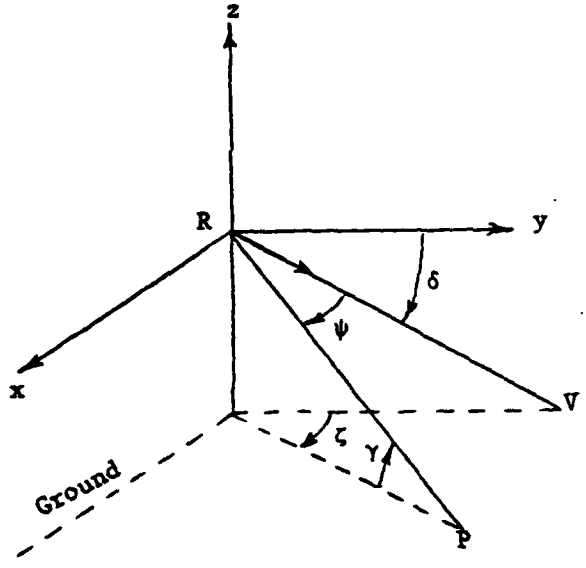

Figure 60. Geometry of Arbitrary Point on Ground

$$\begin{aligned} c_x &= b_x\cos\omega + b_z\sin\omega \\ c_y &= b_y \\ c_z &= -b_x\sin\omega + b_z\cos\omega \end{aligned} \qquad \text{(A-4)}$$

We have now arrived at the geometry of Figure 61 where θ_0 and ϕ_0 are the azimuth and elevation angles, respectively, for the antenna boresight (in this derivation we assume that the longitudinal axis of the missile is coincident with the velocity vector). To define a coordinate system referenced to the antenna, we will first rotate the x-axis in Figure 61 clockwise by θ_0 to obtain the new direction cosines as

$$\begin{aligned} d_x &= c_x\cos\theta_0 - c_y\sin\theta_0 \\ d_y &= c_x\sin\theta_0 + c_y\cos\theta_0 \\ d_z &= c_z \end{aligned} \qquad \text{(A-5)}$$

Now rotate the x-axis counterclockwise by ϕ_0 to obtain the new direction cosines as

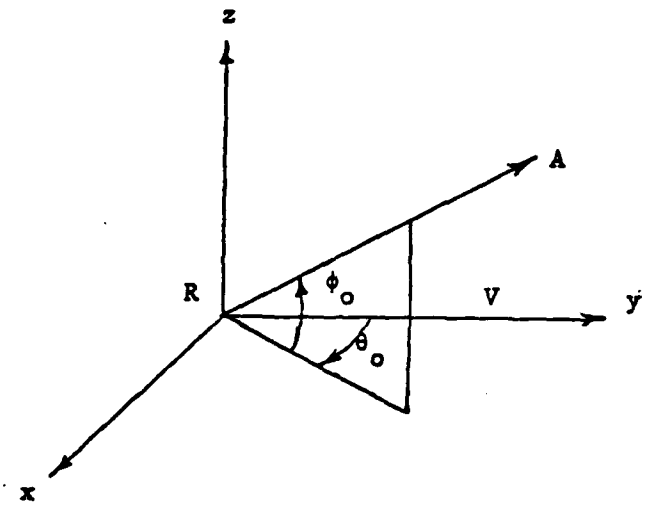

Figure 61. Missile Geometry

$$\begin{aligned} e_x &= d_x \\ e_y &= d_y\cos\phi_0 + d_z\sin\phi_0 \\ e_z &= -d_y\sin\phi_0 + d_z\cos\phi_0 \end{aligned} \tag{A-6}$$

Finally, we can reference Point P to the antenna coordinates as in Figure 62 where the antenna azimuth (θ) and elevation (ϕ) angles are given by

$$\tan\theta = e_x/e_y \tag{A-7}$$

$$\sin\phi = e_z \tag{A-8}$$

Antenna Boresight $(\alpha,\beta) \rightarrow (\theta_o,\phi_o)$

In Figure 60 we can define $\zeta = \alpha$ and $\gamma = \beta$ so that Point P is the intersection of the antenna boresight vector with the ground as shown in Figure 63. The transformation then follows (A-1) through (A-4) so that

$$\begin{aligned} a_x &= \cos\beta\ \sin\alpha \\ a_y &= \cos\beta\ \cos\alpha \\ a_z &= -\sin\beta \end{aligned} \tag{A-9}$$

, and

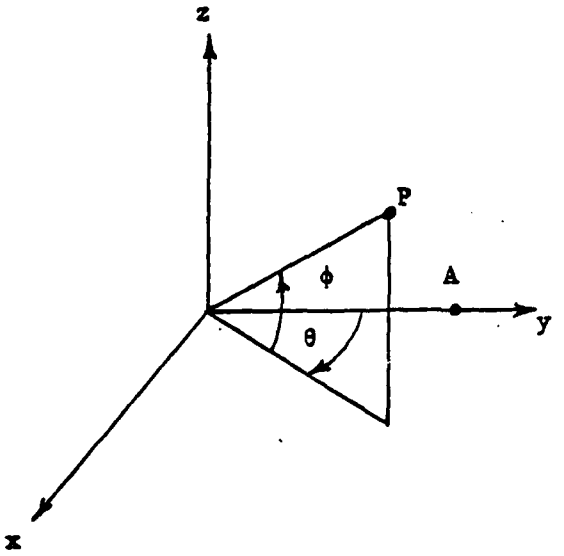

Figure 62. Antenna Geometry

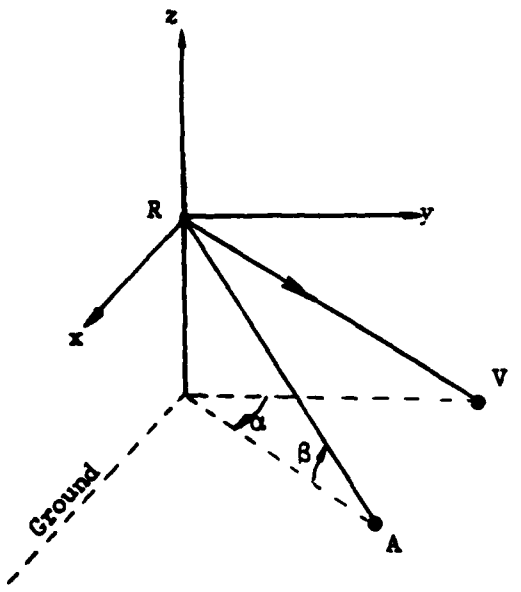

Figure 63. Geometry for Antenna Boresight

$$b_x = a_x$$
$$b_y = a_y\cos\delta - a_z\sin\delta \qquad \text{(A-10)}$$
$$b_z = a_y\sin\delta + a_z\cos\delta$$

and

$$c_x = b_x\cos\omega + b_z\sin\omega$$
$$c_y = b_y \qquad \text{(A-11)}$$
$$c_z = -b_x\sin\omega + b_z\cos\omega$$

These direction cosines define the A-vector in Figure 61, so that

$$\tan\theta_o = c_x/c_y \qquad \text{(A-12)}$$
$$\sin\phi_o = c_z \qquad \text{(A-13)}$$

Antenna Boresight $(\theta_o,\phi_o) \rightarrow (\alpha,\beta)$

This transformation is the inverse of the one just derived. We begin with the A-vector in Figure 61, which has direction cosines

$$c_x = \cos\phi_o\ \sin\theta_o$$
$$c_y = \cos\phi_o\ \cos\theta_o \qquad \text{(A-14)}$$
$$c_z = \sin\phi_o$$

To obtain the direction cosines of the A-vector in a coordinate system that has the z-axis in a plane vertical to the ground we must rotate the old y-axis by ω in the counterclockwise direction (looking in) so that

$$b_x = c_x\cos\omega - c_z\sin\omega$$
$$b_y = c_y \qquad \text{(A-15)}$$
$$b_z = c_x\sin\omega + c_z\cos\omega$$

The missile dive angle δ is referenced to the horizontal so we can define a new coordinate system referenced to the ground, that in Figure 63, by rotating the old x-axis by δ in the counterclockwise direction (looking in). The new direction cosines are

$$
\begin{aligned}
a_x &= b_x \\
a_y &= b_y \cos\delta + b_z \sin\delta \\
a_z &= -b_y \sin\delta + b_z \cos\delta
\end{aligned}
\qquad \text{(A-16)}
$$

The A-vector is now defined by

$$
\begin{aligned}
\tan\alpha &= a_x/a_y \\
\sin\beta &= -a_z
\end{aligned}
$$

APPENDIX B

ANGLE BETWEEN TWO PLANES

Plane 1: Vertical plane containing antenna boresight axis

Plane 2: Plane containing antenna boresight axis and antenna ϕ-axis

Assume that the missile dive angle is δ, the missile roll angle is ω, and the antenna boresight axis is at an angle (θ_o,ϕ_o) from the velocity vector. The direction cosines of the antenna boresight axis in the ground-referenced coordinate system (the A-vector in Figure 63) are given by the coordinate transformations in (A-14) through (A-16), which we denote as (a_x,a_y,a_z). If we replace ϕ_o by $\phi_o + 90°$ in these transformations, we define a vector that is coincident with the antenna ϕ-axis. Let us designate the direction cosines of this vector as (a'_x,a'_y,a'_z). A vector that is perpendicular to the A-vector in the vertical plane has the direction cosines

$$\begin{aligned} a_{xN} &= a_x a_z / a_{zN} \\ a_{yN} &= a_y a_z / a_{zN} \\ a_{zN} &= \sqrt{a_x^2 + a_y^2} \end{aligned} \qquad \text{(B-1)}$$

The two vectors A' and A_N, defined by their direction cosines (a'_x,a'_y,a'_z) and (a_{xN},a_{yN},a_{zN}), respectively, are both perpendicular to the A-vector, which is the intersection of the two planes of interest. The cosine of the angle between these two vectors is the dot product $\bar{A}' \cdot \bar{A}_N$. The sign of the angle is given by the sign of $(\bar{A}' \times \bar{A}_N) \cdot \bar{A}$, which can be rewritten as $(\bar{A}_N \times \bar{A}) \cdot \bar{A}'$. The direction cosines of $(\bar{A}_N \times \bar{A})$ are $(-\cos\alpha, \sin\alpha, o)$, so that

$$(\bar{A}' \times \bar{A}_N) \cdot \bar{A} = (\bar{A}_N \times \bar{A}) \cdot \bar{A}' = -a'_x\cos\alpha + a'_y\sin\alpha \qquad \text{(B-2)}$$

If (B-2) is positive the angle between the two planes is positive, and vice versa.

Instead of beginning with the coordinate (θ_o,ϕ_o) we could have begun with (α,β) as in Figure 63. The procedure then would be to obtain (θ_o,ϕ_o) by the use of (A-9) through (A-13), with the remaining calculation as outlined above.

The use of the above results is straightforward, but somewhat time consuming for real-time applications. We are thus motivated to find a faster method of computing the desired angle. Unfortunately, the direct analysis to find approximate solutions based on small angles is very cumbersome. But with a computer one can find through the process of trial and error the basic behavior of this function of four variables. After many iterations we have found

$$\xi = \omega + \alpha(\beta + (\delta-\beta)\cos\omega) + \frac{1}{4}((\delta-\beta)^2 - \alpha^2)\sin 2\omega - \frac{1}{3}\alpha(\delta-\beta)\omega^2\sin^2 2\omega \qquad \text{(B-3)}$$

as the angle between the two planes of interest, where all angles are in radians. The solution has been evaluated for $0 \leq \alpha \leq 30°$, $-20° \leq \beta \leq 20°$, $-20° \leq \delta \leq 20°$, and $-90° \leq \omega \leq 90°$. The error in the approximation is shown in Table 9. In general, the peak error is less than 1°, except when $|\delta-\beta|$ is large.

Table 9. Residual Errors in Approximation for Angle Between Two Planes (all angles in degrees)

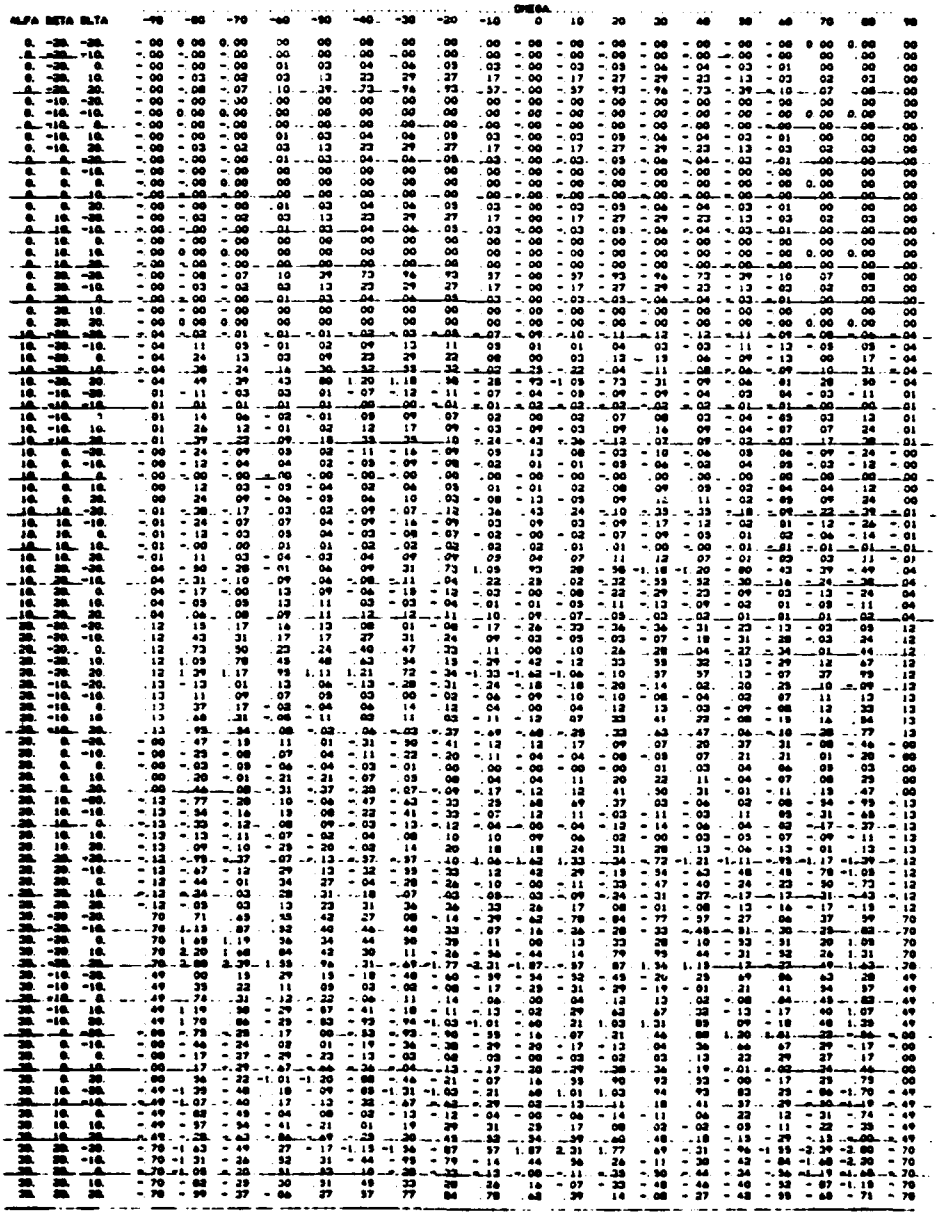

APPENDIX C

FORTRAN PROGRAM FOR GENERATING REAL-TIME CLUTTER SEQUENCES

This Fortran program generates continuous time sequences of ground clutter that would be received on an airborne radar platform for a time-varying engagement geometry. Signals are generated for the three monopulse channels. It is assumed that these signals will be radiated into specific positions on the receive antenna pattern so that each signal will be received by the proper channel and rejected by the others.

This program was written for a single range gate of a pulse-Doppler radar, although it is easily extended to multiple range gates (but not in real time with a single AP120B). The organization of this program is sketched in Figure 64. At the RFSS it is assumed that the real-time state of the environment will be set up in COMMON/C1/ and periodic calls will be made to CLUTTR in the Datacraft/6. The subroutines that actually generate the clutter sequences (FILL, CURVE, PARAB, CONVRT, TIMESQ, GAUSS4, FOURT) will be implemented in the AP120B. Their Fortran equivalents are included in this package.

A test program (TEST) is also included to compare results on different computers. The output of this program is a power spectral estimate of the clutter sequences generated under stationary conditions.

Note: this program does not include an adjustment for Δ on the monopulse difference channel spectra as discussed in Sections 3.7 and 4.2. The modification is minor to include this adjustment, and only the portion of the program that resides in the host computer will be affected.

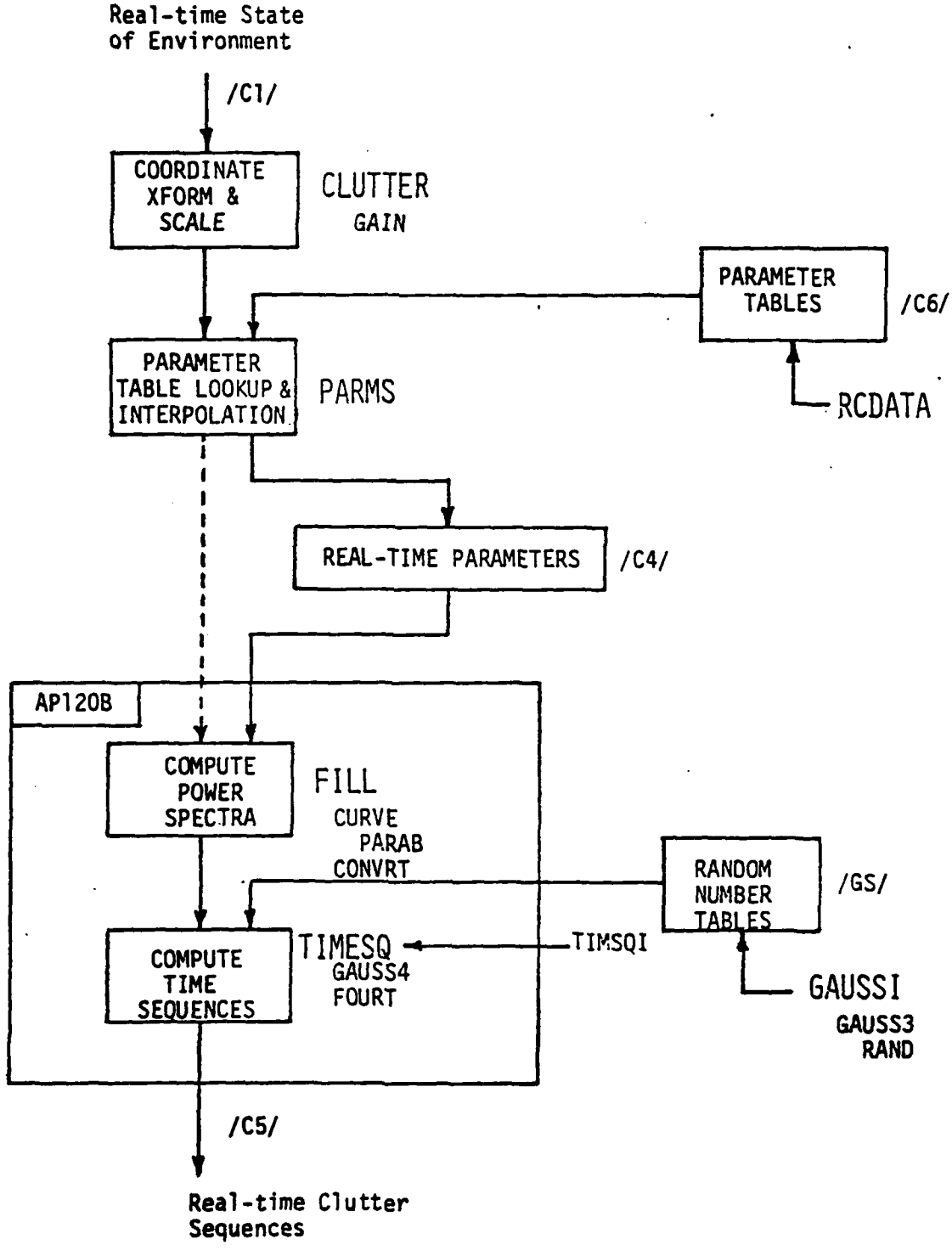

Figure 64. Block Diagram of Clutter Signal Program

PROGRAM SUMMARY

Main or Driver

TEST (for this example)

Initialization

RCDATA
TIMSQI
GAUSSI (GAUSS3,RAND)

Real-time Fortran

CLUTTR(GAIN)
PARMS(AINT)

Utility

PR
ACCUM
POWSPT
XMIT
FOURT

Real-time AP120B

FILL
CURVE
PARAB
CONVRT
TIMESQ
GAUSS4

```
      PROGRAM TEST(INPUT,OUTPUT,TAPE5=INPUT,TAPE6=OUTPUT)
C
C TEST OF SUBROUTINE CLUTTR
C
C THE TEST CASE CORRESPONDS TO ALPHA=20.,BETA=0.,GAMMA=10.,DELTA=0., AND
C OMEGA=-22.5 (ALL DEGREES).
C
      DIMENSION SR(2240,3),SI(2240,3),S(200,3),WORK(600)
      COMMON /C1/ WL,H,V,R,FR,DE,OM,THO,PHO
      COMMON /C2/ PTGDSQ,SIGO,DR
      COMMON /C3/ NFFT,NOVLP,NF,A(64)
      COMMON /C5/ PEFF,
     1            XR1(320),XI1(320),XR2(320),XI2(320),XR3(320),XI3(320)
C
C THE FOLLOWING PARAMETERS MUST BE SET.....
C
      DATA WL,H,R,FR,V/.02,1736.,10000.,10000.,500./
      DATA DE,OM,THO,PHO/0.,-.3927,.3244,.1313/
      DATA PTGDSQ,DR,SIGO/1.,20.,.01/
      DATA NFFT,NOVLP/256,32/
C
C HERE WE INITIALIZE
C
      CALL RCDATA
      CALL TIMSQI
      CALL GAUSSI
C
C HERE WE GENERATE CONTIGUOUS TIME SEQUENCES IN THE SR AND SI ARRAYS
C
      L=1
      DO 20 I=1,10
      CALL CLUTTR
      CALL XMIT(NF,XR1,SR(L,1))
      CALL XMIT(NF,XR2,SR(L,2))
      CALL XMIT(NF,XR3,SR(L,3))
      CALL XMIT(NF,XI1,SI(L,1))
      CALL XMIT(NF,XI2,SI(L,2))
      CALL XMIT(NF,XI3,SI(L,3))
      L=L+NF
   20 CONTINUE
C
C HERE WE COMPUTE THE (AVERAGED) POWER SPECTRUM
C
      L=1
      DO 30 I=1,11
      CALL POWSPT(SR(L,1),SI(L,1),200,200,0.,WORK)
      CALL POWSPT(SR(L,2),SI(L,2),200,200,0.,WORK)
      CALL POWSPT(SR(L,3),SI(L,3),200,200,0.,WORK)
      CALL ACCUM(SR(L,1),S(1,1),200,I)
      CALL ACCUM(SR(L,2),S(1,2),200,I)
```

```
      CALL ACCUM(SR(L,3),S(1,3),200,I)
      L=L+200
   30 CONTINUE
      CALL PR(S,200,3)

      STOP
      END
```

```
      SUBROUTINE RCDATA
C
C THIS SUBROUTINE READS THE CLUTTER DATA BASE INTO COMMON /C6/.
C
      DIMENSION IW(4),W(22)
      COMMON /C6/ S(180),IS(4),A1(216),IA1(36),A2(180),IA2(36),E(216),
     1            IE(36)
      DATA IW/10HIS.......,10HIA1.......,10HIA2.......,10HIE......./
      DATA W/10HS1.......,10HS2.......,10HS3.......,10HS4.......,
     1       10HS5.......,10HA11......,10HA12......,10HA13......,
     2       10HA14......,10HA15......,10HA1P......,10HA22......,
     3       10HA23......,10HA24......,10HA25......,10HA2P......,
     4       10HE1.......,10HE2.......,10HE3.......,10HE4.......,
     5       10HE5.......,10HEP......./

      READ 102,S
      READ 101,IS
      READ 102,A1
      READ 101,IA1
      READ 102,A2
      READ 101,IA2
      READ 102,E
      READ 101,IE

      PRINT 200

      K1=1
      K2=36
      DO 10 L=1,5
      PRINT 202,W(L),(S(K),K=K1,K2)
      K1=K1+36
      K2=K2+36
   10 CONTINUE

      PRINT 201,IW(1),IS

      K1=1
      K2=36
      DO 20 L=6,11
      PRINT 202,W(L),(A1(K),K=K1,K2)
      K1=K1+36
      K2=K2+36
   20 CONTINUE

      PRINT 201,IW(2),IA1

      K1=1
      K2=36
      DO 30 L=12,16
      PRINT 202,W(L),(A2(K),K=K1,K2)
```

```
      K1=K1+36
      K2=K2+36
   30 CONTINUE

      PRINT 201, IW(3), IA2

      K1=1
      K2=36
      DO 40 L=17, 22
      PRINT 202, W(L), (E(K), K=K1, K2)
      K1=K1+36
      K2=K2+36
   40 CONTINUE

      PRINT 201, IW(4), IE

      RETURN
  100 FORMAT(20F4.0)
  101 FORMAT(36I2)
  102 FORMAT(2(9F4.0, 4X))
  200 FORMAT(1H1, 50HGROUND CLUTTER DATA BASE READ BY SUBROUTINE RCDATA/)
  201 FORMAT(/1XA10, 3X36I3)
  202 FORMAT(/1XA10, 3X9F7.3/(14X9F7.3))
      END
```

```
      SUBROUTINE TIMSQI
C
C THIS SUBROUTINE PERFORMS INITIALIZATION FOR SUBROUTINE TIMESQ.
C
C THE INITIALIZATION PARAMETERS ARE.....
C
C     NFFT = SIZE OF FFT (=2**INTEGER)
C    NOVLP = NUMBER OF SAMPLES THAT THE FFTS OVERLAP (NFFT/8 IS OK)
C
C THE ARRAYS MUST BE DIMENSIONED AS LARGE AS.....
C
C          XR1, XI1, ETC          NFFT+NOVLP-1
C                   A             NOVLP-1
C
      COMMON /C3/ NFFT, NOVLP, NF, A(64)
      COMMON /C5/ PEFF,
     1            XR1(320), XI1(320), XR2(320), XI2(320), XR3(320), XI3(320)
      NF=NFFT-NOVLP
      N1=NOVLP-1
      N2=NFFT+N1
      DO 10 K=1, N1
      A(K)=K/FLOAT(NOVLP)
   10 CONTINUE
      CALL XMIT(-N2, 0., XR1)
      CALL XMIT(-N2, 0., XR2)
      CALL XMIT(-N2, 0., XR3)
      CALL XMIT(-N2, 0., XI1)
      CALL XMIT(-N2, 0., XI2)
      CALL XMIT(-N2, 0., XI3)
      RETURN
      END
```

```
      SUBROUTINE GAUSSI
C
C THIS SUBROUTINE FILLS ARRAYS TR AND TI WITH INDEPENDENT GAUSSIAN
C RANDOM NUMBERS FOR USE WITH SUBROUTINE GAUSS4.
C
C ARRAYS TR AND TI MUST BE DIMENSIONED AS LARGE AS NTR+NMAX AND NTI+NMAX
C RESPECTIVELY.
C
C IF N BELOW IS NOT EVEN, ADD 1 TO THE DIMENSION OF TI.
C
      COMMON /GS/ IRSET,NTR,NTI,NMAX,KR,KI,TR(1253),TI(1353)
      DATA NTR,NTI/997,1097/, NMAX/256/, KR,KI/1,1/
      N=NTR+NTI+2*NMAX
      DO 20 K=1,N,2
      CALL GAUSS3(TR(K),TR(K+1),1.)
   20 CONTINUE
      RETURN
      END
```

```
      SUBROUTINE GAUSS3(X,Y,P)
C
C THIS SUBROUTINE GENERATES RANDOM PAIRS FOR THESE DISTRIBUTIONS.....
C
C CALL GAUSS3(X,Y,P)....GAUSSIAN COMPONENTS OF AVERAGE POWER P
C CALL RANG3(X,Y,P).....RANDOM PHASOR COMPONENTS OF POWER P
C
      DATA Z/0./
C                                                          )X(FNAR=)X(DNAR
      IF(P) 30,20,10
   10 E=SQRT(-P*ALOG(RAND(Z)))
      GO TO 15
      ENTRY RANG3
      IF(P) 30,20,12
   12 E=SQRT(P)
   15 A=RAND(Z)
      A=A+A-1.
      B=RAND(Z)
      B=B+B-1.
      A2=A*A
      B2=B*B
      C=A2+B2
      IF(C.GT.1.) GO TO 15
      X=E*(A2-B2)/C
      Y=E*2.*A*B/C
      RETURN
   20 X=0.
      Y=0.
      RETURN
   30 STOP 44
      END
```

```
      FUNCTION RAND(Z)
C FOR TEST PURPOSES ONLY.
      DIMENSION A(8)
      DATA A/.1,.2,.3,.4,.5,.6,.7,.8/
      DATA K/1/
      RAND=A(K)
      K=K+1
      IF(K.GT.8) K=1
      RETURN
      END
```

```
      SUBROUTINE CLUTTR
C
C IN THIS SUBROUTINE WE GENERATE THE CLUTTER MODULATION SIGNALS FOR ONE
C RANGE GATE ON EACH OF THREE MONOPULSE CHANNELS.
C
C THE BACKSCATTER COEFFICIENT OF THE GROUND IS ASSUMED TO VARY AS THE
C SINE OF THE GRAZING ANGLE.
C
C THE REAL-TIME PARAMETERS ON INPUT ARE.....
C
C       WL = WAVELENGTH
C        H = PLATFORM ALTITUDE
C        V = PLATFORM VELOCITY
C        R = RANGE TO RANGE GATE OF INTEREST (UNAMBIGUOUS)
C       FR = EQUIVALENT SAMPLE RATE IN RECEIVER (PROCESSING BAND)
C       DE = DELTA, THE MISSILE DIVE ANGLE
C       OM = OMEGA, THE MISSILE ROLL ANGLE (CCW IS POSITIVE)
C      THO = THETA-ZERO, THE AZIMUTH ANGLE OF THE ANTENNA BORESIGHT
C      PHO = PHI-ZERO, THE ELEVATION ANGLE OF THE ANTENNA BORESIGHT
C
C THE NONREAL-TIME PARAMETERS ON INPUT ARE.....
C
C   PTGDSQ = PRODUCT OF TRANSMIT POWER, GAIN, SQUARE OF CHAMBER LENGTH
C       DR = RANGE RESOLUTION
C     SIGO = GROUND BACKSCATTER COEFFICIENT AT 30-DEG GRAZING ANGLE
C
C THE REAL-TIME OUTPUT FOR THAT PORTION COMPUTED IN THE DATACRAFT IS
C THROUGH /C4/, AND IT IS COMPUTED IN SUBROUTINE PARMS.
C
C SOME OF THE OTHER QUANTITIES USED IN THIS SUBROUTINE ARE.....
C
C       AL = ALPHA, THE AZIMUTH ANGLE OF THE BEAM AXIS IN GROUND COORD.
C       BE = BETA, THE ELEVATION ANGLE OF THE BEAM AXIS IN GROUND COORD.
C       GA = GAMMA, THE GRAZING ANGLE AT THE RANGE RING ON THE GROUND
C
C ALL ANGLES ARE IN RADIANS AND ALL DISTANCES IN METERS.
C
      COMMON /C1/ WL,H,V,R,FR,DE,OM,THO,PHO
      COMMON /C2/ PTGDSQ,SIGO,DR
      COMMON /C3/ NFFT
      DATA FCTR/1./
C
C COMPUTE GEOMETRY AND DOPPLER PARAMETERS
C
     1 SGA=H/R
       CGA=SQRT(1.-SGA**2)
       GA=ATAN(SGA/CGA)
       CPHO=COS(PHO)
       SPHO=SIN(PHO)
       CTHO=COS(THO)
```

```
      STHO=SIN(THO)
      COM=COS(OM)
      SOM=SIN(OM)
      CDE=COS(DE)
      SDE=SIN(DE)
      AX=CPHO*STHO
      AY=CPHO*CTHO
      AZ=SPHO
      BX=AX*COM-AZ*SOM
      BY=AY
      BZ=AX*SOM+AZ*COM
      CX= BX
      CY= BY*CDE+BZ*SDE
      CZ=-BY*SDE+BZ*CDE
      AL=ATAN(CX/CY)
      BE=ATAN(-CZ/SQRT(1.-CZ**2))
      PEFF=.013*PTGDSQ*(2.*SIGO*SGA)*DR*GAIN(GA-BE)/R**3
      FMAX=2.*V/WL
      FMC =FMAX*(CGA*CDE+SGA*SDE)
      FSCL=.9848*FMAX/FMC
      IAMB=FMC/FR
      FNP1=(IAMB-1)*FR*FSCL/FMAX
      DFNP=FNP1/FLOAT((IAMB-1)*NFFT)
      FNP1=.9848-FCTR*(.9848-FNP1)
      DFNP=FCTR*DFNP
      ALD=57.3*AL
      OMD=57.3*OM
      IF(ALD.GT.0.) GO TO 10
      OMD=360.-OMD
      ALD=-ALD
   10 OMDP=OMD
      IF(OMD.GT.315.) OMDP=OMDP-360.
      ICASE=(OMDP+45.)/90.
      OMDP=OMDP-ICASE*90.
      IROT=0
      IF(ICASE.EQ.1.OR.ICASE.EQ.3) IROT=1
C              )/4.21E,4.9F3,1.9F2,1.8F3,4.8F3,4I3/.....RTTULC H21/(TAMROF 0C
C                                                    FFEP,PNFD,1PNF          1
C           ,LCSF,CMF,XAMF,PDMO,DMO,DLA,EB,LA,AG,TORI,ESACI,BMAI,001 TNIRP
C
C COMPUTE REAL-TIME PARAMETERS
C
      CALL PARMS(ALD,OMDP,FNP1,DFNP)
C
C GENERATE REAL-TIME SPECTRA
C
      IROT=0
      IF(ICASE.EQ.1.OR.ICASE.EQ.3) IROT=1
      CALL FILL(IROT)
      RETURN
      END
```

```
      FUNCTION GAIN(PHI)
C
C HERE WE COMPUTE THE 2-WAY POWER GAIN BY TABLE LOOKUP.  PHI IS THE
C ANGLE IN RADIANS.
C
C       NB = NUMBER OF SAMPLES IN TABLE
C       DB = SAMPLE SPACING (DEG)
C
C THE FIRST SAMPLE IS AT PHI=0.
C
      DIMENSION BEAM(101)
      DATA NB/101/,DB/.5/
      DATA A/.00389/,B/2.30/
      DATA NO/0/
      IF(NO.GT.0) GO TO 30
      NO=1
      DO 20 K=1,NB
      BEAM(K)=EXP(-4.*A*((K-1)*DB)**B)
   20 CONTINUE
   30 E=57.3*ABS(PHI)
      IE=E/DB+1.5
      GAIN=0.
      IF(IE.LE.NB) GAIN=BEAM(IE)
      RETURN
      END
```

```
      SUBROUTINE PARMS(ALPHA,OMEGA,F1,DF)
C
C IN THIS SUBROUTINE WE COMPUTE THE REAL-TIME PARAMETERS THAT WILL BE
C SENT TO THE AP120B.  THE PARAMETERS ARE DETERMINED BY INTERPOLATION
C WITHIN THE DATA BASE STORED IN COMMON /C6/.
C
C THE INPUT IS.....
C
C       ALPHA = ABSOLUTE VALUE OF AZIMUTH ANGLE (DEG)
C       OMEGA = MISSILE ROLL ANGLE (DEG,  -45..LE.OMEGA.LE.45.)
C          F1 = NORMALIZED DOPPLER OF FIRST SAMPLE
C          DF = SAMPLE SPACING IN DOPPLER
C
C THE OUTPUT IS THROUGH COMMON /C4/.....
C
C       IS,SPK.....SUM SPECTRUM PARAMETERS
C       IA1,A1PK....DEL-AZ SPECTRUM PARAMETERS, LEFT HALF
C       IA2,A2PK....DEL-AZ SPECTRUM PARAMETERS, RIGHT HALF
C       IE,EPK.....DEL-EL SPECTRUM PARAMETERS
C       PSL.........SIDELOBE LEVEL (SEE SUBROUTINE FILL)
C
C SKP,A1PK,A2PK,EPK,AND PSL MUST BE IN THE SAME UNITS (NEPERS).
C
C                                                          TNIA LANRETXE
      COMMON /C4/ IS(6),IA1(6),IA2(6),IE(6),SPK,A1PK,A2PK,EPK,PSL
      COMMON /C6/ S1(36),S2(36),S3(36),S4(36),S5(36),IST(4),
     1        A11(36),A12(36),A13(36),A14(36),A15(36),A1P(36),IA1T(36),
     2                A22(36),A23(36),A24(36),A25(36),A2P(36),IA2T(36),
     3             E1(36),E2(36),E3(36),E4(36),E5(36),EP(36),IET(36)
      COMMON /CINT/ K1,K2,K3,K4,HOM,HAL
      DATA NAL,NOM/4,9/
      DATA DAL,DOM/10.,11.25/
      ISAMP(A)=(AINT(A)-F1)/DF+1.5
C
C HERE WE FIND THE PARAMETERS FOR INTERPOLATION
C
      AL=ALPHA/DAL
      IAL=AL
      HAL=AL-IAL
      IAL=IAL+1
      IF(IAL.GE.NAL) HAL=1.
      IF(IAL.GE.NAL) IAL=NAL-1
      OMEGA=ABS(OMEGA)/DOM
```

```
      K3=K1+NOM
      K4=K2+NOM
      KAL=ALPHA/DAL+1.5
      KAL=MINO(KAL,NAL)
      KOM=(OMEGA+45.)/DOM+1.5
      K=(KAL-1)*NOM+KOM
C
C HERE WE COMPUTE THE REAL-TIME PARAMETERS
C
      IS(1) =ISAMP(S1)
      IS(2) =ISAMP(S2)
      IS(3) =ISAMP(S3)
      IS(4) =ISAMP(S4)
      IS(5) =ISAMP(S5)
      IA1(1)=ISAMP(A11)
      IA1(2)=ISAMP(A12)
      IA1(3)=ISAMP(A13)
      IA1(4)=ISAMP(A14)
      IA1(5)=ISAMP(A15)
      IA2(1)=IA1(5)
      IA2(2)=ISAMP(A22)
      IA2(3)=ISAMP(A23)
      IA2(4)=ISAMP(A24)
      IA2(5)=ISAMP(A25)
      IE(1) =ISAMP(E1)
      IE(2) =ISAMP(E2)
      IE(3) =ISAMP(E3)
      IE(4) =ISAMP(E4)
      IE(5) =ISAMP(E5)
      SPK =40.
      PSL =0.
      A1PK=AINT(A1P)
      A2PK=AINT(A2P)
      EPK =AINT(EP)
      IS(6) =IST(KAL)
      IA1(6)=IA1T(K)
      IA2(6)=IA2T(K)
      IE(6) =IET(K)
C
C CONVERT DB TO NEPERS (AMPLITUDE)
C
      SPK =.11513*SPK
      A1PK=.11513*A1PK
      A2PK=.11513*A2PK
      EPK =.11513*EPK
      PSL =.11513*PSL

      RETURN
      END
```

```
      FUNCTION AINT(A)
C
C INTERPOLATION FOR SUBROUTINE PARMS
C
      DIMENSION A(1)
      COMMON /CINT/ K1,K2,K3,K4,HOM,HAL
      A1=(1.-HOM)*A(K1)+HOM*A(K2)
      A2=(1.-HOM)*A(K3)+HOM*A(K4)
      AINT=(1.-HAL)*A1+HAL*A2
      RETURN
      END
```

```
      SUBROUTINE PR(A,NX,NY)
C
C IN THIS SUBROUTINE WE PRINT THE 2-DIMENSIONAL ARRAY A WITH THE FORMAT
C EQUIVALENT TO THE DIMENSION A(NX,NY).
C
C THE PRINTING IS ON FILE LU, WHICH MUST BE EQUIPPED.
C
      DIMENSION A(1)
      COMMON /MESGE/ MFLAG
      DATA LU/6/
      IF(MFLAG.NE.1) WRITE (LU,100)
      MFLAG=0
      DO 20 J=1,NY
      L1=(J-1)*NX+1
      L2=L1+9
      L2MAX=J*NX
      L2=MINO(L2,L2MAX)
      DO 20 I=1,NX,10
      IF(I.LE.1) WRITE (LU,101) J,(A(K),K=L1,L2)
      IF(I.GT.1) WRITE (LU,102)   (A(K),K=L1,L2)
      L1=L1+10
      L2=MINO(L2+10,L2MAX)
   20 CONTINUE
      RETURN
  100 FORMAT(1H1)
  101 FORMAT(/I4,2X10E12.4)
  102 FORMAT(6X10E12.4)
      END
```

```
      SUBROUTINE ACCUM(X,Y,N,IREP)
C
C IN THIS SUBROUTINE WE ACCUMULATE AN ARRAY.  AT ALL TIMES ARRAY Y
C REPRESENTS A RUNNING AVERAGE.
C
      DIMENSION X(1),Y(1)
      IF(IREP.EQ.1) GO TO 30
      REP=IREP
      DO 20 K=1,N
      Y(K)=((REP-1.)*Y(K)+X(K))/REP
   20 CONTINUE
      RETURN
   30 CALL XMIT(N,X,Y)
      RETURN
      END
```

```
      SUBROUTINE POWSPT(XR, XI, NIN, NOUT, ALPHA, W)
C
C IN THIS SUBROUTINE WE COMPUTE THE POWER SPECTRUM OF THE COMPLEX TIME
C SEQUENCE IN THE ARRAY-PAIR (XR, XI) OF LENGTH NIN.  THE POWER SPECTRUM
C IS RETURNED IN ARRAY XR, AND IT IS NOW OF LENGTH NOUT.
C
C THE SAMPLE SPACING OF THE POWER SPECTRUM IS 1/NOUT OF THE REPETITION
C FREQUENCY.
C
C A COSINE-ON-A-PEDESTAL WEIGHTING IS APPLIED TO THE INPUT SAMPLES.
C ALPHA IS THE RATIO OF THE WEIGHTING FUNCTION AT THE EDGE TO THE
C CENTER.  ALPHA=.08 FOR HAMMING AND ALPHA=1.0 FOR UNIFORM WEIGHTING.
C
C ARRAY W IS A WORKING ARRAY AND IT MUST BE DIMENSIONED AS LARGE AS....
C
C              NIN            IF NOUT.EQ.2**INTEGER
C              NIN+2*NOUT     IF NOUT.NE.2**INTEGER
C
C THE WEIGHTS ARE NORMALIZED SO THAT THE SUM IS UNITY.
C
      DIMENSION XR(1),XI(1),W(1)
      DATA TWOPI/6.2831853/
      DATA NO/0/
      IF(NO.GT.0) GO TO 25
      NO=1
      N=NOUT-NIN
      A=(1.+ALPHA)/2.
      B=(1.-ALPHA)/2.
      CN=(NIN+1)/2.
      XN=NIN
      DO 10 K=1,NIN
      W(K)=A+B*COS(TWOPI*(K-CN)/XN)
   10 CONTINUE
      SUM=0.
      DO 15 K=1,NIN
      SUM=SUM+W(K)
   15 CONTINUE
      WNORM=SUM
      DO 20 K=1,NIN
      W(K)=W(K)/WNORM
   20 CONTINUE
   25 IF(N) 60,35,30
   30 CALL XMIT(-N,0.,XR(NIN+1))
      CALL XMIT(-N,0.,XI(NIN+1))
   35 DO 40 K=1,NIN
      XR(K)=XR(K)*W(K)
      XI(K)=XI(K)*W(K)
   40 CONTINUE
      CALL FOURT(XR,XI,NOUT,1,1,1,W(NIN+1),W(NIN+NOUT+1))
      DO 50 K=1,NOUT
```

```
      XR(K)=XR(K)**2+XI(K)**2
   50 CONTINUE
      RETURN
   60 PRINT 100, NIN, NOUT
      STOP
  100 FORMAT(/1X49H***ERROR IN POWSPT , NOUT IS SMALLER THAN NIN ***/
     1     /10X4HNIN=I6, 10X5HNOUT=I6)
      END
```

```
      SUBROUTINE XMIT(N,A,B)
C
C IN THIS SUBROUTINE WE EITHER TRANSMIT ARRAY A TO ARRAY B (IF N.GT.0)
C OR WE TRANSMIT THE CONSTANT A TO ARRAY B (IF N.LT.0).   IN EITHER CASE
C THE ARRAY LENGTH IS IABS(N).
C
C THIS SUBROUTINE SHOULD BE WRITTEN IN ASSEMBLY LANGUAGE
C
      DIMENSION A(1),B(1)
      IF(N) 10,20,25
   10 NN=-N
      AA=A(1)
      DO 15 K=1,NN
      B(K)=AA
   15 CONTINUE
   20 RETURN
   25 DO 30 K=1,N
      B(K)=A(K)
   30 CONTINUE
      RETURN
      END
```

```
      SUBROUTINE FILL(IROT)
C
C IN THIS SUBROUTINE WE GENERATE THE REAL-TIME CLUTTER MODULATION
C SIGNALS ON THE THREE MONOPULSE CHANNELS (FOR ONE RANGE GATE ONLY).
C THIS SUBROUTINE, AS WELL AS SUBROUTINES CURVE, CONVRT, PARAB, TIMESQ,
C GAUSS4, AND FFT2, WILL BE IMPLEMENTED ON THE AP120B.
C
C THE REAL-TIME INPUT IS THROUGH /C4/.....
C
C       IS,SPK.....SUM SPECTRUM PARAMETERS
C       IA1,A1PK....DEL-AZ SPECTRUM PARAMETERS, LEFT HALF
C       IA2,A2PK....DEL-AZ SPECTRUM PARAMETERS, RIGHT HALF
C       IE,EPK......DEL-EL SPECTRUM PARAMETERS
C       PSL.........SIDELOBE LEVEL (SEE BELOW)
C
C THE REAL-TIME OUTPUT IS THROUGH /C5/.....
C
C     PEFF = EFFECTIVE POWER RADIATED FROM RFSS ARRAY (FROM SUB. CLUTTR)
C      XR1 = REAL ARRAY CONTAINING SUM CHANNEL MODULATION SIGNAL
C      XI1 = IMAG ARRAY CONTAINING SUM CHANNEL MODULATION SIGNAL
C      XR2 = REAL ARRAY CONTAINING DAZ CHANNEL MODULATION SIGNAL
C      XI2 = IMAG ARRAY CONTAINING DAZ CHANNEL MODULATION SIGNAL
C      XR3 = REAL ARRAY CONTAINING DEL CHANNEL MODULATION SIGNAL
C      XI3 = IMAG ARRAY CONTAINING DEL CHANNEL MODULATION SIGNAL
C
C IROT IS A ROTATION FLAG.  IF IROT.GT.0 THE AZ AND EL ARRAYS ARE
C INTERCHANGED.
C
C THIS PROGRAM GENERATES A CONSTANT-LEVEL SIDELOBE SHOULDER OF (SPK-PSL)
C DB BELOW THE SUM SPECTRUM PEAK.
C
C ARRAYS S,A, AND E ARE FOR TEMPORARY STORAGE OF THE SUM, AZ- AND EL-
C DIFFERENCE SPECTRA.  THEY MUST BE DIMENSIONED AS LARGE AS 2*NFFT.
C
C THE DIMENSIONED ARRAYS IN COMMON /C5/ MUST ACCOMMODATE NFFT+NOVLP
C WORDS (SEE TIMESQ).
C
      COMMON /C3/ NFFT
      COMMON /C4/ IS(6),IA1(6),IA2(6),IE(6),SPK,A1PK,A2PK,EPK,PSL
      COMMON /C5/ PEFF,
     1            XR1(320),XI1(320),XR2(320),XI2(320),XR3(320),XI3(320)
      COMMON /C7/ S(512),A(512),E(512)
      COMMON /LIM/ NFFT2
     ,NFFT2=NFFT*2
C
C INITIALIZE ARRAYS TO SIDELOBE LEVEL
C
      CALL XMIT(-NFFT2,PSL,S)
      CALL XMIT(-NFFT2,PSL,A)
      CALL XMIT(-NFFT2,PSL,E)
```

```
C
C GENERATE LOG-AMPLITUDE SPECTRA
C
      CALL CURVE(S, IS, SPK)
      CALL CURVE(A, IA1, A1PK)
      CALL CURVE(A, IA2, A2PK)
      CALL CURVE(E, IE, EPK)
C
C CONVERT TO LINEAR AMPLITUDE AND FOLDOVER
C
      SNORM=0.
      CALL CONVRT(S, SNORM)
      CALL CONVRT(A, SNORM)
      CALL CONVRT(E, SNORM)
C
C GENERATE TIME SEQUENCES
C
      CALL TIMESQ(S, XR1, XI1)
      IF(IROT.GT.0) GO TO 35
      CALL TIMESQ(A, XR2, XI2)
      CALL TIMESQ(E, XR3, XI3)
      GO TO 40
   35 CALL TIMESQ(A, XR3, XI3)
      CALL TIMESQ(E, XR2, XI2)
   40 RETURN
      END
```

```
      SUBROUTINE CURVE(S,II,PK)
C
C THIS SUBROUTINE GENERATES A CURVE IN ARRAY S BETWEEN SAMPLES II(1) AND
C II(5).  THE CURVE IS DEFINED IN FOUR SEGMENTS BETWEEN FIVE POINTS
C WHERE THE POINTS ARE GIVEN BY.....
C
C                    SAMPLE          VALUE
C
C                    II(1)           0.
C                    II(2)           PK/2.
C                    II(3)           PK
C                    II(4)           PK/2.
C                    II(5)           0.
C
C II(6)=ITYP IS A PARAMETER THAT DEFINES THE TYPE OF SEGMENTS.....
C
C                    ITYP            SEGMENTS
C
C                    0               LINE,LINE,LINE,LINE
C                    1               LINE,PARAB,LINE,LINE
C                    2               LINE,PARAB,PARAB,LINE
C
C THE PARABOLA IS ALWAYS CONSTRAINED TO HAVE ZERO SLOPE AT THE CENTER
C POINT.
C
      DIMENSION S(1),II(6)
      COMMON /ABC/ A,B,C

      IF(PK.LE.0.) RETURN
      P2=.5*PK
      ITYP=II(6)
C
C COMPUTE FIRST SEGMENT
C
      C=0.
      B=P2/AMAX0(II(2)-II(1),1)
      A=-B*II(1)
      CALL PARAB(S,II(1),II(2))
C
C COMPUTE SECOND SEGMENT
C
      IF(ITYP.GT.0) GO TO 20
      C=0.
      B=P2/AMAX0(II(3)-II(2),1)
      A=P2-B*II(2)
      GO TO 25
   20 C=-P2/AMAX0(II(3)-II(2),1)**2
      B=-2.*C*II(3)
      A=P2-B*II(2)-C*II(2)**2
   25 CALL PARAB(S,II(2)+1,II(3))
```

```
C
C COMPUTE THIRD SEGMENT
C
      IF(ITYP.GT.1) GO TO 30
      C=0.
      B=-P2/AMAXO(II(4)-II(3),1)
      A=PK-B*II(3)
      GO TO 35
   30 C=-P2/AMAXO(II(4)-II(3),1)**2
      B=-2.*C*II(3)
      A=PK-B*II(3)-C*II(3)**2
   35 CALL PARAB(S,II(3)+1,II(4))
C
C COMPUTE FOURTH SEGMENT
C
      C=0.
      B=-P2/AMAXO(II(5)-II(4),1)
      A=P2-B*II(4)
      CALL PARAB(S,II(4)+1,II(5))

      RETURN
      END
```

```
      SUBROUTINE PARAB(S, II1, II2)
C
C THIS SUBROUTINE GENERATES A PARABOLA OF THE FORM.....
C
C                S(I) = A + B*I + C*I**2
C
      DIMENSION S(1)
      COMMON /ABC/ A, B, C
      COMMON /LIM/ LIM
      I1=MAXO(II1, 1)
      I2=MINO(II2, LIM)
      IF(I1. GT. I2) RETURN
      DO 20 I=I1, I2
      S(I)=(C*I+B)*I+A
   20 CONTINUE
      RETURN
      END
```

```
      SUBROUTINE CONVRT(S,SNORM)
C
C IN THIS SUBROUTINE WE CONVERT THE SPECTRUM IN ARRAY S OF LOG-AMPLITUDE
C UNITS TO LINEAR-AMPLITUDE UNITS.  IN ADDITION, TWO PRF INTERVALS ARE
C FOLDED (SUMMED).  THE INPUT S-ARRAY IS OF LENGTH 2*NFFT AND THE OUTPUT
C S-ARRAY IS OF LENGTH NFFT.  AN APPROXIMATION IS USED IN THE DO-20 LOOP
C FOR A FASTER COMPUTATION.
C
C FOR THE SUM SPECTRUM SET SNORM=ZERO ON INPUT (DO NOT USE THE CONSTANT
C 0., HOWEVER).  THE NORMALIZATION FACTOR SNORM WILL BE RETURNED.  FOR
C THE DIFFERENCE SPECTRA USE THIS SAME VALUE ON INPUT.
C
      DIMENSION S(1)
      COMMON /C3/ NFFT
      DO 20 K=1,NFFT
      S(K)=EXP(S(K)+S(K+NFFT))
   20 CONTINUE
      IF(SNORM.GT.0.) GO TO 35
      SUM=0.
      DO 30 K=1,NFFT
      SUM=SUM+S(K)**2
   30 CONTINUE
      SNORM=1./SQRT(SUM)
   35 DO 40 K=1,NFFT
      S(K)=S(K)*SNORM
   40 CONTINUE
      RETURN
      END
```

AD-A093 052 MARK RESOURCES INC MARINA DEL REY CA F/G 17/9
RFSS. VOLUME 1. DISTRIBUTED CLUTTER MODEL: REAL-TIME FFT PROGRA--ETC(U)
NOV 78 R L MITCHELL DAAK40-78-C-0031
UNCLASSIFIED MRI-149-38 NL

2 OF 2
AD A
093052

END
DATE FILMED
-81
DTIC

```
      SUBROUTINE TIMESQ(SA, XR, XI)
C
C IN THIS SUBROUTINE WE GENERATE A CORRELATED TIME SEQUENCE THAT HAS AN
C AMPLITUDE SPECTRAL FUNCTION DESCRIBED BY ARRAY SA OF LENGTH NFFT.  THE
C METHOD USED IS THE ON-LINE FFT APPROACH DESCRIBED IN SECTION 6 OF MRI
C REPORT 132-44, WHERE SUCCESSIVE CALLS TO TIMESQ WILL CREATE CONTIGUOUS
C TIME SEQUENCES BASED ON OVERLAPPING FFTS IN THE FREQUENCY DOMAIN.
C
C ON INPUT.....
C
C      NFFT = SIZE OF FFT (=2**INTEGER)
C     NOVLP = NUMBER OF SAMPLES THAT THE FFTS OVERLAP (NFFT/8 IS OK)
C     SA(K) = SPECTRAL AMPLITUDE OF KTH SAMPLE, K=1,...,NFFT
C
C ON OUTPUT.....
C
C     XR(K) = KTH SAMPLE OF IN-PHASE SIGNAL, K=1,...,NF
C     XI(K) = KTH SAMPLE OF QUADRATURE SIGNAL, K=1,...,NF
C
C WHERE  NF=NFFT-NOVLP.
C
C THE ARRAYS MUST BE DIMENSIONED AS LARGE AS.....
C
C                       SA          NFFT
C                       XR          NFFT+NOVLP-1
C                       XI          NFFT+NOVLP-1
C                       A           NOVLP-1
C
C NOTE THAT THE INFORMATION IS STORED IN THE XR AND XI ARRAYS FROM
C NFFT+1 TO NFFT+NOVLP+1 THAT WILL BE USED ON THE NEXT CALL.  PRIOR TO
C THE FIRST CALL TO TIMESQ THE INITIALIZATION SUBROUTINE (TIMSQI) MUST
C BE CALLED.
C
C THE WORK ARRAYS WRKR AND WRKI NEED BE DIMENSIONED ONLY IF NFFT.NE.
C 2**INTEGER, IN WHICH CASE THE DIMENSION SIZE MUST BE NFFT.
C
      DIMENSION WRKR(160),WRKI(160)
      DIMENSION SA(1),XR(1),XI(1)
      COMMON /C3/ NFFT,NOVLP,NF,A(1)
      CALL GAUSS4(SA,XR,XI,NFFT)
      CALL FOURT(XR,XI,NFFT,1,0,1,WRKR,WRKI)
      N1=NOVLP-1
      DO 20 K=1,N1
     ,XR(K)=A(K)*(XR(K)-XR(K+NFFT))+XR(K+NFFT)
      XI(K)=A(K)*(XI(K)-XI(K+NFFT))+XI(K+NFFT)
      XR(K+NFFT)=XR(K+NFFT-NOVLP)
      XI(K+NFFT)=XI(K+NFFT-NOVLP)
   20 CONTINUE
      RETURN
      END
```

```
      SUBROUTINE GAUSS4(A,XR,XI,N)
C
C GENERATES RANDOM PHASOR COMPONENTS (XR(K),XI(K)) OF ZERO MEAN WITH THE
C AVERAGE POWER OF  XR(K)**2+XI(K)**2  GIVEN BY A(K)**2 FOR K=1,...,N.
C
C THE RANDOM NUMBERS ARE ACCESSED FROM RECIRCULATING TABLES.  NTR AND
C NTI ARE THE CIRCULATION PARAMETERS AND NMAX=MAX(N).  WE SHOULD CHOOSE
C NTR AND NTI RELATIVELY PRIME.
C
C ARRAYS TR AND TI MUST BE DIMENSIONED AS LARGE AS NTR+NMAX AND NTI+NMAX
C RESPECTIVELY.
C
C IF IRSET=1 IN COMMON /GS/, THE POINTERS WILL BE RESTORED ON EXIT TO
C THEIR ORIGINAL VALUES WHEN GAUSS4 WAS ENTERED.  THIS MEANS THAT THE
C SAME GAUSSIAN SEQUENCE (EXCEPT FOR THE WEIGHTS A) WILL BE GENERATED ON
C THE NEXT CALL.
C
C PRIOR TO CALLING GAUSS4, THE RANDOM NUMBERS IN ARRAYS TR AND TI MUST
C BE INITIALIZED WITH A CALL TO GAUSSI.
C
      DIMENSION A(1),XR(1),XI(1)
      COMMON /GS/ IRSET,NTR,NTI,NMAX,KR,KI,TR(1253),TI(1353)
      IF(N.GT.NMAX) STOP
      DO 35 I=1,N
      XR(I)=A(I)*TR(KR)
      XI(I)=A(I)*TI(KI)
      KR=KR+1
      KI=KI+1
   35 CONTINUE
      IF(IRSET.NE.1) GO TO 40
      KR=KR-N
      KI=KI-N
   40 IF(KR.GT.NTR) KR=KR-NTR
      IF(KI.GT.NTI) KI=KI-NTI
      RETURN
      END
```